IN-71
156306
P.72

Aeroacoustic Diffraction and Dissipation by a Short Propeller Cowl in Subsonic Flight

Rudolph Martinez
Cambridge Acoustical Associates, Inc.
Cambridge, Massachusetts

April 1993

NASA
National Aeronautics and
Space Administration

AEROACOUSTIC DIFFRACTION AND DISSIPATION BY A SHORT PROPELLER COWL IN SUBSONIC FLIGHT

TABLE OF CONTENTS

NOMENCLATURE

Roman

a	cowl radius, dimensional up to Section C.3 and nondimensional thereafter
A	one of three parameters used to characterize the inflow nonuniformity chopped by the propeller, Eq. 56 and Fig. 6a
B	number of blades in the fan
c	speed of sound of the medium
$\bar{c}$	nondimensional blade chord for Sears' function
H_ν	Hankel function of the first kind of order ν
I_ν	modified Bessel function of order ν
J_ν	Bessel function of order ν
k	cowl's reduced frequency, $\omega L/2U$
$\bar{k}$	transform wavenumber, dimensional up to Section C.3
K_ν	modified Hankel function of order ν
L/2	cowl's halflength or halfchord; also the normalizing constant in Section C.3
L_{liner}	length of lined segment, Fig. 5a
L_ν	two-dimensional lift [Force/length] acting on an elemental ring of chord "$d\bar{z}$"
m	index of the series elements for the assumed lifting solution, Eq. 54a. Also serves as temporal harmonic counter in Eqs. 57a,b
M	flight or freestream Mach number, U/c
n	index of the series elements for the assumed nonlifting solution, Eq. 54b

p	time-dependent pressure
$\bar{p}, \bar{p}_v$	frequency-domain pressure, and its circumferential v mode
$\bar{p}_v^{inc}$	incident field pressure
$\bar{p}_v^{\ell}, \bar{p}_v^{th}$	lifting and thickness contributions to the scattered pressure
$r, \bar{r}$	field and source values of the radial coordinate, dimensional up to Section C.3
r^*	running radial variable distinguishing among blade stations, nondimensional
R_o	nondimensional range to the farfield observer, with origin at the cowl's geometric center $r=0$, $z=0$. $\hat{R}_o$ is its dimensional version, $R_o L/2$
S	Sears function, Eq. 59
t	time
T_n	Chebyshev polynomial of the first kind, Eq. 54b
$\bar{T}_n$	aerodynamic transfer function, Eqs. 57a,b
$\bar{u}$	one of three parameters used to describe the inflow inhomogeneity which the propeller blades must cut, Eq. 56 and Fig. 6a
$\bar{u}_{r,v}^{\ell}$	axial velocity induced by an elemental lifting ring
U	freestream or flight speed
U_n	Chebyshev polynomials of the second kind, Eq. 54a
$\bar{w}_v^{\ell}$	radial velocity induced by a lifting ring
$\bar{w}_v^{inc}$	incident field's radial particle velocity over $r=a^+$
$z, \bar{z}$	axial coordinates for receiver and source, respectively, dimensional up to Section C.3
z^*	propeller's axial station
z_{mid}	midpoint axial position for the liner ring patch, Fig. 5a
Z_{liner}	liner impedance, Eq. 49

Greek

α axially variable admittance of the liner, normalized by the fluid's characteristic admittance $1/\rho c$, Eq. 52

β^2 $1-M^2$

γ transform wavenumber for the radial direction, Eqs. 8 and 50

$\Delta\bar{p}, \Delta\bar{w}$ unknown diffraction loading $\bar{p}^+ - \bar{p}^-$ in the lifting problem, and unknown monopole strength $\bar{w}^+ - \bar{w}^-$ for the nonlifting problem; each of these two quantities takes on a ν subscript when it becomes the circumferential mode of the parent variable; "+" and "−" denote $r=a^+$ and $r=a^-$

η liner loss factor, Eq. 49

θ_o directivity angle, Figs. 7a,b

$K_\nu^{l,l}$ lifting kernel, or influence function linking the induced radial velocity to the virtual lift

$K_\nu^{l,th}$ kernel linking the radial upwash to thickness source strength, or pressure to the virtual lift

$K_\nu^{th,th}$ kernel linking pressure to the thickness source strength

ν circumferential mode

ρ background fluid density

$\phi, \bar{\phi}$ field and source values of the circumferential angle, Fig. 1b

ϕ^* running angular variable in Eq. 56

$\hat{\phi}$ angular position around the propeller disk of the maximum momentum deficit in the inflow inhomogeneity, Fig. 6a

Ω propeller's rotational speed

ω frequency, $mB\Omega$ in the tonal problem of Eqs. 57a,b

AEROACOUSTIC DIFFRACTION AND DISSIPATION BY A

SHORT PROPELLER COWL IN SUBSONIC FLIGHT

R. Martinez
Cambridge Acoustical Associates, Inc.
Cambridge, Massachusetts

I   ABSTRACT

This report develops and applies a new acoustic diffraction theory for a ring wing in unsteady compressible flow. The motivation of the study is the current need to predict the sound scattered and absorbed by a short duct, or cowl, placed around typical sources of propeller noise. The modelled cowl's inner wall contains a liner with axially variable properties. Its exterior is rigid. The analysis replaces both sides with an unsteady lifting surface coupled to a dynamic thickness problem. The resulting pair of aeroacoustic governing equations for a lined ring wing is valid both for passive and for active liners.

The independent character of the incident field that drives these two equations implies no approximations[‡]. The new theory is thus ideally suited to "marriages" with existing sophisticated predictors of the propeller nearfield for the unducted configuration. These predictors will supply the new cowl diffraction theory with its known "right side", on a case by case basis.

The solution of the coupled integral equation pair yields the effective dipole and monopole distributions of the shrouding system, and thus determines the cowl-diffracted component of the total field. The sample calculations presented here include a preliminary parametric search for that passive liner layout which in some sense minimizes the shrouded propulsor's radiated field.

The main conclusion of the study is that a short cowl passively lined should provide moderate reductions in propeller noise.

[‡]Perhaps a better term than "independent character" is "modular character". This statement simply declares that the thin-shape diffraction analysis proceeds without approximations once its incident field has been defined.

II INTRODUCTION

A. Motivation and Objectives of the Research

There is a need for rigorous and affordable predictions of the acoustic field diffracting from a lined propeller cowl of finite length[1] (Fig. 1a). The hope is that a properly designed short duct, e.g., one that takes due note of the position of its edges and liner relative to the sources it contains, will either reduce or favorably alter the radiation emerging from its ends. Recent estimates of planar edge diffraction by Dittmar[2] and by Amiet[3a] suggest that this could indeed be the case.

This report develops and applies an aeroacoustic diffraction theory for a lined ring wing of finite chord (the cowl) in unsteady subsonic flow (Fig. 1b). The modelled cowl's internal liner is axisymmetric, but with physical and geometric characteristics that are otherwise left arbitrary. The liner contributes, by virtue of its finite reactance and resistance, a nonlifting unsteady flow of strength which is unknown a priori. This virtual flow from the dynamic "thickness problem" combines with that of the cowl as a lifting surface in satisfying the geometry's boundary conditions, e.g., in satisfying flow tangency over the rigid parts of the shroud's inner and outer sides. The lifting and nonlifting unsteady problems are coupled.

The cowl's static angle of attack is zero. The sole source of incident flow normal to its surfaces is the propeller-generated acoustic field insonifying it from within. The mathematical descriptions of the acoustics and the aerodynamics of the system are really the same. Put more specifically: the boundary conditions which diffraction theory imposes on an open-ended duct in a freestream by default are, or become, a lifting-surface aerodynamic theory for a ring wing (coupled to a nonlifting problem due to the liner, as explained above).

This lifting-surface theory automatically isolates the phenomenon of edge diffraction when the liner is taken away: the thickness problem disappears then. The treatment here of the remaining pure-lift equation is unorthodox. The approach uses a circumferential modal expansion to remove the ring wing's spanwise direction and all of its anticipated liabilities, e.g., its Mangler singularity. The result is a benign but rigorous integral equation for the cowl's fore/aft chord that trades these classical difficulties for the need to compute a simple product of Bessel functions and an associated circumferential modal series in terms of these functions.

2

This new analysis for a three-dimensional cowl of finite length takes a spectral approach to the representation of its lifting and nonlifting kernels. The final forms of these are in terms of contour integrals in wavenumber space. These contours expose the "guts" of the influence functions they describe; e.g., the transform of the lifting kernel displays its formal wake-shedding capability explicitly through a simple pole. The spectral analysis also serves to connect the new theory to its predecessors, thereby checking it, e.g., to the "pure" diffraction case of the author's Refs. 4a,b for U=0. Section A.2 thus shows how the contour of integration of general aeroacoustics links steady and unsteady aerodynamics for ring wings to the theory of (flowless) diffraction for open-ended ducts.

The demonstrated steady limit of the novel lift theory (with its steady trailing vortices) could predict already the airloads that a cowl would experience when placed at an angle of attack, as well as the steady but spatially nonuniform interference flows that the system would induce over the plane of its internal propeller.

The new model for the cowl shares an important feature with Amiet's simpler two-dimensional analysis[3a] for a planar airfoil in subsonic flow: both include the effect of the freestream on the propagating incident and diffracted fields. The fully coupled theory for the cowl also accounts rigorously for the very different kind of acoustic scattering that occurs at the liner's axial discontinuities (note the three discrete liner rings in Fig. 1b, as an example). The cowl's virtual flows contribute only small disturbances to the medium. The analysis is linear.

These virtual flows, once found, furnish the dipole and monopole strengths of the cowl's diffracted or scattered field, which added to that which is incident from the propeller produces the total acoustic pressure as a function of listener position. A primary objective of the study is to predict this last quantity for two kinds of observers:

(1) Passengers in the aircraft to which the cowl belongs. Here the field positions correspond to points along the cabin's outer wall. Arriving rays must cut through a uniform meanflow of Mach number M.

(2) Listeners on the ground, where the medium is still and the overhead acoustic sources are in motion. The propagation of

3

sound in this reference frame includes such familiar effects as Doppler shifts and the enhancement of ray amplitudes in the forward direction.

The differences in the fields heard by these two types of observers disappear with a vanishing value of the Mach number M.

The first task for the calculations presented here is to determine the theoretical degree of edge shielding provided by a completely rigid short cowl without a liner. A second set of predictions explores the sensitivity of the field radiated by the complete lined system to differing geometric layouts of its liner. The idea is to maximize the combined, and generally coupled effects of liner dissipation, finite-liner scattering, and edge diffraction at the cowl's two circular ends.

B. Context of the New Work

The presence or absence of a meanflow U has tended to split cleanly the kinds of acoustic analyses performed for finite or semi-infinite ducts. Horowitz et al.'s study is typical of investigations with a freestream[5]. This paper describes a computational fluid dynamics solution of an inlet-geometry problem. The duct is semi-infinite. On the other hand, Refs. 6a,b by Hamdi & Ville, Refs. 7a,b by Fuller and by Fuller & Silcox, and Refs. 4a,b by the author, are examples of studies which have not modelled flow effects.

This second group has focused instead on predicting pure acoustic diffraction for a finite duct driven by relatively simple internal sources of sound. Fuller & Silcox's analysis and experiments addressed the problems of edge diffraction and of diffraction and dissipation by a circumferentially nonuniform and axially finite liner. The geometry in Refs. 7a,b included a flange, or baffle, at the finite duct's single opening (the other end was closed). The solution procedure was to split the medium artificially into duct-internal and duct-external parts and to describe the interior in terms of axial modes with cut-on frequencies, etc. A system of linear equations coupled the interior and exterior parts and generated the final solution.

Hamdi & Ville used a variational formulation of the boundary-element type to treat unflanged ducts with both ends open in a still medium. Their calculations, however, were only for the relatively simple case without a liner[6a,b].

The author developed in Ref. 4a a spectral formulation for

4

the boundary kernels that arise in the analysis of diffraction and dissipation for a partially lined pipe of finite length. The duct was unflanged and with both ends open. The model accounted formally for the strong acoustic coupling that exists among the two circular edges when the distance separating them was acoustically short; i.e., when $\omega L/c = O(1)$.

Eversman's numerical model has improved on all of the above by bringing freestream effects to a system of finite length[8]. His approach is to apply finite elements to a fluid volume surrounding the cowl and the internal engine core on which the propeller is mounted.

The theory developed here incorporates a subsonic freestream in the analysis of the author's Ref. 4a. It neglects the engine core but otherwise matches Eversman's model in terms of physics. The new treatment is "boundary-element" in philosophy, i.e., it is a rational melding of lifting- and nonlifting-surface theories, each of which describes the relevant spatial domain in a manner that requires one global dimension less than finite elements. The new construction also includes unequivocally the influence of shed vorticity on the coupled processes of edge diffraction and liner dissipation (remember that the cowl is really a ring wing). The main purpose of section A.2 is, in fact, to confirm the correctness of the potential-vortex flows embedded in the new theory.

C. Organization of the Report

Section III is a detailed development of the new formulation. Subsection A contains the lifting half of the problem; B poses the nonlifting half contributed by the liner. Section C puts A and B together: C.3 states the final pair of coupled integral equations in nondimensional form. Readers not primarily concerned with these specifics should proceed directly to C.3.

Section III.E builds a simple model of the incident field that drives the integral equations. The current Phase I study considers a tonal signal resulting from a propeller chopping a generic inflow inhomogeneity. Each blade in this fan is a spanwise continuum of strips that are chordwise compact and unpitched, i.e., that lay flat on their plane of rotation. Future applications of the new cowl theory will replace this driver with more sophisticated predictors of propeller radiation in free field; see, for example, Hanson[9], and Dunn & Farassat[10].

Section F writes down the final farfield equations both for incident and diffracted fields, both for aircraft- and ground-reference frames. Section IV discusses sample calculations.

5

III FORMULATION OF THE AEROACOUSTIC DIFFRACTION/DISSIPATION PROBLEM OF A SHORT LINED PROPELLER COWL INSONIFIED FROM WITHIN

A The "Lifting" Unsteady-Aerodynamics Problem for the Virtual Dipoles making up the Cowl's Two-Sided Surface

A.1 Development

A convenient starting point in the development of the relevant influence function for the lifting problem is the Helmholtz integral equation for a medium generalized to include a uniform meanflow U. A standard reference is Goldstein[11], who incorporates the effects of freestream U in his definition of the freefield Green's function G:

$$\tilde{p}(r,\phi,z) = a \int_{-L/2}^{L/2} d\bar{z} \int_{0}^{2\pi} d\bar{\phi} \left[\Delta\left(\frac{\partial \tilde{p}}{\partial \bar{r}}(\bar{r}=a,\bar{\phi},\bar{z}) \right) \cdot G(r,\phi,z;a,\bar{\phi},\bar{z}) \right.$$
$$\left. - \frac{\partial G}{\partial \bar{r}}(r,\phi,z;\bar{r}=a,\bar{\phi},\bar{z}) \, \Delta\tilde{p}(\bar{r}=a,\bar{\phi},\bar{z}) \right] \quad . \quad (1)$$

The dependent variable on the left side of Eq. 1 is the scattered pressure field $\tilde{p}$ in the frequency domain ω. The corresponding symbol p, without the tilde, will eventually denote pressure in the time domain and will enter the development here in the "incident field analysis" carried out below. Eq. 1 describes a cowl that extends from $\bar{z}=-L/2$ to L/2, with an infinitesimally thin wall that is at a radial distance "a" from the axis r=0. Angle $\bar{\phi}$ runs in the circumferential direction as depicted on the right part of Fig. 1b.

Eq. 1 is actually the jump version of Goldstein's form for the same equation: E.g, quantity $\Delta\tilde{p}_v \cdot ad\bar{\phi}d\bar{z}$ in Eq. 1 is the elemental virtual force straddling the cowl's thin wall at axial position $\bar{z}$,

$$[\tilde{p}(\bar{r}=a^+,\bar{\phi},\bar{z}) - \tilde{p}(\bar{r}=a^-,\bar{\phi},\bar{z})] \cdot ad\bar{\phi}d\bar{z} \equiv [\tilde{p}^+(a,\bar{\phi},\bar{z}) - \tilde{p}^-(a,\bar{\phi},\bar{z})] \cdot ad\bar{\phi}d\bar{z}$$
$$\equiv [\Delta\tilde{p}(a,\bar{\phi},\bar{z})] \cdot ad\bar{\phi}d\bar{z} \quad . \quad (2)$$

The lifting kernel about to be derived could be interpreted as being the result of a number of analytical operations on Eq. 1's $-\partial G/\partial \bar{r}$ term. But the analysis here will be self contained in

6

that it will begin by adding the few extra steps needed to produce $-\partial G/\partial \bar{r}$ itself.

This influence function $\check{p}_e$, to be defined as the product of $-\partial G/\partial \bar{r}$ and its elemental force-dipole strength $\Delta \bar{p}_v \cdot ad\bar{\phi} d\bar{z}$, is the solution of

$$\beta^2 \frac{\partial^2 \check{p}_e^{\ell}}{\partial z^2} + \nabla_{2-D}^2 \check{p}_e^{\ell} + \frac{\omega^2}{c^2} \check{p}_e^{\ell} + 2i \frac{\omega U}{c^2} \frac{\partial \check{p}_e^{\ell}}{\partial z}$$
$$= -\left[\Delta \bar{p}(a,\bar{\phi},\bar{z}) ad\bar{\phi} d\bar{z}\right] \cdot \lim_{\bar{r} \to a} \frac{\partial}{\partial \bar{r}} \cdot \frac{\delta(r-\bar{r})}{r} \delta(z-\bar{z}) \delta(\phi-\bar{\phi}) \quad . \quad (3)$$

Subscript "e" and superscript "ℓ" denote, respectively, "elemental" and "lifting problem". Symbol c stands for the spatially uniform sound speed of the medium and M=U/c, the flight Mach number. Parameter β^2 is $1-M^2$. Subscript "2-D" on the Laplacian operator on the left side applies to the r,ϕ cross-sectional plane. The complete differential operator displayed is the frequency-domain (ω) version of that from the linearized convected-wave equation; see, for example, Eq. 1.61 of Ref. 11.

The following standard change of dependent variables,

$$\check{p}_e^{\ell}(r,\phi,z) = p_e^*(r,\phi,z) e^{-i\frac{\omega}{c}\frac{M}{\beta^2}z} \quad , \quad (4)$$

turns Eq. 3 into

$$\beta^2 \frac{\partial^2 p_e^*}{\partial z^2} + \nabla_{2-D}^2 p_e^* + \frac{\omega^2}{c^2} \frac{1}{\beta^2} p_e^*$$
$$= -e^{i\frac{\omega}{c}\frac{M}{\beta^2}z} \left[\Delta \bar{p}(\bar{\phi},\bar{z}) ad\bar{\phi} d\bar{z}\right] \lim_{\bar{r} \to a} \frac{\partial}{\partial \bar{r}} \frac{\delta(r-\bar{r})}{r} \delta(z-\bar{z}) \delta(\phi-\bar{\phi}) \quad . \quad (5)$$

The $(\omega M/c)/\beta^2$ factor in the exponent of Eq. 4 matches that in the first term of the argument of the exponential in Adamczyk's[12] Eq. 15, after specifying his result to the case of zero sweep.

The "a" radial argument has disappeared from what would have been $\Delta \bar{p}(a,\ldots)$ on the right side of Eq. 5, for the sake of simplicity of notation. The next step is to define the transform pair

$$P^*(r,\phi;\overline{K}) = \int_{-\infty}^{\infty} \frac{dz}{2\pi}\, e^{i\overline{K}z}\, p_e^*(r,\phi,z) \quad ; \quad p_e^*(r,\phi,z) = \int_{-\infty}^{\infty} d\overline{K}\, e^{-i\overline{K}z}\, P^*(r,\phi;\overline{K}) \quad (6a,b)$$

and to apply Eq. 6a to Eq. 5. The result is

$$\nabla^2_{2-D} P^* + \gamma^2 P^* = -\,[\Delta \tilde{p}(\overline{\phi},\overline{z})\, a d\overline{\phi} d\overline{z}]\, \frac{e^{i\left(\overline{K} + \frac{\omega}{c}\frac{M}{\beta^2}\right)\overline{z}}}{2\pi}\, \lim_{\overline{r}\to a} \frac{\partial}{\partial \overline{r}} \frac{\delta(r-\overline{r})}{\overline{r}}\, \delta(\phi-\overline{\phi}) \quad , \quad (7)$$

with

$$\gamma = \sqrt{\frac{\omega^2}{c^2}\frac{1}{\beta^2} - \beta^2 \overline{K}^2} \quad . \qquad (8)$$

Eq. 7 has solution

$$P^* = -\,[\Delta \tilde{p}(\overline{\phi},\overline{z})\, a d\overline{\phi} d\overline{z}]\, \frac{e^{i\left(\overline{K} + \frac{\omega}{c}\frac{M}{\beta^2}\right)\overline{z}}}{2\pi}$$

$$\cdot \lim_{\overline{r}\to a} \frac{\partial}{\partial \overline{r}} \left(-\frac{i}{4}\right) H_o^{(1)}\!\left[\gamma \sqrt{r^2 + \overline{r}^2 - 2r\overline{r}\cos(\phi-\overline{\phi})}\right] \quad , \quad (9)$$

where the group $-i/4 \cdot H_o^{(1)}[\gamma \sqrt{\,..}\,]$ satisfies $(\nabla^2 + \gamma^2)(.) = \delta(r-\overline{r})/\overline{r}$ $\cdot \delta(\phi-\overline{\phi})$. Eqs. 6b, 4, and the familiar modal break up of the "origin-displaced" Hankel function $H_o^{(1)}$, give that

$$\tilde{p}_e^!(r,\phi,z) = \left(\frac{i}{8\pi}\right)[\Delta\tilde{p}(\overline{\phi},\overline{z})\, a d\overline{\phi} d\overline{z}]\; e^{-i\frac{\omega}{c}\frac{M}{\beta^2}(z-\overline{z})}$$

$$\cdot \sum_{v=-\infty}^{\infty} e^{-iv(\phi-\overline{\phi})} \int_{-\infty}^{\infty} d\overline{K}\, e^{-i\overline{K}(z-\overline{z})}\, \gamma \begin{cases} H_v(\gamma r)\, J_v'(\gamma a) & \text{for } r>a \\ H_v'(\gamma a)\, J_v(\gamma r) & \text{for } r<a \end{cases} \quad . \qquad (10)$$

The next step is to consider a circumferential continuum of virtual elemental lifting elements in order to build a singular

ring at $z=\bar{z}$. One defines $\bar{p}_r^{\prime}(r,\phi,z)$ as the pressure field due to this constructed elemental lifting ring:

$$\bar{p}_r^{\prime}(r,\phi,z;a,\bar{z}) \equiv \int_0^{2\pi} \bar{p}_e^{\prime}(r,\phi,z;\bar{\phi},\bar{z}) \qquad .\qquad (11)$$

The integral in Eq. 11 is over $\bar{\phi}$: The $d\bar{\phi}$ differential is part of the definition of $\bar{p}_e^{\prime}$ in Eq. 10. The result is a compound ring dipole source of strength given by

$$\int_0^{2\pi} d\bar{\phi}\, e^{iv\bar{\phi}} \Delta\tilde{p}(\bar{\phi},\bar{z}) \equiv 2\pi\, \Delta\tilde{p}_v(\bar{z}) \qquad \left(\to \Delta\tilde{p}(\bar{\phi},\bar{z}) = \sum_{v=-\infty}^{\infty} e^{-iv\bar{\phi}} \Delta\tilde{p}_v(\bar{z})\right). \quad (12)$$

This leads naturally to the physical interpretation of circumferential mode $\Delta\bar{p}_v(\bar{z})$ as the effective amplitude of the elemental ring at axial station $\bar{z}$. A similar reasoning will eventually identify the circumferential modal form of the left side of Eq. 10 as given by the function within the v sum on the right side of that expression.

The development will postpone this second modal definition and will now instead determine the full three-dimensional velocity field associated with $\bar{p}_r^{\prime}$. The component of interest in the boundary-value problem will be the radial velocity $\bar{w}_r^{\prime}(r=a,\phi,z)$ across the cowl's infinitesimally separated surfaces: across $r=a^\pm$, $-L/2<z<L/2$. This velocity field is available from the inverted radial momentum equation with the constant of integration $\bar{w}_r^{\prime}(z=-\infty)$ prescribed to be zero on physical grounds:

$$\bar{w}_r^{\prime}(a^\pm,\phi,z) = -\frac{e^{i\frac{\omega}{U}z}}{\rho U} \int_{-\infty}^{z} dz^* \frac{\partial \tilde{p}_r^{\prime}}{\partial r}(r=a^\pm,\phi,z^*)\, e^{-i\frac{\omega}{U}z^*} \qquad . \qquad (13)$$

In Eq. 13 ρ is the medium's background density. From Eqs. 10 and 12 it now follows that

$$\tilde{w}_r^l(r=a^{\pm}, \phi, z) = \left(\frac{-ia}{4\rho U}\right) \sum_{\nu=-\infty}^{\infty} e^{-i\nu\phi} [\Delta\tilde{p}_\nu(\bar{z}) \, d\bar{z}] \, e^{i\frac{\omega}{U}z + i\frac{\omega}{c}\frac{M}{\beta^2}\bar{z}}$$

$$\cdot \int_{-\infty}^{\infty} d\bar{k} \, e^{i\bar{k}\bar{z}} \gamma^2 \, H_\nu'(\gamma a) \, J_\nu'(\gamma a) \cdot \int_{-\infty}^{z} dz^{\bullet} e^{-i\left(\bar{k} + \frac{\omega}{U}\frac{1}{\beta^2}\right)z^{\bullet}} \qquad . \qquad (14)$$

The indicated continuity of velocity across the wall of the elemental ring, as implied by the radial argument on the left side of the equation, stems from the fact that the derivative with respect to r of the right side of Eq. 10 yields the same thing whether r>a or r<a. This is as should be for the lifting problem because the distribution of virtual dipoles to be postulated over -L/2<z̄<L/2 will be equivalent to a superposition of bound vortex rings. And it is well known that an unbroken vortex sheet induces a continuous flow field normal to itself.

The "-∞" bottom limit of the z* integral that appears last in Eq. 14 causes that part of Eq. 14 to exist only for

$$Im[\bar{k}] > Im\left[-\frac{\omega}{U}\frac{1}{\beta^2}\right] \qquad . \qquad (15)$$

This relationship has temporarily generalized frequency ω to be complex for the sake of emphasis. For k̄ wavenumbers satisfying Eq. 15, then

$$\int_{-\infty}^{z} dz^{\bullet} e^{-i\left(\bar{k} + \frac{\omega}{U}\frac{1}{\beta^2}\right)z^{\bullet}} = \frac{i}{\bar{k} + \frac{\omega}{U}\frac{1}{\beta^2}} e^{-i\left(\bar{k} + \frac{\omega}{U}\frac{1}{\beta^2}\right)z} \qquad , \qquad (16)$$

which upon substitution into Eq. 14 finally yields that

$$\tilde{w}_r^l(a, \phi, z) = \frac{a}{4\rho U} \sum_{\nu=-\infty}^{\infty} e^{-i\nu\phi} [\Delta\tilde{p}_\nu(\bar{z}) \, d\bar{z}] \, e^{-i\frac{\omega}{c}\frac{M}{\beta^2}(z-\bar{z})}$$

$$\cdot \int_c \frac{d\bar{k} \, e^{-i\bar{k}(z-\bar{z})}}{\bar{k} + \frac{\omega}{U}\frac{1}{\beta^2}} \gamma^2 \, H_\nu'(\gamma a) \, J_\nu'(\gamma a) \qquad . \qquad (17)$$

10

The integration contour C is as depicted in Fig. 2a. Its passage below the branch point at $+(\omega/c)/\beta^2$ and above that at $-(\omega/c)/\beta^2$ [these are the zeros of γ in Eq. 8] is consistent with the chosen temporal behavior $\exp(-i\omega t)$. And its passage above the pole at $-(\omega/U)/\beta^2$ embodies, and is the result of, Eq. 15.

Eq. 17 holds whether or not the boundary-value problem is separable in the cross-sectional circumferential coordinate ϕ. From this point on the development will confine itself to axisymmetric liners and thus to a formulation that is strictly separable in ϕ. The liner will be able to vary arbitrarily in the axial direction z, however.

Separability in ϕ will lead below to a set of independent integral equation pairs for the single variable z: one system, i.e., a coupled pair, for each mode ν for the lifting and thickness problems. So with

$$\tilde{w}_r^l(a,\phi,z) = \sum_{\nu=-\infty}^{\infty} \tilde{w}_{r,\nu}^l(a,z)\, e^{-i\nu\phi} \qquad , \qquad (18)$$

one now identifies $\tilde{w}_{r,\nu}^l$ as everything on the right side of Eq. 17 other than the summation sign and the $\exp(-i\nu\phi)$ term.

Section A.2 below will return to a detailed discussion of the flows induced by a single dipole ring. The lifting-surface equation for the complete cowl requires now the induced velocity field due to a continuum of such rings extending over $-L/2<\bar{z}<L/2$. This collectively induced radial velocity will here be $\bar{w}_\nu^l$. The final modal integral equation for the lift distribution is then

$$\tilde{w}_\nu^l(z) = \int_{-L/2}^{L/2} d\bar{z}\, K_\nu^{l,l}(z-\bar{z})\, \Delta\tilde{p}_\nu(\bar{z}) \qquad , \qquad (19a)$$

where the indicated lifting kernel is

$$K_v^{\ell,\ell}(z-\bar{z}) = \frac{\beta}{2\pi\rho U} \cdot \frac{e^{-i\frac{\omega}{c}\frac{M}{\beta^2}(z-\bar{z})}}{z-\bar{z}}$$

$$+ \frac{a\, e^{-i\frac{\omega}{c}\frac{M}{\beta^2}(z-\bar{z})}}{4\rho U} \int_C d\bar{K}\, e^{-i\bar{K}(z-\bar{z})} \left[\frac{\gamma^2 H_v'(\gamma a)\, J_v'(\gamma a)}{\bar{K} + \frac{\omega}{U}\frac{1}{\beta^2}} - \frac{i\beta}{\pi a}\frac{|\bar{K}|}{\bar{K}} \right] . \quad (19b)$$

The reason for the "ℓ,ℓ" superscript will become obvious below, with the analysis of the nonlifting problem. Eq. 19b's first line showcases the locally steady, singular behavior of the kernel as z approaches $\bar{z}$. This first term on the right side comes from the subtraction of the high-wavenumber asymptote of the transform's $\bar{K}$ integrand. The second line of the equation is consequently integrable in z as $\bar{z}$ approaches z (it behaves as $\log(z-\bar{z})$; cf. Wong[13a] for the precise form of the remainder term, determined from a spatial-domain rather than a spectral analysis of the kernel function for the special case of pure diffraction, U=0). The second line in Eq. 19b also contains the bulk of the unsteady aeroacoustic information of the complete influence function.

This split of the kernel into its regular and singular parts resulted from the following analytical observations: first the limit,

$$\lim_{\bar{K}\to\infty} \gamma^2 H_v'(\gamma a)\, J_v'(\gamma a) = \frac{i}{\pi}\frac{\beta|\bar{K}|}{a} \quad , \quad (20)$$

so that

$$\lim_{z\to\bar{z}} \int_C \frac{d\bar{K}\, e^{-i\bar{K}(z-\bar{z})}}{\bar{K} + \frac{\omega}{U}\frac{1}{\beta^2}} \gamma^2 H_v'(\gamma a)\, J_v'(\gamma a) = \frac{i\beta}{\pi a} \int_{-\infty}^{\infty} d\bar{K}\, \frac{|\bar{K}|}{\bar{K}}\, e^{-i\bar{K}(z-\bar{z})} . \quad (21)$$

The spectrum on the right side of Eq. 21 furnishes the term that was subtracted from the $\bar{K}$ integrand in Eq. 19b. The limit on the right side of Eq. 20 requires the intermediate conversion of the standard Bessel functions to their modified forms. To find what the right side of Eq. 21 is, in $(z-\bar{z})$ space, one recalls the familiar spectral breakup of the zeroth-order Hankel

function [see, for example, Goldstein[11], p. 244, first equation in Appendix 5.B]:

$$i \lim_{k \to 0} \frac{\partial}{\partial z} \int_{-\infty}^{\infty} \frac{d\lambda \, e^{-i\lambda(z-\bar{z})}}{\sqrt{\lambda^2 - k^2}} = -\pi \lim_{k \to 0} \frac{\partial}{\partial z} H_o^{(1)}(k|z-\bar{z}|) \qquad . \qquad (22)$$

Here "k" is a temporary constant. Taking the indicated limit of the two sides individually yields

$$\int_{-\infty}^{\infty} d\lambda \, \frac{\lambda}{|\lambda|} e^{-i\lambda(z-\bar{z})} = -2i \frac{\partial}{\partial z} \log|z-\bar{z}| = -\frac{2i}{z-\bar{z}} \quad \text{both for } z>\bar{z} \text{ and } z<\bar{z} . \quad (23)$$

In conclusion,

$$\lim_{z \to \bar{z}} \int_c \frac{d\bar{k} \, e^{-i\bar{k}(z-\bar{z})}}{\bar{k} + \frac{\omega}{U} \frac{1}{\beta^2}} \gamma^2 H_\nu'(\gamma a) J_\nu'(\gamma a) = \frac{2\beta}{\pi a} \cdot \frac{1}{z-\bar{z}} \qquad . \qquad (24)$$

A.2 Physical Interpretation of the Lifting Kernel $K_\nu^{l,l}$, and the Unification of Aerodynamics and Diffraction Theory (U=0) for Thin-Walled Shapes of Revolution

The analysis in Eqs. 21-24 has determined the character of the lifting kernel as the source and control points approach each other. Its $(z-\bar{z})^{-1}$ Cauchy-Principal local dependence is fundamentally different from that of the associated diffraction problem lacking a meanflow[4a,b]. The discussion will return to this, after Eq. 30b below.

This first term on the right side of Eq. 19b is neither a function of the cowl radius "a" nor of the circumferential mode ν. This nondependence is the result of the dipole ring appearing locally straight to fluid points close to it. It acts locally as if it were in an unbounded two-dimensional medium without length scales. The first term on the right side of Eq. 19b accordingly matches the familiar influence function for lift and induced upwash in two dimensions (see Ref. 14's Eq. 5-58, where the bound vorticity "$\gamma(x_1)$" becomes $-\Delta\bar{p}_\nu/\rho U$ in the present terminology due to Bernoulli's equation for the locally steady limit $\bar{z} \to z$).

13

This deduction of $K_v^{',}$'s local behavior is the first of several strong checks on the formulation. It came, as seen above, from the large-$\bar{k}$ form of the kernel's spectrum. The second check comes instead from the spectral behavior for finite $\bar{k}$, specifically from $\bar{k}$ in the vicinity of the three singularities in Fig. 2a.

First, to dispose of the role of the branch points, which is qualitatively the same as that in the familiar case of pure diffraction with U=0: Deforming contour C to the lower half $\bar{k}$ plane for $z>\bar{z}$ and wrapping it around the point $-(\omega/c)/\beta^2$ produces an acoustic ray that spreads spherically as $1/(z-\bar{z})$ for $z-\bar{z}\to+\infty$. Its phase is the issue. This is determined by the product of the exponential inside the transform evaluated at $\bar{k}=-(\omega/c)/\beta^2$ and the exponential term outside the transform on the first line of Eq. 17:

$$e^{-i\frac{\omega}{c}\frac{M}{\beta^2}(z-\bar{z})+i\frac{\omega}{c}\frac{1}{\beta^2}(z-\bar{z})-i\omega t} = e^{i\frac{\omega}{c(1+M)}[(z-\bar{z})-(c+U)t]} \qquad . \qquad (25)$$

For $z<\bar{z}$ a similar result springs from the neighborhood of the branch point at $+(\omega/c)/\beta^2$: A spatially spreading ray with phase factor $\exp\{-i[\omega/c(1-M)][(z-\bar{z})+(c-U)t]\}$.

These phase terms have included the $\exp(-i\omega t)$ temporal factor for the sake of clarity. The downstream wave in Eq. 25 "rides" the meanflow -- its speed relative to the cowl is $c+U$; whereas the wave traveling upstream must fight the current -- its speed relative to the cowl is $c-U$. Both rays display a correct spatial "Doppler" shift: The spatial variation of the shortened acoustic signal going upstream is that prescribed by the relatively high wavenumber $\omega/[c(1-M)]$, while that of the stretched-out downstream signal comes from $\omega/[c(1+M)]$.

Consider now the pole in the first term within brackets in Eq. 19b's second line. It has no effect upstream of the elemental lifting ring, $z<\bar{z}$. For $z>\bar{z}$, i.e., downstream of the ring, contour C picks up the pole upon dropping down to the lower half plane of Fig. 2a. The residue, by definition, does not decay with increasing distance $z-\bar{z}$ if ω is real (i.e., it does not spread, unlike the branch-points field). The part contributed by the exponential inside the integrand must be combined again with the exponential outside which appears on the first line of Eq. 17. The complete residue of Eq. 19b's second line is, times $\exp(-i\omega t)$

14

$$\underset{@\ \bar{k}=-\frac{\omega}{U}\frac{1}{\beta^2}}{Residue} = \left(\frac{a}{4\rho U}\right)\left(\frac{-2i}{\pi}\right)\left(\frac{\omega}{U}\right)^2 K'_v\left(\frac{\omega a}{U}\right) I'_v\left(\frac{\omega a}{U}\right) e^{i\frac{\omega}{c}\left[\frac{1}{M}\frac{1}{\beta^2}-\frac{M}{\beta^2}\right](z-\bar{z})-i\omega t} . \quad (26a)$$

The above phase factor is

$$e^{i\frac{\omega}{c}\left[\frac{1}{M}\frac{1}{1-M^2}-\frac{M}{1-M^2}\right](z-\bar{z})-i\omega t} = e^{i\frac{\omega}{U}[(z-\bar{z})-Ut]} , \quad (26b)$$

so that Eq. 26a describes a convected, nondecaying velocity pattern that exists only along the z>z̄ half of the infinite fluid shell defined by r=a, −∞<z<∞: <u>The anticipated shed/trailed wake of the elemental lifting ring</u>. The residue in Eq. 26a is not a function of Mach number M, which is as should be because the speed of sound is irrelevant in the still-fluid frame of reference of the shed/trailed vortex system.

It is important to admit now that this argument regarding the interpretation of the correctness of the lifting ring's free vortex flows has really been only qualitative. That is because the lifting problem makes no a priori physical demands on the induced normal upwash $\tilde{w}_v{}'$ other than continuity across r=a, which the construction has satisfied trivially. There is no independent gauge on Eq. 19a's left side. The wake check in Eqs. 26a,b is therefore not as persuasive as it could be.

What is needed is a frontal attack on the component of induced velocity "$\tilde{u}$" in the direction of the cowl's z axis. That analysis would be definitive because it would relate unambiguously the shed vorticity field $\Delta\tilde{u}$ to the oscillatory force that causes it, i.e., to $\Delta\bar{p}_v(\bar{z})ad\bar{z}$ on the right side of the equation. The expected identity is a well known variant of Kelvin's theorem of vorticity conservation: The ring-shaped vortices shed, shown at the bottom right corner of Fig. 1b, must cancel the temporal change in bound strength associated with $\Delta\bar{p}_v(\bar{z})ad\bar{z}.\exp(-i\omega t)$.

This calculation will be a digression because once checked, the shed vortices need never again be referred to. The lifting-surface theory, Eq. 19a, contains all of their induction effects implicitly. The first step is to invoke the z-momentum version of Eq. 13 in order to compute the lifting ring's $\bar{u}_{r,v}^{\ell}$ perturbation velocity component in line with freestream U:

15

$$\tilde{u}^l_{r,\nu}(a^\pm, z) = -\frac{e^{i\frac{\omega}{U}z}}{\rho U} \int_{-\infty}^{z} dz^* \frac{\partial \tilde{p}^l_{r,\nu}}{\partial z^*}(r=a^\pm, z^*) e^{-i\frac{\omega}{U}z^*} \qquad . \qquad (26c)$$

From Eqs. 10-12, this field is

$$\tilde{u}^l_{r,\nu}(a^\pm, z) = \left(-\frac{ia}{4\rho U}\right) [\Delta\tilde{p}_\nu(\bar{z}) d\bar{z}] \; e^{-i\frac{\omega}{c}\frac{M}{\beta^2}(z-\bar{z})}$$

$$\cdot \int_C d\bar{k} \, e^{-i\bar{k}(z-\bar{z})} \left[\frac{\bar{k}+\frac{\omega}{c}\frac{M}{\beta^2}}{\bar{k}+\frac{\omega}{U}\frac{1}{\beta^2}}\right] \gamma \left\{ \begin{matrix} H_\nu(\gamma a^+) \, J'_\nu(\gamma a) \\ H'_\nu(\gamma a) \, J_\nu(\gamma a^-) \end{matrix} \right\} \qquad . \qquad (26d)$$

The term within large curly brackets that appears last in the integrand contains, in its upper line, the Bessel function product of the $r=a^+$ solution. The lower line contains the $r=a^-$ part corresponding to the lower of the two signs in the "$a^\pm$" argument of the equation's left side. It follows that the strength of clockwise vorticity at a freefield axial position z is

$$\tilde{u}^l_{r,\nu}(a^+, z) - \tilde{u}^l_{r,\nu}(a^-, z) \equiv \Delta\tilde{u}^l_{r,\nu}(a, z)$$

$$= \left(-\frac{ia}{4\rho U}\right) [\Delta\tilde{p}_\nu(\bar{z}) d\bar{z}] \; e^{-i\frac{\omega}{c}\frac{M}{\beta^2}(z-\bar{z})}$$

$$\cdot \int_C d\bar{k} \, e^{-i\bar{k}(z-\bar{z})} \left[\frac{\bar{k}+\frac{\omega}{c}\frac{M}{\beta^2}}{\bar{k}+\frac{\omega}{U}\frac{1}{\beta^2}}\right] \gamma \left\{ H_\nu(\gamma a) \, J'_\nu(\gamma a) - H'_\nu(\gamma a) \, J_\nu(\gamma a) \right\}. \qquad (26e)$$

Contour C in Fig. 2a threads out a spectrum for Eq. 26e that seems to be still singular at the branch-point zeros of the radial wavenumber γ. This must only be apparent, however, since otherwise the solution would produce vortical signals not only downstream of the lifting ring but also ahead of it. The expected removal of γ comes about from the Wronskian relationship $H_\nu(\gamma a) J_\nu'(\gamma a) - H_\nu'(\gamma a) J_\nu(\gamma a) = -2i/\pi\gamma a$, which gives

16

$$\Delta \tilde{u}_{r,v}^{\prime}(a,z) = -\frac{[\Delta \tilde{p}_v(\bar{z})\,d\bar{z}]}{2\pi \rho U}\, e^{-i\frac{\omega}{c}\frac{M}{\beta^2}(z-\bar{z})} \int_C d\bar{k} \left[\frac{\bar{k}+\frac{\omega}{c}\frac{M}{\beta^2}}{\bar{k}+\frac{\omega}{U}\frac{1}{\beta^2}}\right] e^{-i\bar{k}(z-\bar{z})} \qquad . \quad (26f)$$

It follows from the empty upper half $\bar{k}$ plane which now results from Fig. 2a without branch cuts that the vorticity is exactly zero for $z<\bar{z}$ on $r=a$, while downstream of the elemental lifting ring it is

$$\Delta \tilde{u}_{r,v}^{\prime}(a,z)\, e^{-i\omega t} = -\frac{i\omega}{\rho U^2}\,[\Delta \tilde{p}_v(\bar{z})\,d\bar{z}]\, e^{i\frac{\omega}{U}[(z-\bar{z})-Ut]} \implies$$

$$\Delta u_{r,v}^{\prime}(a,z,t) = -\frac{1}{\rho U^2}\frac{dL_v}{dt}\left(z=\bar{z};\ t-\frac{z-\bar{z}}{U}\right)$$

$$= -\frac{1}{U}\frac{d\Gamma_v}{dt}\left(z=\bar{z};\ t-\frac{z-\bar{z}}{U}\right) \qquad . \qquad (26g)$$

The constant $-i\omega$ on the first line of Eq. 26g's right side is equivalent to the time derivative d/dt. The second line has removed the tilde from the dependent variable on either side and has thereby returned each to its time domain. The new equality has also identified $L_v=-\Delta p_v d\bar{z}\equiv[p_v^- - p_v^+]d\bar{z}$ as the sectional lift acting on the elemental ring wing's chord $d\bar{z}$.

The first argument of dL_v/dt accounts for the source position $z=\bar{z}$ on which the strength $\Delta p_v(\bar{z},t)$ obviously depends. The second, $t-(z-\bar{z})/U$, is the wake's retarded time. The third line has invoked the difference in the locally steady version of Bernoulli's equation between upper and lower ring surfaces: From Eq. 26c with $\omega=0$, one obtains $\Delta p_v=-\rho U\Delta u_{r,v}^\ell$, which upon multiplication by $d\bar{z}$ gives $L_v=\rho U\Gamma_v$ ($\Gamma_v = \Delta u_{r,v}^\ell d\bar{z}$). This, in turn, connects sectional lift L_v to the standard definition of the clockwise circulation Γ_v and casts the result in one of its more recognizable canonical forms; e.g., Ref. 14's Eq. 13.27. The lifting theory in Eqs. 19a,b above is correct.

There have been previous appearances of Eq. 19b's dramatic pole. In Ref. 4c the author applied the Wiener-Hopf technique to solve the problem of gust/airfoil interaction at high frequencies and speeds. This mathematical method is fundamentally a spectral one. Its application produced then a spectrum for the velocity

17

potential that already contained the pole in question: see Eq. 12 and Fig. 2 of Ref. 4c, which used exp(+iωt) instead of exp(-iωt).

This earlier solution, however, masked the _wake_ role of the pole for two reasons. First, it addressed the problem of an airfoil whose chord was semi-infinite, i.e., an airfoil with no trailing edge and therefore no wake. Secondly, the dependent variable was the velocity potential. And the discontinuity in velocity potential across the far wake of a finite-chord airfoil bearing a noncompact airload is known to be precisely the same as that across the semi-infinite chord of a leading-edge airfoil (cf. Howe's spatial-domain analysis[15]).

The interpretation of the pole's wake role came after Eq. A.17 of Ref. 4d. That later work noted that the shed wake produced from arbitrarily cutting off the leading-edge solution kept canceling the gust's downwash along the newly created "wake points": I.e., the flow past this trailing edge, in spite of having the strange ability to cancel the input downwash there, was, nonetheless, a wake. It followed that the spectrum's pole, whose original mission had been to account for true flow tangency in the semi-infinite airfoil, was just as much a _wake_ pole. Ref. 4d made this connection obliquely immediately before its Eq. A8 and chose instead to pursue a wake analysis in the spatial domain through a number of equivalent manipulations on the Possio kernel.

The wake pole, incidentally, arises regardless of the direction of the lifting element. Here this direction has been radial because the cowl's surface is normal to r. But the incident-field model discussed below in section E analyzes instead a continuum of axial thrust dipoles prescribed over a set of propeller blades. And the wake pole shows up still: see Eq. 57b, where the pole's position, $-\omega/U\beta^2$, has turned into the nondimensional wavenumber $-mB\Omega L/2U\beta^2$.

Amiet[3b] has recently performed a thorough analysis of airfoil-shed vorticity in the spatial domain. That study includes the case of a gust straggling behind the freestream that otherwise would convect it.

The Steady Aerodynamics Limit: A Three-Dimensional Benchmark Check, and a Specialized Theory for Future Applications

The analysis of the shed vorticity has taken a sideways look at the process of wake generation on the r,z plane of Fig. 1b.

The final conclusions in Eq. 26g certainly seem to give kernel $K_v^{i,i}$ its needed seal of approval, and yet, they really say nothing about the three-dimensional character of the shed/trailed vortex system.

The check for the three-dimensionality of $K_v^{i,i}$ comes from the steady-aerodynamics limit $\omega \to 0$. The shed vortex system disappears then and the remaining trailing vortices isolate the elemental ring wing's Trefftz flow. These straight vortices must then obey Kelvin's theorem of unchanging strength with distance z down the wake, as suggested in Fig. 1b's bottom right edge.

This invariance with z is immediately apparent from the fact that the exponential in Eqs. 26a,b turns into 1 for $\omega = 0$. But one notes also that the product of modified Bessel functions in the algebraic part of the calculated residue becomes then (Ref. 16)

$$\lim_{\omega \to 0} K_v'\left(\frac{\omega a}{U}\right) I_v'\left(\frac{\omega a}{U}\right) = \begin{cases} const. & for\ v = 0 \\ (\omega/U)^{-2} \cdot (-v/2 a^2) & for\ v \neq 0 \end{cases} \qquad (27a)$$

It follows that in Eq. 26a,

$$\lim_{\omega \to 0} \left(\frac{\omega}{U}\right)^2 K_v'\left(\frac{\omega a}{U}\right) I_v'\left(\frac{\omega a}{U}\right) = \begin{cases} 0 & for\ v = 0 \\ -v/2a^2 & for\ v \neq 0 \end{cases} \qquad (27b)$$

The first line on Eq. 27b's right side states that when the ring's steady loading pattern is uniform in the ring's circumferential (spanwise) direction, i.e., when the circumferential mode v is zero, the trailed vortex system disappears too.

This is again as should be, because each trailed vortex filament is the result of a differential change in bound vortex strength along ϕ. I.e., the purpose of each trailed filament is to avoid a violation of Kelvin's theorem along ϕ by the bound circulation. The trailed vortex system becomes superfluous (zero) when the lifting ring's loading distribution is circumferentially uniform: when v=0, or more precisely, when $\Delta \bar{p}_v = 0$ for $v \neq 0$.

The second line on the right side of Eq. 27b declares that when this loading is circumferentially nonuniform the trailed

19

vortex system is born naturally out of the product of the constant $-\nu/2a^2$ and $\Delta\bar{p}_\nu$. This extra factor of ν times $-i$ acts as a derivative with respect to ϕ on $\Delta\bar{p}(\bar{z},\phi)$, so that it is this derivative which then determines the circumferential pattern of vorticity in the ring's Trefftz, or wake plane.

Eq. 27b has demonstrated that the lifting-surface theory in Eqs. 19a,b for a ring wing in unsteady subsonic flow collapses, in the limit $\omega \to 0$, to a steady lifting-surface formulation with a system of trailing vortices that is consistent with the spanwise variation of the loading imposed. Fig. 2b shows the spectral structure of steady aerodynamics: All three of its fundamental singularities converge upon the $\bar{k}=0$ origin.

Thinking in reverse, this picture pries apart the three invisible and confluent singular points of the steady case and thereby provides a simple generalization to unsteady flows. Fig. 2b represents an analytically compact and liberating alternative to the usual construction in the spatial domain relying on horseshoe vortices (see Ref. 14's Eq. 5-35 and then Eq. 7-32).

This steady-limit form of the development could address steady inflow conditions that are clearly already covered by the present model but that are beyond the scope of the current study. E.g., the steady limit could generate the potential interference flow field produced by the cowl over the internal fan stage when the whole system is at a static angle of attack. This "potential-flow shadow" cast by the tilted cowl's inlet on part of the propeller station would cause the blades rotating there to feel an additional spatial nonuniformity. The new nonuniformity in turn becomes an additional cause of unsteady blade forces and therefore of aerodynamically generated sound.

The canonical interpretation of this theoretically predictable steady interference field is that of a small perturbation on the incident freestream. However, it obviously could be of the first order of importance as a source of propeller noise.

Yet another Benchmark Check: Unification With the Theory of Pure Diffraction

Fig. 2a, by means of Fig. 2b, has already unified steady and unsteady subsonic aerodynamics for ring wings. The purpose of this section is to show how this picture also contains standard diffraction theory for thin shapes of revolution in the zero

20

freestream limit U→0. The resulting new picture, Fig. 2c, will end up linking quantitatively the apparently disconnected disciplines of steady aerodynamics for ring wings and acoustic diffraction theory for "free-flooded" cylindrical scatterers.

Before writing down the U→0 limit of Eqs. 19a,b, it is well to state beforehand what one expects of the resulting diffraction theory.

(1) First of all, a diffracting thin shape of finite size does not shed or trail vorticity when its bound vortices do not buck a mean flow [in terms of linear variables at least]. The shed and trailed vortex systems found above must somehow go away for U→0.

(2) Secondly, the shape's diffracted field, which includes the pattern of self-induced normal flows (Eqs. 19a,b), must be acoustically reciprocal: Any pair of source and receiver points must be interchangeable in the basic influence function.

(3) And third, the resulting kernel should be "hypersingular", i.e., of the Mangler type, because the mutual local influence of a source and receiver pair of points is the same for pure acoustic diffraction as for the spanwise problem of classical aerodynamics: The perturbed cross velocities of an unswept flat wing in subsonic flow by definition do not see a freestream either, and therefore may be regarded as the result of pure "Trefftz diffraction".

Passing the U^{-1} factor in the coefficient of Eq. 19b's second line on to its two integrand terms within large square brackets gives

$$K_v^{l,l}(z-\overline{z}) = \frac{\beta}{2\pi\rho U} \cdot \frac{e^{-i\frac{\omega}{c}\frac{M}{\beta^2}(z-\overline{z})}}{z-\overline{z}}$$

$$+ \frac{a e^{-i\frac{\omega}{c}\frac{M}{\beta^2}(z-\overline{z})}}{4\rho} \int_C d\overline{k} e^{-i\overline{k}(z-\overline{z})} \left[\frac{\gamma^2 H_v'(\gamma a) J_v'(\gamma a)}{\overline{k} U + \frac{\omega}{\beta^2}} - \frac{i\beta}{\pi a U} \frac{|\overline{k}|}{\overline{k}} \right] . (28a)$$

For U→0 the first term on the right side and the second integrand term within brackets dominate Eq. 28a as they grow indefinitely. However, they cancel by construction (recall Eq. 23). Moreover, the wake pole term turns into a multiplicative

21

constant for U=0 and so drops entirely out of the problem, thereby fulfilling expectation #1 immediately. The result of the U→0 limit is thus

$$K_v^{l,l}(z-\overline{z}) \Big|_{U\to 0} = \frac{a}{4\rho\omega} \int_C d\overline{K} e^{-i\overline{K}(z-\overline{z})} \gamma^2 H_v'(\gamma a) J_v'(\gamma a) \qquad . \qquad (28b)$$

In Eq. 28b the radial wavenumber γ now comes from Eq. 8 with $\beta=1$ (i.e., U=0 → M=0 for a finite sound speed c). The zeros of Eq. 8 are then the familiar branch points of diffraction analysis: they are at ± the acoustic wavenumber ω/c (cf., for example, Noble's[17] Fig. 1.1). Fig. 2c here shows the movements for U→0 of the three basic singularities from Fig. 2a as deduced from these demands of pure diffraction.

From Eqs. 20 and 21 with $\beta=1$ it follows that

$$\lim_{z\to\overline{z}} \int_C d\overline{K} e^{-i\overline{K}(z-\overline{z})} \gamma^2 H_v'(\gamma a) J_v'(\gamma a) = \frac{i}{\pi a} \int_{-\infty}^{\infty} d\overline{K} |\overline{K}| e^{-i\overline{K}(z-\overline{z})} , \qquad (29a)$$

while i times the z derivative of Eq. 23 yields that

$$i \frac{\partial}{\partial z} \int_{-\infty}^{\infty} d\lambda \frac{\lambda}{|\lambda|} e^{-i\lambda(z-\overline{z})} = \int_{-\infty}^{\infty} d\lambda |\lambda| e^{-i\lambda(z-\overline{z})} = i \frac{\partial}{\partial z} \left[-\frac{2i}{z-\overline{z}} \right] = -\frac{2}{(z-\overline{z})^2} . \qquad (29b)$$

Incorporating Eqs. 29a,b and 30 in Eq. 28b finally gives

$$K_v^{l,l}(z-\overline{z}) \Big|_{U\to 0} = -\frac{i}{2\pi\rho\omega} \frac{1}{(z-\overline{z})^2}$$

$$-\frac{i}{\rho\omega} \int_C d\overline{K} e^{-i\overline{K}(z-\overline{z})} \left[\frac{i\gamma^2 a}{4} H_v'(\gamma a) J_v'(\gamma a) + \frac{|\overline{K}|}{4\pi} \right] , \qquad (30a)$$

and so,

22

$$U \to 0 : \qquad \tilde{w}_v{}'(z) = \oint_{-L/2}^{L/2} d\bar{z}\, K_v{}^{l,l}(z-\bar{z})\, \Delta \tilde{p}_v(\bar{z}) \qquad . \qquad (30b)$$

The $\tilde{K}$ spectrum in Eq. 30a's second line is even in the running wavenumber $\tilde{K}$. Its transform is even in $(z-\bar{z})$ because the $\exp[-i\tilde{K}(z-\bar{z})]$ factor becomes $\cos[-i\tilde{K}(z-\bar{z})]$, which is even in $z-\bar{z}$. And this evenness translates into the reciprocity hoped for in item #2 above.

The first term on the right side of Eq. 30a displays the expected Mangler behavior and so confirms requirement #3. The second line of Eq. 30a is integrable for $\bar{z} \to z$ in the usual sense. Note that the analysis that gave Eq. 30a has actually cut out the delicate limiting process $(r \to a^+)$ that contributes the infinite negative trough "$-2/\epsilon$" that cancels the two positive infinities of the $(z-\bar{z})^{-2}$ term that appears on the first term on the equation's right side. Eqs. 24-28 of Ref. 4a contain these missing steps which justify the finite-part "X" Mangler sign in Eq. 30b.

The relative constant $-i/\rho\omega$, between the result in Eq. 30a above and that in Ref. 4a's Eq. 29, accounts for the fact that the left side of Eq. 19a is a velocity while that of Ref. 4a's Eq. 29 is a pressure gradient. And $-i/\rho\omega$ is their constant of proportionality in the r momentum equation when $U=0$: $(-i/\rho\omega)\partial \bar{p}_v{}'/\partial r = \bar{w}_v{}'$.

B The Dynamic "Thickness" Problem due to the Compliant Dissipative Liner

Eq. 19a, along with 19b, provides the lifting component $\bar{w}_v{}'$ of the total virtual flow induced by the cowl across its own two-sided surface. The cowl's liner over part or all of the inner surface contributes a similar but "nonlifting" component $\bar{w}_v{}^{th}$ that must be added to that of Eq. 19a to complete the virtual flow picture for the boundary-value problem. The sum $\bar{w}_v{}' + \bar{w}_v{}^{th}$, for example, will be called upon to cancel the incident fluid particle velocities along the duct's rigid outer surface at $r=a^+$, and will thereby generate one of the problem's two coupled integral equations. The formulation will be valid whether the liner is passively compliant or actively pulsating, or a combination of the two.

The construction of the nonlifting flow $\bar{w}_v{}^{th}$ will begin again

23

with its associated pressure, this time given by the first term
in the integrand of the Helmholtz integral equation: Eq. 1 above.
This term implies the following solution for the elemental
influence of a small patch of cowl surface $ad\bar{\phi}.d\bar{z}$ (hence the "e"
subscript, the same as before for the lifting problem):

$$\tilde{p}_e^{th}(r,\phi,z) = \left(-\frac{i}{8\pi}\right)\left[\Delta\left(\frac{\partial\tilde{p}}{\partial\bar{r}}(\bar{r}=a,\bar{\phi},\bar{z})\right)ad\bar{\phi}d\bar{z}\right]e^{-i\frac{\omega}{c}\frac{M}{\beta^2}(z-\bar{z})}$$

$$\cdot\sum_{\nu=-\infty}^{\infty}e^{-i\nu(\phi-\bar{\phi})}\int_C d\bar{K}\,e^{-i\bar{K}(z-\bar{z})}\begin{cases}H_\nu(\gamma r)\,J_\nu(\gamma a) & \text{for } r>a \\ H_\nu(\gamma a)\,J_\nu(\gamma r) & \text{for } r<a\end{cases} \qquad (31)$$

The difference in the signs of the $\pm i/8\pi$ coefficients of Eqs. 31
and 10 reflects the basic sign difference of the two parts of the
integrand of Eq. 1 (see Eq. 61 of Ref. 4a).

The indicated jump in radial pressure gradient in the
"strength" coefficient of Eq. 31 is

$$\Delta\left(\frac{\partial\tilde{p}}{\partial\bar{r}}(\bar{r}=a,\bar{\phi},\bar{z})\right) \equiv \left(\frac{\partial\tilde{p}}{\partial\bar{r}}(\bar{r}=a,\bar{\phi},\bar{z})\right)^+ - \left(\frac{\partial\tilde{p}}{\partial\bar{r}}(\bar{r}=a,\bar{\phi},\bar{z})\right)^-$$

$$\equiv \frac{\partial\tilde{p}}{\partial\bar{r}}(\bar{r}=a^+,\bar{\phi},\bar{z}) - \frac{\partial\tilde{p}}{\partial\bar{r}}(\bar{r}=a^-,\bar{\phi},\bar{z}) \qquad . \qquad (32)$$

The first task is to convert the above relationship into one
for the jump in the fluid particle velocity across the
temporarily invisible two-side surface of the cowl. The radial
momentum equation in barred source variables is

$$\Delta\left(\frac{\partial\tilde{p}}{\partial\bar{r}}(\bar{\phi},\bar{z})\right) = -\rho\left[-i\omega + U\frac{\partial}{\partial\bar{z}}\right]\Delta\tilde{w}(\bar{\phi},\bar{z}) \qquad . \qquad (33)$$

And so, Eq. 31 now reads

24

$$\tilde{p}_e^{th}(r,\phi,z) = \frac{i\rho a\, d\overline{\phi}\, d\overline{z}}{8\pi}\; e^{-i\frac{\omega}{c}\frac{M}{\beta^2}(z-\overline{z})}$$

$$\cdot \sum_{\nu=-\infty}^{\infty} e^{-i\nu(\phi-\overline{\phi})}\int_C d\overline{k}\, e^{-i\overline{k}(z-\overline{z})} \begin{Bmatrix} H_\nu(\gamma r)\, J_\nu(\gamma a)\,;\; r>a \\ H_\nu(\gamma a)\, J_\nu(\gamma r)\,;\; r<a \end{Bmatrix} \left[-i\omega + U\frac{\partial}{\partial\overline{z}}\right]\Delta\tilde{w}(\overline{\phi},\overline{z})\,. \quad (34)$$

Eq. 33 has suppressed the $\overline{r}=a$ argument of the dependent variable on either side of the equation for the sake again of a simpler notation.

The nonlifting velocity field associated with the pressure in Eq. 34 results from application of the integral operator in Eq. 13. That operator produces again the $\overline{k}+(\omega/U)/\beta^2$ wake pole that appeared in the $\overline{k}$ spectrum on the right side of Eq. 17:

$$\tilde{w}_e^{th}(r,\phi,z) = \frac{a\, d\overline{\phi}\, d\overline{z}}{8\pi}\; e^{-i\frac{\omega}{c}\frac{M}{\beta^2}(z-\overline{z})}$$

$$\cdot \sum_{\nu=-\infty}^{\infty} e^{-i\nu(\phi-\overline{\phi})}\int_C \frac{d\overline{k}\, e^{-i\overline{k}(z-\overline{z})}}{\overline{k}+\dfrac{\omega}{U}\dfrac{1}{\beta^2}}\, \gamma \begin{Bmatrix} H_\nu'(\gamma r_{>a})\, J_\nu(\gamma a) \\ H_\nu(\gamma a)\, J_\nu'(\gamma r_{<a}) \end{Bmatrix} \left[-i\frac{\omega}{U} + \frac{\partial}{\partial\overline{z}}\right]\Delta\tilde{w}(\overline{\phi},\overline{z})\,. \quad (35)$$

The situation regarding the singularities of the spectrum in Eq. 35 is precisely the opposite of that faced earlier in Eq. 26e. The challenge there was to justify the removal of the branch points while keeping the wake pole untouched. The Wronskian for Bessel functions performed that task perfectly. Here the pole must somehow go away and the branch points alone must stay, because it would be nonsensical for the nonlifting problem to shed or trail vorticity.

The thickness flow $\tilde{w}^{th}(r,\phi,z)$ generated by the whole surface results from integrating over $d\overline{\phi}\cdot d\overline{z}$. This operation eventually leads to the same natural definition of the circumferential-mode versions of the dependent variables in Eq. 35. E.g., it leads to the definition of $\tilde{w}_\nu^{th}(r,z)$ for the left side of the equation as a function of r and z only. The surface integration produces

25

$$\tilde{w}^{th}(r,\phi,z) = \frac{a}{8\pi} e^{-i\frac{\omega}{c}\frac{M}{\beta^2}z} \int_0^{2\pi} d\bar{\phi} \sum_{v=-\infty}^{\infty} e^{-iv(\phi-\bar{\phi})} \int_c \frac{d\bar{K}\,e^{-i\bar{K}z}}{\bar{K}+\frac{\omega}{U}\frac{1}{\beta^2}} \gamma \begin{Bmatrix} H_v'(\gamma\,r_{>a})\,J_v(\gamma a) \\ H_v(\gamma a)\,J_v'(\gamma\,r_{<a}) \end{Bmatrix}$$

$$\cdot \int_{-L/2}^{L/2} d\bar{z}\,e^{i\left(\bar{K}+\frac{\omega}{c}\frac{M}{\beta^2}\right)\bar{z}} \left[-i\frac{\omega}{U}+\frac{\partial}{\partial\bar{z}}\right]\Delta\tilde{w}(\bar{\phi},\bar{z}) \qquad . \qquad (36)$$

Further analytical treatment of the $\bar{z}$ integral on the second line of Eq. 36 now proceeds on a v-modal basis. First there is the split of this $\bar{z}$ integral into its two added terms,

$$\int_{-L/2}^{L/2} d\bar{z}\,e^{i\left(\bar{K}+\frac{\omega}{c}\frac{M}{\beta^2}\right)\bar{z}}\left[-i\frac{\omega}{U}+\frac{\partial}{\partial\bar{z}}\right]\Delta\tilde{w}_v(\bar{z}) = -i\frac{\omega}{U}\int_{-L/2}^{L/2}d\bar{z}\,e^{i\left(\bar{K}+\frac{\omega}{c}\frac{M}{\beta^2}\right)\bar{z}}\Delta\tilde{w}_v(\bar{z})$$

$$+\int_{-L/2}^{L/2}d\bar{z}\,e^{i\left(\bar{K}+\frac{\omega}{c}\frac{M}{\beta^2}\right)\bar{z}}\frac{\partial}{\partial\bar{z}}\Delta\tilde{w}_v(\bar{z}) \quad , \quad (37)$$

followed by the integration of the second one by parts:

$$\int_{-L/2-\epsilon}^{L/2+\epsilon}d\bar{z}\,e^{i\left(\bar{K}+\frac{\omega}{c}\frac{M}{\beta^2}\right)\bar{z}}\frac{\partial}{\partial\bar{z}}\Delta\tilde{w}_v(\bar{z}) = -i\left(\bar{K}+\frac{\omega}{c}\frac{M}{\beta^2}\right)\int_{-L/2}^{L/2}d\bar{z}\,e^{i\left(\bar{K}+\frac{\omega}{c}\frac{M}{\beta^2}\right)\bar{z}}\Delta\tilde{w}_v(\bar{z}) \quad . \quad (38)$$

The temporary "ϵ" parameter in the integration limits of Eq. 38's left side ensures that the integration's end points are just beyond the spatial extent of the liner. Parameter ϵ is obviously analytically unnecessary if the liner treatment does not extend all the way to $\bar{z}=-L/2$ and to $\bar{z}=+L/2$.

Adding now the right side of Eq. 38 to the first term on the right side of Eq. 37 results in the following simplification for the constant inside the coefficient of the resulting integral:

$$\frac{\omega}{U}+\frac{\omega}{c}\frac{M}{\beta^2} = \frac{\omega}{U}\frac{1}{\beta^2} \qquad . \qquad (39)$$

And so, finally,

$$\int\limits_{-L/2}^{L/2} d\bar{z} \, e^{i\left(\bar{k} + \frac{\omega}{c}\frac{M}{\beta^2}\right)\bar{z}} \left[-i\frac{\omega}{U} + \frac{\partial}{\partial\bar{z}}\right] \Delta \tilde{w}_\nu(\bar{z})$$

$$= -i\left(\bar{k} + \frac{\omega}{U}\frac{1}{\beta^2}\right) \int\limits_{-L/2}^{L/2} d\bar{z} \, e^{i\left(\bar{k} + \frac{\omega}{c}\frac{M}{\beta^2}\right)\bar{z}} \Delta \tilde{w}_\nu(\bar{z}) \quad . \quad (40)$$

The multiplicative factor on the right side of Eq. 40 removes the wake pole in the spectrum of Eq. 36, as expected for this nonlifting problem: The thickness solution neither sheds nor trails. Eq. 40 in Eq. 36 gives

$$\tilde{w}_\nu^{th}(r, z) = -i\frac{a}{4} \int\limits_{-L/2}^{L/2} d\bar{z} \, \Delta \tilde{w}_\nu(\bar{z}) \, e^{-i\frac{\omega}{c}\frac{M}{\beta^2}(z-\bar{z})}$$

$$\cdot \int\limits_C d\bar{k} \, e^{-i\bar{k}(z-\bar{z})} \gamma \begin{cases} H_\nu'(\gamma r) \, J_\nu(\gamma a) \; ; \; r > a \\ H_\nu(\gamma a) \, J_\nu'(\gamma r) \; ; \; r < a \end{cases} \quad . \quad (41)$$

The last step in the development is to isolate the self behavior, i.e., the behavior as $\bar{z} \to z$ and $r \to a^\pm$ of the influence function contained in Eq. 41. The procedure is similar to that employed in Eqs. 20-24 above for the lifting kernel. The corresponding analysis for the integrand in Eq. 41 yields that

$$\lim_{\bar{k} \to \infty} \gamma \begin{cases} H_\nu'(\gamma a^+) \, J_\nu(\gamma a) \\ H_\nu(\gamma a) \, J_\nu'(\gamma a^-) \end{cases} = \pm \frac{i}{\pi a} \quad , \quad (42)$$

where the "+" sign on the right side stands for $r = a^+$ and the "−" for $r = a^-$. It follows that the $\bar{k}$ transform integral in Eq. 41 becomes, as the control and running source points approach each other on $r \to a^+$,

27

$$\int_C dK\, e^{-iK(z-\bar{z})}\, \gamma\, H'_\nu(\gamma a^+)\, J_\nu(\gamma a) = \frac{2i}{a}\, \delta(z-\bar{z})$$

$$+ \int_C dK\, e^{-iK(z-\bar{z})} \left[\gamma\, H'_\nu(\gamma a)\, J_\nu(\gamma a) - \frac{i}{\pi a} \right]. \quad (43)$$

Substitution of Eq. 43 turns the r>a part of Eq. 41 into

$$\tilde{w}_\nu^{th}(r=a^+, z) = \frac{\Delta \tilde{w}_\nu(z)}{2} + \int_{-L/2}^{L/2} d\bar{z}\, \Delta \tilde{w}_\nu(\bar{z})\, e^{-i\frac{\omega}{c}\frac{M}{\beta^2}(z-\bar{z})}$$

$$\cdot \int_C dK\, e^{-iK(z-\bar{z})} \left[-i\frac{\gamma a}{4} H'_\nu(\gamma a)\, J_\nu(\gamma a) - \frac{1}{4\pi} \right], \quad (44a)$$

while for r=a⁻,

$$\tilde{w}_\nu^{th}(r=a^-, z) = -\frac{\Delta \tilde{w}_\nu(z)}{2} + \int_{-L/2}^{L/2} d\bar{z}\, \Delta \tilde{w}_\nu(\bar{z})\, e^{-i\frac{\omega}{c}\frac{M}{\beta^2}(z-\bar{z})}$$

$$\cdot \int_C dK\, e^{-iK(z-\bar{z})} \left[-i\frac{\gamma a}{4} H_\nu(\gamma a)\, J'_\nu(\gamma a) + \frac{1}{4\pi} \right]$$

$$= -\frac{\Delta \tilde{w}_\nu(z)}{2} + \int_{-L/2}^{L/2} d\bar{z}\, \Delta \tilde{w}_\nu(\bar{z})\, e^{-i\frac{\omega}{c}\frac{M}{\beta^2}(z-\bar{z})}$$

$$\cdot \int_C dK\, e^{-iK(z-\bar{z})} \left[-i\frac{\gamma a}{4} H'_\nu(\gamma a)\, J_\nu(\gamma a) - \frac{1}{4\pi} \right]. \quad (44b)$$

The second equality in Eq. 44b has again invoked the Wronskian from the discussion following Eq. 26e, in its replacement of $-i(\gamma a/4)H_\nu J_\nu' + 1/4\pi$ with $-i(\gamma a/4)H_\nu' J_\nu - 1/4\pi$.

The first term on the right side of Eq. 44a is the special-case result of the general mathematical operation contained in the second term on the right side of Eq. 13a of Ref. 4e. A similar statement holds for the first term on the right of Eq. 44b and Ref. 4e's Eq. 13b. That operation here has been locally equivalent to "$\partial G/\partial r$", while in Ref. 4e it stood for $-\partial G/\partial \bar{r}$

28

because the dependent variable there was the pressure in the Helmholtz integral equation instead of the velocity used here. These two derivatives of G match as $\bar{r}$ approaches r because G then becomes a function of $|r-\bar{r}|$ (to see this, put $\phi=\bar{\phi}$ in the radical in the argument of $H_o^{(1)}$ in Eq. 9. That radical then turns into $|r-\bar{r}|$).

The second term on the right sides of Eqs. 44a and b are equal, as predicted by the match of the third term on right sides of Ref. 4e's Eqs. 13a and b. These terms contain the "remote", or nonplanar effects of Eqs. 44a,b and accordingly vanish as the radius "a" of the cowl approaches infinity.

The boundary condition along the cowl's lined surface on $r=a^-$ will invoke not only the above velocity, but also the pressure field associated with it. Its analysis follows a line very similar to that of the lifting velocity $\bar{w}_v^\ell$, described in detail above. The discussion will return to this unexpected similarity shortly.

The pressure generated by the nonlifting problem over $r=a^-$ turns out to be

$$\bar{p}_v^{th}(a^{\pm},z) = -\frac{\rho U}{2\pi\beta} \int\limits_{-L/2}^{L/2} d\bar{z} \frac{\Delta \tilde{w}_v(\bar{z})}{z-\bar{z}} e^{-i\frac{\omega}{c}\frac{M}{\beta^2}(z-\bar{z})}$$

$$+ \frac{\rho a U}{4} \int\limits_{-L/2}^{L/2} d\bar{z} \, \Delta \tilde{w}_v(\bar{z}) \, e^{-i\frac{\omega}{c}\frac{M}{\beta^2}(z-\bar{z})}$$

$$\cdot \int\limits_{C} d\bar{k} \, e^{-i\bar{k}(z-\bar{z})} \left[H_v(\gamma a) \, J_v(\gamma a) \left(\bar{k} + \frac{\omega}{U}\frac{1}{\beta^2} \right) + \frac{i}{\pi a\beta} \frac{|\bar{k}|}{\bar{k}} \right] . \quad (45)$$

This solution applies both for $r=a^-$ and $r=a^+$, true to the fact that it stands for a monopole distribution; note the argument $a^{\pm}$ on the left side of the equation.

The remaining dependent variable needed below to complete the statement of the boundary condition for the cowl's inner surface is the lifting component of the pressure field there. The development for $\bar{p}_v^\ell$ follows essentially the same steps as Eq. 44b:

$$\tilde{p}_v^l(a^-,z) = -\frac{\Delta\tilde{p}_v(z)}{2} - \int_{-L/2}^{L/2} d\bar{z}\,\Delta\tilde{p}_v(\bar{z})\,e^{-i\frac{\omega}{c}\frac{M}{\beta^2}(z-\bar{z})}$$

$$\cdot \int_C d\bar{K}\,e^{-i\bar{K}(z-\bar{z})}\left[-i\frac{\gamma a}{4}H_v'(\gamma a)\,J_v(\gamma a) - \frac{1}{4\pi}\right]\,. \quad (46)$$

The second term on the right side of Eq. 46 this time reflects the nonplanar character of the lifting surface and therefore vanishes for a→∞ (cf. comments immediately preceding Eq. 15 of Ref. 4e). All of the above results collapse to Ref. 4a's corresponding terms upon setting U=0, as they must.

Regarding now the similarity alluded to above, of $\bar{p}_v^{th}$ in Eq. 45 to $\tilde{w}_v^l$ in Eq. 19a, one notes that the match among the first terms on the right side of the two equations is tantamount to a statement of local reciprocity for two ratios of <u>dependent</u> variables that are apparently unrelated. The observation is worth making because it may be of practical value both to future experimental work and to the interpretation of old data. Eqs. 45 and 19a therefore state that

$$\lim_{z\to\bar{z}}\left(-\frac{\bar{p}_v^{th}(z)}{[\rho U/\beta]\,\Delta\tilde{w}_v(\bar{z})\,d\bar{z}}\right) = \left(\frac{[\rho U/\beta]\,\tilde{w}_v^l(z)}{\Delta p_v(\bar{z})\,d\bar{z}}\right) = \frac{1}{2\pi}\frac{e^{-i\frac{\omega}{c}\frac{M}{\beta^2}(z-\bar{z})}}{z-\bar{z}}\,. \quad (47)$$

Perhaps the most interesting feature of Eq. 47 is that its first equality does not hold for the case of pure diffraction, touted above for its <u>spatial</u> reciprocity z↔z̄ when U=0. Eq. 47 is true because the freestream U has the local (steady) effect of turning a generating element of thickness flow, $\Delta\tilde{w}_v$, into an axial ring doublet -- recall the $\partial/\partial\bar{z}$ derivative on the right side of Eq. 33. Figs. 3a,b summarize the mathematical and physical details behind Eq. 47.

The context of Eq. 47 vis-à-vis past work is, as far as the author knows, as follows. The effective conversion of a monopole source into an axial dipole is a well-known consequence of having a freestream U; see, for example, Amiet's comments at the top of Ref. 3a's p. 8. That conversion suggested here the possibility of the type of reciprocity displayed by Eq. 47, because the fore/aft oddness of the new "thickness dipole" is similar to that of the upwash of a bound vortex in the lifting problem. The multiplicative constant of proportionality remained to be worked out. Eq. 47 has established that this constant is simply -1, a

30

number checked independently and semi-graphically in Figs. 3a,b.

C The Coupled Pair of Singular Integral Equations

C.1 Statement of the Boundary Conditions for $r=a^-$, a^+, and Qualitative Sign Check amongst the Terms of the Lifting and Nonlifting Problems

The coupled integral equations that describe the fluid dynamics of the cowl as a diffractive/dissipative two-sided object result from the enforcement of boundary conditions on its inner and outer surfaces. These conditions, which apply over $-L/2 < z < L/2$, are

$$r = a^+ \quad : \quad -\tilde{w}_v^{inc} = \tilde{w}_v^l + \tilde{w}_v^{th} \quad , \tag{48a}$$

$$r = a^- \quad : \quad
\begin{cases}
Z_{liner}(z;\omega)\left[\tilde{w}_v^{inc} + \tilde{w}_v^l + \tilde{w}_v^{th}\right] = \tilde{p}_v^{inc} + \tilde{p}_v^l + \tilde{p}_v^{th} \quad , & (48b) \\
\\
-Z_{liner}(z;\omega)\,\Delta\tilde{w}_v(z) = \tilde{p}_v^{inc} + \tilde{p}_v^l + \tilde{p}_v^{th} \quad . & (48c)
\end{cases}$$

Eq. 48a states that the total fluid particle velocity normal to the cowl's outer rigid wall must vanish there (flow tangency). Symbol $\bar{w}_v^{inc}$ denotes the contribution of the incident field. Eqs. 48b and c, which are equivalent, introduce the axially and frequency-variable dynamics of the liner[‡] through its locally reacting impedance $Z_{liner}(z;\omega)$. Eq. 48c is considerably simpler to implement than Eq. 48b. It combines Eqs. 48a and b as follows:

Bringing $\bar{w}_v^{inc}$ to the right side of Eq. 48a, one first notes that the added subfield $\bar{w}_v^{inc} + \bar{w}_v^l$ is continuous across $r=a$ because its two constituents are individually continuous everywhere: for them the implied radial argument $r=a^+$ could just as well be $r=a^-$. Thus Eq. 48a also declares that $\bar{w}_v^{inc}(a^-) + \bar{w}_v^l(a^-) = -\bar{w}_v^{th}(a^+)$, which upon substitution in the left side of Eq. 48b generates the left side of Eq. 48c, because $\bar{w}_v^{th}(a^-,z) - \bar{w}_v^{th}(a^+,z) = \bar{w}_v^{total}(a^-,z) = \bar{w}_v^{total}(a^-,z) - \bar{w}_v^{total}(a^+,z) \equiv -\Delta\bar{w}_v(z)$, this last equality following from the definition of $\Delta\bar{w}_v$ in Eqs. 32 and 33. The quantity $\bar{w}_v^{total}(a^-,z) - \bar{w}_v^{total}(a^+,z)$ becomes $\bar{w}_v^- - \bar{w}_v^+$ for short in Fig. 4a, which summarizes part of the sign-check argument that now follows.

[‡]Eqs. 48b,c enforce continuity of normal velocity between the fluid and the liner-material particles. Nayfeh et al. (AIAA J., 13(2), 1975, pp. 130-153; see p. 135) have discussed the flow conditions under which these statements hold, and when they should be replaced with corresponding expressions for the continuity of particle displacement.

31

The first term on the right sides of each of Eqs. 44a and 46 has isolated the local delta-function behavior imparted by the respective kernel. The results are the terms $\Delta \bar{w}_v(z)/2$ and $-\Delta \bar{p}_v(z)/2$ lying outside the $\bar{z}$ integrations. These separated terms are useful for checking the relative signs of the several parts of Eqs. 48a and c, and for interpreting these parts physically.

Eq. 48a strikes a balance between $-\bar{w}_v^{inc}$ and $\Delta \bar{w}_v/2 + \ldots$ and so implies that $-\bar{w}_v^{inc} - (\bar{w}_v^+ - \bar{w}_v^-)/2 = \ldots$ The effective thickness velocity $-\bar{w}_v^+$ is thus in line with that of the incident field, which is as should be (Fig. 4a). Quantity $\bar{w}_v^-$ subtracts from that sum [$\bar{w}_v^+$ is zero in the present study because the cowl's outer surface is taken to be hard].

Similarly, bringing in the first term on the right side of Eq. 46 into Eq. 48c's right side leads to a balance between $-Z_{liner}\Delta \bar{w}_v$ ($=Z_{liner}\bar{w}_v^-$) and the difference $\bar{p}_v^{inc}-\Delta \bar{p}_v/2$ (Fig. 4b). This second term becomes $\bar{p}_v^{inc}+ \bar{p}_v^-/2 - \bar{p}_v^+/2$, so that the lower lifting pressure $\bar{p}_v^-$ pushes in the direction of $\bar{p}_v^{inc}$, which is again as should be.

In the way of final remark, note that Eqs. 48b,c are valid whether Z_{liner} refers to a passive or an active liner. The development will specialize itself now to the former type. This will result in integral-equation drivers that are in terms only of propeller-incident field quantities. An active liner would obviously contribute to these known right-hand sides: $\Delta \bar{w}_v$ would then be the prescribed inward velocity "$-\bar{w}_v^{active}(a^-,z)$" of the active source at z backed by the cowl's outer structure. $Z_{liner}(z;\omega)$ would then stand for the known internal impedance of that particular active source, and the sum of the second and third terms on the right sides of Eqs. 48b,c would then be interpreted as the radiation loading bearing down on that source.

C.2 **The Liner Model**

The formulation limits itself here to modeling liners that are axisymmetric at every axial station z along the cowl's interior, although properties may vary with axial distance z. The present study considers a single axisymmetric band of axial extent L_{liner} with its midpoint at $z=z_{mid}$ (Fig. 5a). An important objective is to determine the sensitivity of the scattered-plus-incident acoustic field to the position of this band within the cowl.

The liner material will be locally reacting and its impedance signature will be that of a blocked acoustic layer of thickness h_{liner} and complex compressional wave speed c_{liner} (the blocking is provided by the cowl's "outer" wall, which is of infinite impedance, see Fig. 5b). The dissipation mechanism will be a material loss factor η associated with this compressional speed. Normalized by the medium's characteristic impedance ρc, Z_{liner} is

$$\frac{Z_{liner}(\omega;z)}{\rho c} = i \cot\left(\frac{\omega h_{liner}}{c_{liner}}\right)$$

$$= i \cot\left(\frac{15}{B\sqrt{1-i\eta}} \cdot \frac{\omega}{RPM_{choice}}\right) \quad ; \quad |z - z_{MID}| < \frac{L_{liner}}{2} \quad . \quad (49)$$

The second equality has fixed the real part of the liner's compressional wave speed to make impedance Z_{liner} pass through its first null, i.e., through its first thickness resonance, at a value of frequency ω corresponding to a propeller RPM of choice, RPM_{choice}. B is the number of blades in the propeller. Together with RPM_{choice}, B obviously determines the blade-passage frequency of choice. The discussion will describe below a tonal model for the incident field adopted for the current study.

C.3 Final Nondimensional Form for the Coupled System of Singular Integral Equations

Sections II.A and B have generated the different parts of the coupled lifting and nonlifting problems for a lined ring wing in aerodynamically noncompact unsteady subsonic flow. This section puts those parts together. First, however, it nondimensionalizes every distance and wavenumber by the cowl's halfchord L/2. The cowl's left and right ends will now be at z= -1, +1, as shown between parentheses in Fig. 5a. A new symbol, "k", will stand for the ring wing's reduced frequency $\omega L/2U$ following standard nomenclature. Radius "a" will now be nondimensional, and the radial wavenumber of Eq. 8 will be given by

$$\gamma = \sqrt{\left(\frac{kM}{\beta}\right)^2 - \beta^2 \bar{k}^2} \quad . \quad (50)$$

Contour C now traces the path shown in Fig. 2d.

The first of the two coupled integral equations applies to the r=a$^+$ outer surface of the cowl. It is

$$I: \quad -\frac{\tilde{w}_v^{inc}(z)}{U} = \frac{1}{2}\frac{\Delta\tilde{w}_v(z)}{U} + \oint_{-1}^{1} d\bar{z}\, K_v^{l,l}(z-\bar{z})\, \frac{\Delta\tilde{p}_v(\bar{z})}{\rho U^2}$$

$$+ \int_{-1}^{1} d\bar{z}\, K_v^{l,th}(z-\bar{z})\, \frac{\Delta\tilde{w}_v(\bar{z})}{U} \quad . \tag{51a}$$

The second equation comes from the boundary condition along $r=a^-$:

$$II: \quad -M\alpha_{liner}(\omega;z)\,\frac{\tilde{p}_v^{inc}(z)}{\rho U^2} = \frac{\Delta\tilde{w}_v(z)}{U} - \frac{M}{2}\,\alpha_{liner}(\omega;z)\,\frac{\Delta\tilde{p}_v(z)}{\rho U^2}$$

$$- M\alpha_{liner}(\omega;z) \int_{-1}^{1} d\bar{z}\, K_v^{l,th}(z-\bar{z})\, \frac{\Delta\tilde{p}_v(\bar{z})}{\rho U^2}$$

$$+ M\alpha_{liner}(\omega;z) \oint_{-1}^{1} d\bar{z}\, K_v^{th,th}(z-\bar{z})\, \frac{\Delta\tilde{w}_v(\bar{z})}{U} . \tag{51b}$$

Eq. 51b has divided Eq. 48c throughout by the liner impedance Z_{liner}, and has defined the normalized liner admittance α as

$$\alpha(\omega;z) = \frac{\rho c}{Z_{liner}(\omega;z)} \quad . \tag{52}$$

The reason for Eq. 52 is numerical stability: Along the unlined parts of the cowl's interior, where the compliance $\alpha(z)$ is zero, the coefficients of Eq. 51b that contain it simply contribute zero. The remaining term, which appears first on the right side of the equation, is then balanced by nothing and therefore states that the thickness solution $\Delta\tilde{w}_v(z)$ is identically zero over these unlined z's -- a sanity check. Not dividing throughout by Z_{liner} leads to the same conclusion but requires the practical use of artificially large numbers to account for the arbitrarily large impedance of the unlined segments.

Note finally that Eq. 51b collapses to the statement $\Delta\bar{w}_v(z)\equiv 0$ if there are no lined segments at all along the cowl's

interior. Eq. 51a then turns into an old-fashioned lifting problem unencumbered by the one-sided nonlifting effects of the liner:

$$- \frac{\tilde{w}_v^{inc}(z)}{U} = \int\limits_{-1}^{1} d\bar{z} \, K_v^{\ell,\ell}(z-\bar{z}) \, \frac{\Delta \tilde{p}_v(\bar{z})}{\rho U^2} \quad .$$

Kernels $K_v^{\ell,\ell}$, $K_v^{\ell,th}$, and $K_v^{th,th}$ in Eqs. 51a,b are

$$K_v^{\ell,\ell}(z-\bar{z}) = \frac{\beta}{2\pi} \cdot \frac{e^{-i\frac{kM^2}{\beta^2}(z-\bar{z})}}{z-\bar{z}}$$

$$+ \frac{e^{-i\frac{kM^2}{\beta^2}(z-\bar{z})}}{4} \int_C d\bar{k} \, e^{-i\bar{k}(z-\bar{z})} \left[\frac{\gamma^2 a \, H_v'(\gamma a) \, J_v'(\gamma a)}{\bar{k} + \frac{k}{\beta^2}} - \frac{i\beta}{\pi} \frac{|\bar{k}|}{\bar{k}} \right] \,, \quad (53a)$$

$$K_v^{\ell,th}(z-\bar{z}) = - \frac{e^{-i\frac{kM^2}{\beta^2}(z-\bar{z})}}{4} \int_C d\bar{k} \, e^{-i\bar{k}(z-\bar{z})} \left[i\gamma a \, H_v'(\gamma a) \, J_v(\gamma a) + \frac{1}{\pi} \right] \,, \quad (53b)$$

$$K_v^{th,th}(z-\bar{z}) = - \frac{1}{2\pi\beta} \cdot \frac{e^{-i\frac{kM^2}{\beta^2}(z-\bar{z})}}{z-\bar{z}}$$

$$+ \frac{e^{-i\frac{kM^2}{\beta^2}(z-\bar{z})}}{4} \int_C d\bar{k} \, e^{-i\bar{k}(z-\bar{z})} \left[H_v(\gamma a) \, J_v(\gamma a) \left(\bar{k} a + \frac{ka}{\beta^2} \right) + \frac{i}{\pi\beta} \frac{|\bar{k}|}{\bar{k}} \right] \,. \quad (53c)$$

The division of the pressure jump by ρU^2 in Eq. 51a, and likewise of all velocities by the freestream U, has prompted a redefinition of the kernel $K_v^{\ell,\ell}$ in Eq. 19b to be now without the $1/\rho U$ factor included there.

D Form of the Solution

The solution technique will be conventional: A pair of series that introduce unknown coefficients A_m and B_n for the lifting and nonlifting problems, respectively:

$$\frac{\Delta \tilde{p}_v(z)}{\rho U^2} = A_o \sqrt{\frac{1-z}{1+z}} + \sqrt{1-z^2} \sum_{m=1}^{M} A_m U_m(z) \qquad , \qquad (54a)$$

$$\frac{\Delta \tilde{w}_v(z)}{U} = \sum_{n=0}^{N} B_n T_n(z) \qquad . \qquad (54b)$$

Eq. 54a is equivalent to Ref. 11's expansion on p. 230. Its first term accounts for the square-root singularity of the aeroacoustic loading at the cowl's assumed-sharp leading edge $z=-1$. The numerator of this factor brings the diffraction loading down to zero at the trailing edge $z=+1$ and thus simulates a Kutta condition there. The sum part of Eq. 54a is in terms of Chebyshev polynomials U_m of the second kind. Its square root-factor also satisfies the Kutta condition. The T_n functions in Eq. 54b are Chebyshev polynomials of the first kind.

The relationship of the solution prescribed in Eq. 54a (Ref. 4f's Eq. 25), to that used in Ref. 4a for the pure diffraction problem in the absence of a freestream, is as follows: The scatterer's bound vorticity $\Delta u(z)$ blows up as $(z+1)^{-1/2}$ for $z \to -1$ whether or not a freestream is present. Accordingly, the discontinuity in the velocity potential Φ, which by definition is obtainable from the integration of Δu with respect to z, vanishes as $(z+1)^{1/2}$ for $z \to -1$ regardless of the presence or absence of a meanflow U (see, for example, Noble's[17] p. 74 for $U=0$, and Amiet[3c] for the case with U).

The difference of $U=0$ versus $U \neq 0$ is obviously in the diffraction loading $\Delta \bar{p}$. This is given by $-\rho \partial [\Delta \Phi]/\partial t = i\omega \rho \Delta \Phi$ for the flowless case ("Bernoulli's equation" for acoustics), which, by the above arguments, vanishes at any of the scatterer's thin edges. Ref. 4a, which dealt with the flowless version of the present problem, accordingly skipped the first term on the right of Eq. 54a and began the remaining sum with $m=0$. The solution thus resembled that usually implemented for subsonic flow along the spanwise direction in thin-wing theory (see, for example, Ref. 14's Eq. 7-96, and recall the comments made above regarding the analogy between spanwise aerodynamics and diffraction theory,

in item #3 of "Yet Another Benchmark Check: Unification with the Theory of Pure Diffraction").

The situation changes radically when there is a freestream. Bernoulli's equation then states that $\Delta\bar{p} = i\rho\omega\Delta\Phi - \rho U\Delta\bar{u} \approx - \rho U\Delta\bar{u}$ for $z \rightarrow -1$, and $\Delta\bar{p}$ is therefore automatically singular at those edges recognized to be the geometry's leading edges: see Adamczyk[12]'s Eq. 37 for the pressure field along the semi-infinite chord of a "leading-edge" airfoil, and Ref. 4g's Eq. 14 for its analytic continuation by the present author to any nearfield point. This second result is in closed form, just as Adamczyk's had been, despite its generality of field position.

Unlike in the problem of pure diffraction just discussed (U=0), the process of bringing $\Delta\bar{p}$ down to zero at any other edge exposed to the meanflow now requires human intervention. It is worth restating that the Kutta condition and its implication of a vanishing trailing-edge load are viscous effects that must be injected into potential theory by hand.

A recent report by Amiet[3a] has argued independently for the singular behavior of the first term on the right side of Eq. 54a above, which had also been postulated in Eq. 25 of Ref. 4f and had been based then on the above simple observations.

The expansions in Eqs. 54a,b, once substituted in Eqs. 51a,b, generate a number of integrals familiar to workers in aerodynamics, e.g.,

$$\int_{-1}^{1} d\bar{z} \sqrt{\frac{1-\bar{z}}{1+\bar{z}}}\ e^{i\left(\bar{k} + \frac{kM^2}{\beta^2}\right)\bar{z}} = \pi\left[J_o\left(\bar{k} + \frac{kM^2}{\beta^2}\right) - iJ_1\left(\bar{k} + \frac{kM^2}{\beta^2}\right)\right] \quad , \qquad (55a)$$

and

$$\int_{-1}^{1} d\bar{z}\sqrt{1-\bar{z}^2}\ U_m(\bar{z})\ e^{i\left(\bar{k} + \frac{kM^2}{\beta^2}\right)\bar{z}} = \pi\ (m+1)\ i^m \cdot \frac{J_{m+1}\left(\bar{k} + \frac{kM^2}{\beta^2}\right)}{\bar{k} + \frac{kM^2}{\beta^2}} \quad . \qquad (55b)$$

The last step is to multiply Eqs. 51a,b by convenient functions containing the same indices as Eqs. 54a,b, i.e., m and

n, and to integrate again from -1 to +1, this time with respect to the control variable z. The result is an M+N+2 x M+N+2 system of equations to be solved for the unknown coefficients A_m and B_n.

E Model of the Incident Field

The aeroacoustic field that insonifies the cowl from within will come here from a propeller, or fan, with B thin blades cutting through a "general" inhomogeneity in the axial meanflow: $u(\phi^*, r^*)$. Asterisked variables will describe the inhomogeneity spatially on the plane of this fan stage, which accordingly will be at axial station z^*.

Such an inhomogeneity could be due, for example, to

(1) the wake-momentum deficit of upstream vanes or supporting struts (neither of which exists for the configuration of Fig. 1a, although the statement could then apply to the indicated downstream structural member, which is in the wake of the upstream rotating blades);

or to

(2) a cross flow when the cowl is at an angle of attack while climbing or turning -- either type of maneuver would cause the cowl's inlet region to contribute a relatively smooth inflow inhomogeneity by effectively shielding sectors of the propeller from the incoming flow (recall the comments made after Eq. 27b).

The model of the nonuniform inflow will be contained in a simple Gaussian curve of effective width "A^{-1}" that puts the maximum momentum deficit $\bar{u}$ at an absolute circumferential position $\hat{\phi}$ (three parameters, see Fig. 6a). Its discrete circumferential spectrum of amplitudes $u_n(r^*)$ is

$$u_n(r^*) = \int_0^{2\pi} \frac{d\phi^*}{2\pi} e^{-in\phi^*} u(\phi^*, r^*) = \bar{u} \int_0^{2\pi} \frac{d\phi^*}{2\pi} \exp[-in\phi^* - A(\phi^* - \hat{\phi})^2] \quad . \quad (56)$$

This implies a spectrum of gusts with fronts parallel to the unswept blades, which sense a chordwise wavenumber n/r^* at radial station r^* (Fig. 6b).

The blades' chord $\bar{c}$ will be constant from hub radius R_h to the effective tip at $r^* = R_t$. Moreover, all of the airfoil elements making them up will lay flat on their nominal plane of rotation at the axial station $z = z^*$ (no pitch, no rake). The model's unsteady aerodynamics will be those of strip theory in the aeroacoustically compact regime:

(1) Each blade element, of local spanwise width dr^*, will sense an airload due to the chopping process in a state of isolation from the rest of the airfoil segments on the same blade, and

(2) The aerodynamic transfer function $\bar{T}_n$ defined below in Eq. 58 will not include compressibility or high-frequency effects: it will be the Sears function evaluated for "wavenumber" n/r^*. The units of the product $u_n \bar{T}_n$ below are force/running length.

The aeroacoustic field along $r = a$ radiated by the thrust-dipole field from "B" such blades is

$$p^{inc}(a,\phi,z,t) = -\frac{B}{4\pi} \sum_{m=-\infty}^{\infty} e^{-imB\Omega t - i\frac{mB\Omega LM}{2c\beta^2}(z-z^*)} \sum_{n=-\infty}^{\infty} e^{-i(mB-n)\phi}$$

$$\cdot \int_{R_h}^{R_t} dr^* \frac{u_n(r^*)\,\bar{T}_n(n/r^*)}{\rho U^2 L} \int_C d\bar{K}\left(\bar{K} + \frac{mB\Omega LM}{2c\beta^2}\right) e^{-i\bar{K}(z-z^*)} H_{mB-n}^{(1)}(\gamma_m a)\, J_{mB-n}(\gamma_m r^*), \quad (57a)$$

and the corresponding incident fluid particle velocities are

$$\frac{w^{inc}(a,\phi,z,t)}{U} = \frac{iB}{4\pi} \sum_{m=-\infty}^{\infty} e^{-imB\Omega t - i\frac{mB\Omega LM}{2c\beta^2}(z-z^*)} \sum_{n=-\infty}^{\infty} e^{-i(mB-n)\phi}$$

$$\cdot \int_{R_h}^{R_t} dr^* \frac{u_n(r^*)\,\bar{T}_n(n/r^*)}{\rho U^2 L} \int_C d\bar{K}\left(\frac{\bar{K} + \dfrac{mB\Omega LM}{2c\beta^2}}{\bar{K} + \dfrac{mB\Omega L}{2U\beta^2}}\right) e^{-i\bar{K}(z-z^*)} \gamma_m H_{mB-n}'(\gamma_m a)\, J_{mB-n}(\gamma_m r^*)$$

$$(57b)$$

The cowl's halfchord $L/2$ continues to normalize all length variables in Eqs. 57a,b; e.g., r^*, blade chord $\bar{c}$, and blade length $R_t - R_h$ are all nondimensional. Ω is the fan's rotational speed and the first sum on the right side of both equations accounts for the problem's tonal harmonics m. E.g., $mB\Omega$ are the blade-passage frequency ($m=1$) and its harmonics ($m = 2, 3, \ldots$).

Discrete frequency $mB\Omega$ thus replaces the symbol ω in all of the earlier equations. For example, radial wavenumber γ becomes γ_m in all of the $\tilde{k}$ transforms, still given by Eq. 50 but with reduced frequency k now given by "k_m"$=mB\Omega L/2U$.

Everything inside the m sum except for the $\exp[-imB\Omega t]$ factor becomes $\tilde{p}$ in Eq. 57a: the incident pressure field's frequency spectrum (recall the purpose of the tilde over all of the dependent variables in the foregoing analysis). And the effective circumferential modes of this driving acoustic field are mB-n, which replaces symbol ν throughout the above.

The product $u_n \bar{T}_n$ is

$$\frac{u_n(r^*)\,\bar{T}_n(n/r^*)}{\rho U^2 L} = \frac{\pi}{4J}\left(\frac{\bar{u}}{U}\right)\left(\frac{\bar{c}}{R_t}\right)\left[\int_0^{2\pi} d\phi^* \exp[-in\phi^* - A(\phi^* - \hat{\phi})^2]\right] r^* S\left(\frac{n\bar{c}}{2r^*}\right), \quad (58)$$

where S is the Sears function, conveniently approximated by

$$S\left(\frac{n\bar{c}}{2r^*}\right) = \frac{\exp\left\{-\dfrac{in\bar{c}}{2r^*}\left[1 - \dfrac{\pi^2}{2(1+\pi n\bar{c}/r^*)}\right]\right\}}{\sqrt{1 + \dfrac{\pi n\bar{c}}{r^*}}} \quad . \qquad (59)$$

(Quantity $n\bar{c}/2r^*$ is "σ_1" in Goldstein's nomenclature[11], see the discussion surrounding his Eq. 3.64).

Parameter J in the denominator of the coefficient on the right side of Eq. 58 is short for the propeller's advance ratio $\pi U/[\Omega \cdot (R_t L/2)]$ (remember that R_t has been normalized by the ring wing's halfchord L/2). This use of J is somewhat misleading because it suggests that the blades are pitched when in fact they are not: their chords lie flat on the plane of rotation, as stated earlier. J comes about solely from the normalization by $\rho U^2 L$ on the left side of Eq. 58.

As a weak check on the meaning of Eqs. 56 through 59, consider the circumferential average of the nonuniformity's upwash on the plane of rotation, given by the n=0 term of Eq. 56. The unsteady chopping mechanism should then go away and the only noise given off by the modelled fan stage should be of the Gutin

type. And putting n=0 on the right sides of Eqs. 57a,b in fact generates just that kind of acoustic field, with subscript mB-n on the Bessel functions collapsing to mB.

For n=0 the Sears coefficient of lift as given by Eq. 59 becomes unity, which is again as should be, and Eq. 58 accordingly provides the incremental steady running (strip) lift experienced by the blades as they cut through the ϕ^* average of the signature in Fig. 6a. This lift would be "incremental" because it would obviously be additional to what real blades would feel by virtue of their angle-of-attack distribution.

It is also interesting to note that the much higher Fourier mode n=mB (v=0) of the inflow inhomogeneity is special, because it, and only it, will determine the incident and diffracted farfields along the cowl's axis r=0. The $\Delta \bar{p}_{v=0}$ part of the cowl's virtual sources does not contribute even then: the dipoles' nodal planes coincide with the cowl's axis in the farfield. The liner will thus be responsible for all on-axis scattering.

Regarding the incident field by itself, one could fairly call v=0 the propeller's "impulsive" chopping mode, because if each of the blades cut the nonuniformity in rectilinear motion (i.e., nonperiodically) the response would, in fact, be nonzero on axis. Goldstein[11] discusses other interesting aspects of the mB-n index of the above equations on p. 165 of his book.

F The FarField Analysis

There are two kinds of farfields that are of interest to the present research program. Each applies to both the incident and the scattered component:

(1) The field produced by the ducted propulsor along the aircraft cabin's exterior wall (the relevant frequencies are high enough to put these points in the acoustic farfield; see Fig. 7a); and

(2) Acoustic radiation as heard by someone on the ground, where all real and virtual sources appear to be flying by (Fig. 7b).

Recent interest seems to be leaning increasingly toward the second of the above: the community noise problem. The current project considers both. Their analyses follow standard asymptotic steps which need not be repeated here.

41

First for the fan's incident radiated field: As seen from the aircraft's reference frame (item 1 above), this is

$$
\frac{\tilde{p}_\nu{}^{inc}(R_o \to \infty, \theta_o)}{\rho U^2 \dfrac{e^{i\frac{kM}{\beta}R_o - i\frac{kM^2}{\beta^2}z}}{R_o}} \sim \frac{B}{8}\frac{kM}{J}\frac{1}{\beta^3}\left(\frac{\overline{u}}{U}\right)\left(\frac{\overline{c}}{R_t}\right) e^{-i(\nu-1)\pi/2 + i\frac{kM}{\beta}\left[\frac{M}{\beta} + \cos\theta_o\right]z^*}
$$

$$
\cdot \left[\int_0^{2\pi} d\phi^* \exp\{-in\phi^* - A(\phi^* - \hat{\phi})^2\}\right]
$$

$$
\cdot (\cos\theta_o + M)\int_{R_h}^{R_t} dr^* r^* S\left(\frac{n\overline{c}}{2r^*}\right) J_\nu\left(\frac{kM}{\beta}r^*\sin\theta_o\right) . \quad (60a)
$$

The corresponding ground-perceived incident signal is

$$
\frac{\tilde{p}_\nu{}^{inc}(R_o \to \infty, \theta_o)}{\rho U^2 \dfrac{e^{-i\frac{\omega}{1-M\cos\theta_o}\left(t - \frac{R_o}{c}\right)}}{R_o}} \sim \frac{B}{8}\frac{kM}{J}\left(\frac{\overline{u}}{U}\right)\left(\frac{\overline{c}}{R_t}\right) e^{-i(\nu-1)\pi/2 + i\frac{kz^* M\cos\theta_o}{1-M\cos\theta_o}}
$$

$$
\cdot \left[\int_0^{2\pi} d\phi^* \exp\{-in\phi^* - A(\phi^* - \hat{\phi})^2\}\right]
$$

$$
\cdot \frac{\cos\theta_o}{(1-M\cos\theta_o)^2}\int_{R_h}^{R_t} dr^* r^* S\left(\frac{n\overline{c}}{2r^*}\right) J_\nu\left(\frac{kr^* M\sin\theta_o}{1-M\cos\theta_o}\right) . \quad (60b)
$$

Here ν continues to be mB-n, as earlier explained.

In the aircraft-based result of Eq. 60a, the nondimensional range R_o and the directivity angle θ_o are respectively defined by (Fig. 7a):

$$
R_o = \sqrt{(z/\beta)^2 + r^2} \quad ; \quad \theta_o = -\arctan\left(\frac{\beta r}{z}\right) . \quad (61a,b)
$$

And on the ground frame these same variables stand for (Fig. 7b)

42

$$R_o = \sqrt{z^2 + r^2} \qquad ; \qquad \theta_o = -\arctan\left(\frac{r}{z}\right) \qquad . \qquad (62a,b)$$

The range $\hat{R}_o$ that appears in the retarded time $t-\hat{R}_o/c$ in the exponential in the denominator of Eq. 60b's left side is the dimensional version of R_o, i.e., $\hat{R}_o=R_oL/2$. The analysis for Eq. 60b began by including the problem's $\exp(-i\omega t)$ temporal factor in the calculated function. This becomes $\exp(-i\omega t/[1-M\cos\theta_o])$, which displays the classically familiar Doppler shift $1-M\cos\theta_o$. This factor squared also appears in the denominator on the right side of Eq. 60b. It amplifies the solution in the upstream direction and reduces it in the downstream direction, consistent with the similar behavior found by Goldstein for jet noise (see, for example, Ref. 11's Eq. 2-29, where the power of $1-M\cos\theta_o$ is "-5" rather than "-2").

Recall now that the propeller's sources of aerodynamic sound are thrust dipoles only (the blades lie flat on their plane of rotation, and there are no "drag" dipoles). One's first inclination might therefore be to say that the incident acoustic field should be zero on the $\theta_o=\pi/2$ plane of the propeller regardless of reference frame. This actually occurs for the ground frame of reference: the $\cos\theta_o$ on the third line of Eq. 60b is zero there. But the aircraft-frame result in Eq. 60a instead displays a corresponding null at $\theta_o=\cos^{-1}(-M)$, which is $\geq\pi/2$. The propeller's nodal plane gets washed downstream by that much. Note that Eqs. 60a and b merge for $M\to0$, as they must. The product "kM" then becomes $\omega L/2c$, the normalized acoustic wavenumber.

As for the scattered field radiated by the virtual source distributions $\Delta\bar{p}_v(\bar{z})$ and $\Delta\bar{w}_v(\bar{z})$, both of which are known by now, this is, in the aircraft's reference frame of Fig. 7a,

43

$$\frac{\tilde{p}_v{}^!(R_o \to \infty, \theta_o) + \tilde{p}_v{}^{th}(R_o \to \infty, \theta_o)}{\rho U^2 \dfrac{e^{i\frac{kM}{\beta}R_o - i\frac{kM^2}{\beta^2}z}}{R_o}}$$

$$\sim -\left(\frac{ka}{2}\right) e^{-i(v-1)\pi/2} \left[\frac{iM}{\beta^2} \sin\theta_o \, J_v'\left(\frac{ka}{\beta} M\sin\theta_o\right) \int_{-1}^{1} d\overline{z} \, \frac{\Delta \tilde{p}_v(\overline{z})}{\rho U^2} e^{i\frac{k\overline{z}M}{\beta}\left(\frac{M}{\beta}+\cos\theta_o\right)} \right.$$

$$\left. + \frac{1}{\beta^3}(M\cos\theta_o + 1) J_v\left(\frac{ka}{\beta} M\sin\theta_o\right) \int_{-1}^{1} d\overline{z} \, \frac{\Delta \tilde{w}_v(\overline{z})}{U} e^{i\frac{k\overline{z}M}{\beta}\left(\frac{M}{\beta}+\cos\theta_o\right)} \right]$$

$$(63a)$$

Ground-based listeners perceive the same diffracted signal as (Fig. 7b)

$$\frac{\tilde{p}_v{}^!(R_o \to \infty, \theta_o) + \tilde{p}_v{}^{th}(R_o \to \infty, \theta_o)}{\rho U^2 \dfrac{e^{-i\frac{\omega}{1-M\cos\theta_o}\left(t - \frac{R_o}{c}\right)}}{R_o}}$$

$$\sim -\left(\frac{ka}{2}\right) e^{-i(v-1)\pi/2} \left[\frac{iM\sin\theta_o}{(1-M\cos\theta_o)^2} J_v'\left(\frac{ka\,M\sin\theta_o}{1-M\cos\theta_o}\right) \int_{-1}^{1} d\overline{z} \, \frac{\Delta \tilde{p}_v(\overline{z})}{\rho U^2} e^{i\frac{k\overline{z}M\cos\theta_o}{1-M\cos\theta_o}} \right.$$

$$\left. + \frac{1}{(1-M\cos\theta_o)^2} J_v\left(\frac{ka\,M\sin\theta_o}{1-M\cos\theta_o}\right) \int_{-1}^{1} d\overline{z} \, \frac{\Delta \tilde{w}_v(\overline{z})}{U} e^{i\frac{k\overline{z}M\cos\theta_o}{1-M\cos\theta_o}} \right]$$

$$(63b)$$

The sum of Eqs. 60a and 63a gives the total pressure field as a function of the cowl elevation angle θ_o, for observers in an aircraft, while the sum of Eqs. 60b and 63b yields the corresponding quantity relevant to community noise studies.

IV REPRESENTATIVE PREDICTIONS OF THE MODEL

A Selected Values for the Input Parameters

Ref. 18 lists operational parameters for a prototype of a
modern ducted propulsor. The sample calculations about to be
discussed will apply, alter somewhat, and supplement these values
as needed to complete the input set. The flight Mach number M is
.8.

Cowl parameters: length L = 6 feet
                  radius a = 2.5 feet
                  position of propeller station $z^* = +L/10$
                  length of liner patch $L_{liner} = .6$ L

Propeller parameters: number of blades B = 18
                     hub radius $R_h = .25$ a
                     tip radius $R_t = .70$ a
                     average blade chord $\bar{c} = .10\ (R_t - R_h)$
                     RPM = 1000

Inflow nonuniformity parameters (see Fig. 6a here):

$$\bar{u}/U = .2$$
$$\hat{\phi} = 0$$
$$A = (2/\pi)^2 \log_e 10$$

The indicated value of "A" causes the Gaussian in Fig. 6a to
reach its 10-percent-of-maximum mark at $\phi^* = \hat{\phi} \pm \pi/2$ (the maximum
occurs at $\phi = \hat{\phi}$ by design). The chosen propeller rotational speed
of 1000 RPM generates a blade-passage frequency of 300 Hz. It is
roughly one third that of the actual specification in Ref. 18.
And yet, 1000 RPM already implies relatively large values for the
noncompactness parameters of the cowl as a ring wing. E.g., the
acoustic wavenumber normalized by the cowl's radius is $\omega a/c = 4.28$
($\omega = B\Omega$, the blade-passage frequency). The aerodynamically
relevant form of this quantity, $\omega a/(\beta c)$, is 7.11. As for the
cowl's length, or chord, its reduced frequency "k" is 12.86, and
$\omega L/c$ is 10.29.

B Discussion of Numerical Results

Fig. 8a plots the total farfield v-modal pressure, in the
aircraft's reference frame, for three possible layouts of the
cowl's interior liner. The value of v is zero, corresponding to
the $n = mB^{th}$ circumferential mode of the inflow inhomogeneity in
Fig. 6a (recall the text after Eq. 59 regarding the significance

of this null value). The solid curve belongs to a ring liner patch beginning just after the cowl's leading edge. The dash curve is for the same patch centered at the cowl's z=0 middle (i.e., with $z_{mid}=0$ in Eq. 49). The remaining dot curve is for a ring patch that almost reaches the cowl's trailing edge.

The patch length L_{liner} displayed in each of the insert sketches in Fig. 8a is .6L, as per the above list. RPM_{choice} in Eq. 49 is 2000, so that the layer in Fig. 5b is stiffness-controlled at the operating rotational speed of 1000 RPM. The loss factor η does not play a strong role at this frequency (its actual value was .05 for Fig. 8a).

Each of the three curves in Fig. 8a shows $20\log_{10}|R_o(\text{total pressure})/\rho U^2|$ as given by the sum of Eqs. 60a and 63a. The sense of the directivity angle θ_o follows from Fig. 7a. The differences in the $\theta_o=0$ pressures among the three plots are attributable solely to differences in the radiative performance of the thickness solution among the three liner cases investigated (recall that each coupled lifting solution, $\Delta\bar{p}_v$, cannot affect on-axis levels directly because its effective dipoles are radial). The same is true of the $\theta_o=180°$ downstream direction. The message of the figure is that the spatial layout of a finite cowl's lined patches can have a significant impact on most of its radiated rays, even when these patches are not tuned for maximum energy absorption.

Fig. 8b removes the liner (note the cowl sketch along the bottom right of the picture), and compares the total to the incident pressure. The sector marked "IL≥0" contains those field positions where the diffracting cowl has a beneficial shielding effect. "IL" stands for "insertion loss", following standard terminology. I.e., "insertion loss" denotes here the loss of field pressure due to the "insertion", or introduction, of the cowl.

There are two such IL≥0 zones in Fig. 8b. The larger one agrees very roughly with the cowl's geometric shadow by extending from about $\theta_o=50°$ to 110°. Its largest IL values are only a few dB, however. The narrower rearward zone, which is off the cowl's shadow as defined neglecting again the effects of convection U, is the result of a subtle destruction of the incident field by the lifting distribution over the cowl. Incidentally, the total pressures at $\theta_o=0$, 180° match those of the incident field (i.e., the two plotted curves merge), as a result of the absence of a liner and of its associated monopoles. The incident field has a null at the propeller's convected nodal plane at $\theta_o=143°$

=$\cos^{-1}(-M)=\cos^{-1}(-.8)$, as anticipated above after Eqs. 62a,b. The insertion loss is doomed to be negative there: the total field is locally due strictly to (undesirable) diffraction by the cowl.

Fig. 8c is a composite of the positive insertion-loss zones from Figs. 8a and b. The solid curve is the same incident-field pattern from Fig. 8b. The purpose of the new figure is to show the <u>potential</u> noise-reduction effect of the investigated ensemble of liner configurations coupled to the mechanism of edge diffraction at the cowl's two ends. The best compound results occur approximately over the cowl's shadow, which appears to be further accentuated by the liner, or liners, relative to that cast by the unlined case of Fig. 8b.

Figs. 8a-c have addressed the aircraft reference frame in Fig. 7a. Figs. 9a-c now show results corresponding to the ground frame of reference in Fig. 7b. Fig. 9a uses the same three lined cases of Fig. 8a. The curves are again for the total normalized pressure farfield, this time given by the sum of Eqs. 60b and 63b. E.g., Fig. 9b is Fig. 9a's ground-reference counterpart. The solid curve contains again the incident farfield, which vanishes at $\theta_o=90°$ as demanded by the $\cos\theta_o$ factor on the third line of Eq. 60b. The broken curve is for the total farfield for the unlined cowl. The large detrimental bulge between 60° and 70° in Figs. 9a,b, which incidentally does not show up elsewhere in Figs. 8a,b, remains to be resolved. The larger of the two zones of positive insertion loss is now somewhat narrower and more forward-directive than in Fig. 8b. The rearward IL≥0 zone, on the other hand, widens relative to that in Fig. 8b. Fig. 9c shows the union of the IL≥0 sectors of Figs. 9a,b.

A few comments are in order regarding the nulls of the incident fields in Figs. 8b and 9b. These are the result of having used only thrust dipoles to describe the unsteady aerodynamics of the propeller/inflow-inhomogeneity chopping process. The present model for the incident field neglected blade-thickness effects on blade radiation (monopole in nature), blade pitch, or more generally, blade twist. It has also not accounted for "drag" dipoles for the blade sections. Any one of these omissions, once included, would remove the nodal planes of the solid curves in Figs. 8b,c and 9b,c, which in some sense are therefore artifacts of the propeller model chosen here to test or drive the cowl theory.

The $\theta_o=90°$ null of Fig. 9b's community-noise calculation represents a particular strain on the present diffraction study because it causes the cowl's insertion loss always to be negative

near this direction. The cowl's shielding performance should be better for real-life incident fields which typically reach their maximum, not minimum, near $\theta_o=90°$ (see Ref. 19).

Figs. 8a-c and 9a-c have presented calculations for the n=mB (v=0) circumferential mode of the inflow inhomogeneity. Figs. 10a,b now show ground-frame predictions for n=mB+5, so that $|v|$=5. One objective of these results is simply to drive home the point that the new code for the cowl diffractor can tackle a general value of v and can thus map the radiation in three dimensions by weighing coherently each v pattern by a factor $\exp(-iv\phi)$. Another purpose of Figs. 10a,b is to explore the effects of a tuned liner having a high loss factor: RPM_{choice} in Eq. 49 is now 1028 and so essentially matches the operational RPM, which remains at 1000. The loss factor η is 1 (one). The layer in Fig. 5b is now resistance-controlled.

Fig. 10a compares the incident (the solid curve) to the total farfield for the liner patch whose left end is just inside the cowl's inlet edge (see insert). Fig. 10b displays the other two patch cases analyzed in earlier figures. The new high-loss factor results contain fewer undesirable IL≤0 zones relative to the reactive liners discussed above. The extremely low levels of these IL≤0 zones now make the cowl's performance essentially all good. These $|v|$=5 results are representative of predictions in which the shrouding system was found to play an almost global positive role in noise reduction.

V CONCLUSIONS AND RECOMMENDATIONS

A Conclusions

1. The present study has generated a new formulation, in terms of boundary values only, for the coupled problems of cowl diffraction and liner dissipation of propeller noise at high subsonic flight speeds. A new computer code based on that theory now exists. The $\omega\to 0$ limit of the analysis can already predict the steady but nonuniform interference flows which a cowl at an angle of attack would induce on its internal propulsion system (thereby generating additional propeller noise). The new code predicts cowl diffraction both for aircraft-cabin and ground-based listeners.

2. The new formulation is valid both for passive and for active liners, although the Phase I study has addressed only the former kind.

3. The theory uses <u>freefield</u> propeller nearfield quantities to

drive its diffraction system equations. This requires no sacrifice in rigor. The right-hand side of the pair of singular integral equations in Eqs. 51a,b could be saved, so that only their freefield drivers need be replaced from propeller case to case (for a specific frequency of interest).

4. The calculations produced here to demonstrate the new theory suggest that a short cowl having passive lined segments should provide moderate shielding of propeller noise (see the shaded parts of Fig. 8c, for example). These passive-liner results imply that the significantly better performance that one would expect of a smart liner should be within the reach of present technology, at least in terms of power requirements.

B Recommendations

The recommendations of the present Phase I study are almost self-suggesting given the above conclusions:

1. Turn the new diffraction software into a user-friendly code that will allow for the "fast" testing of propellers in terms of the freefield nearfields with which they would insonify a candidate design for the shrouding cowl. Apply the new theory to realistic and relevant propulsion systems. Adapt existing predictors of freefield propeller noise to provide the input quantities needed in the new cowl theory. E.g., make part of their output the directional derivative of the pressure nearfield normal to what will later correspond to the cowl's surface, in order to yield $\bar{w}_v^{inc}$ for use in Eq. 51a.

2. Include in a future model a number of features missing from the current version. These include

(a) a formal coupling of the existing cowl-only theory to a boundary-element analysis of the axisymmetric engine core in Fig. 1a (see the author's Ref. 13b and Ref. 13a by Wong, for one such analysis for an unshrouded, but otherwise general axisymmetric body in a still acoustic medium);

(b) possible changes in the liner model and its subroutine;

(c) the addition of camber/taper and static thickness to the cowl's geometry, which is now straight and thin.

3. Develop and apply an active-liner control algorithm to further reduce acoustic radiation from the ducted system.

REFERENCES

1 J.F. Groeneweg, "Aeroacoustics of Advanced Propellers", NASA TM 103137, 17th Congress of the International Council of Aeronautics and Astronautics, Stockholm, Sept. 9-14, 1990.

2 J.H. Dittmar, "An Estimate of the Noise Shielding on the Fuselage Resulting from Installing a Short Duct Around an Advanced Propeller", NASA TM 100262, 1988.

3 R.K. Amiet, (a) "Unified Aeroacoustics Analysis for High Speed Turboprop Aerodynamics and Noise", Vol. II -- Development of Theory for Wing Shielding, NASA CR 185192, May 1991; (b) "Gust Response for Flat-Plate Airfoils and the Kutta Condition", AIAA J., 28(10), 1990, pp. 1718-1727; (c) "High-Frequency Thin-Airfoil Theory for Subsonic Flow", AIAA J., 14(8), 1976, pp. 1076-1082, Eq. 15, where the Fresnel integral "E" vanishes as the square root of its argument.

4 R. Martinez, (a) "A Boundary-Integral Formulation for Thin-Walled Shapes of Revolution", J. Acoust. Soc. Am., 87(2), 1990, pp. 523-531; (b) "Diffracting Open-Ended Pipe Treated as a Lifting Surface", AIAA J., 26(4), 1988, pp. 396-404; (c) "Unified Aerodynamic Acoustic Theory for a Thin Rectangular Wing Encountering a Gust", AIAA J., 18(6), 1980, pp. 636-645; (d) "Predictions of Wing and Pylon Forces Caused by Propeller Installation", NASA CR 178298, May 1987; (e) "The Thin-Shape Breakdown of the Helmholtz Integral Equation", J. Acoust. Soc. Am., 90(5), 1991, pp. 2728-2738; (f) "Aeroacoustic Diffraction and Dissipation by a Short Propeller Cowl in Subsonic Flight", SBIR proposal, submitted July 1991; (g) (with S.E. Widnall) "An Aeroacoustic Model for High-Speed, Unsteady Blade-Vortex Interaction", AIAA J., 21(9), 1983, pp. 1225-1231, Eq. 14.

5 S.J. Horowitz, R.K. Sigman, and B.T. Zinn, "An Iterative Finite-Element/Integral Technique for Predicting Sound Radiation from Turbofan Inlets in Steady Flight", AIAA J., 24(8), 1986, pp. 1256-1261.

6 M.A. Hamdi and J.M. Ville, (a) "Sound Radiation from Ducts: Theory and Experiment", J. Sound & Vib., 107, 1986, pp. 231-242; (b) "Development of a Sound Radiation Model for a Finite Length Duct of Arbitrary Shape", AIAA J, 20, 1982, 1687-1692.

7 C.R. Fuller, (a) "Propagation and Radiation of Sound from Flanged Circular Ducts with Circumferentially Varying Wall

Admittances: II Finite Ducts with Sources", J. Sound & Vib., 93(3), 1984, pp. 321-351; (b) with R.J. Silcox, "Experiments on Sound Radiation from a Duct with a Circumferentially Varying Liner", AIAA J., Vol. 22, 1984, pp. 781-785.

8   W. Eversman, "Radiated Noise of Ducted Fans", AIAA Paper 92-02-139, 14th Aeroacoustics Conf., Aachen, May 11-14, 1992.

9   D.B. Hanson, "Unified Aeroacoustics Analysis for High Speed Turboprop Aerodynamics and Noise", NASA CR 4329, March 1991.

10   M.H. Dunn and F. Farassat, "State of the Art of High Speed Propeller Noise Prediction -- A Multidisciplinary Approach and Comparison with Measured Data", AIAA Paper 90-3934, 1990.

11   M.A. Goldstein, Aeroacoustics, McGraw-Hill, 1976.

12   J.J. Adamczyk, "The Passage of an Infinite Swept Airfoil through an Oblique Gust", NASA CR-2395, 1974.

13   (a) S.K. Wong, "The Singular Kernels of the Helmholtz Integral Equation for Axisymmetric Bodies", to appear, Eq. 17; (b) R. Martinez, "Regarding the Helmholtz Integral for Axisymmetric Bodies", Proceedings of the First International Congress on Recent Developments in Air and Structureborne Sound, Auburn University, March 6-8, 1990, Vol. II, 727-734.

14   H. Ashley and M.T. Landahl, Aerodynamics of Wings and Bodies, Addison Wesley, 1965, 1st Ed.

15   M.S. Howe, "The Influence of Vortex Shedding on the Generation of Sound by Convected Turbulence", J. Fluid Mech., 1976, Vol. 76, pp. 711-740.

16   M. Abramowitz and I.A. Stegun, Handbook of Mathematical Functions, Dover, 1968 (5th Printing), p. 375, Eq. 9.6.7-9.

17   B. Noble, Methods Based on the Wiener-Hopf Technique, Pergamon Press, 1958.

18   S.W. Kandebo, "Pratt to Ground-Test Advanced Ducted Prop Demonstrator in 1991", Aviation Week & Space Technology, February 5, 1990, pp. 34-45.

19   B. Magliozzi, D.B. Hanson, and R.K. Amiet, "Propeller and Propfan Noise", from Aeroacoustics of Flight Vehicles: Theory and Practice, Vol. 1: Noise Sources, NASA Ref. Pub. 1258, Tech. Rep. 90-3052, 1991, Figs. 7a,b.

NEAR-FIELD NOISE

THIN COWL
ACOUSTIC
TREATMENT —

MINIMUM COWL DRAG
(LENGTH AND THICKNESS)

PROPELLER VS.
FAN DESIGN:
SWEEP: M_{AXIAL}: M_{TIP}

BLADE STRESSES
AT HIGH ANGLE
OF ATTACK —

COWL LIP
SEPERATION
AT HIGH ANGLE
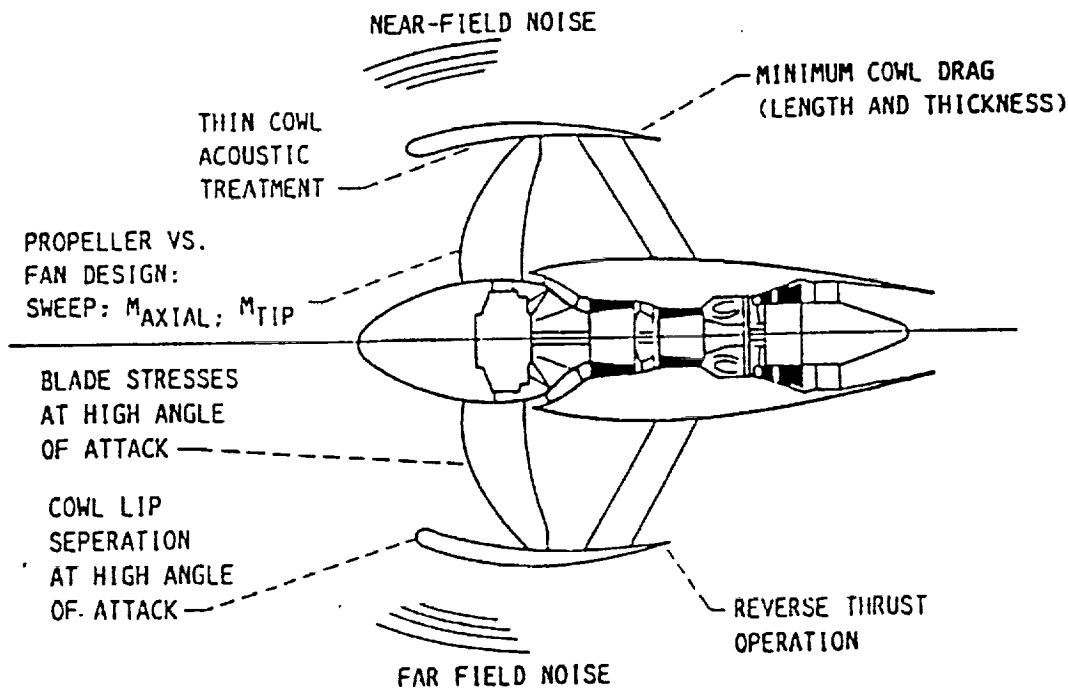OF ATTACK —

REVERSE THRUST
OPERATION

FAR FIELD NOISE

Fig. 1a   [From Refs. 1 and 2]: Typical cowl design for the new
generation of advanced ducted fans. The picture lists
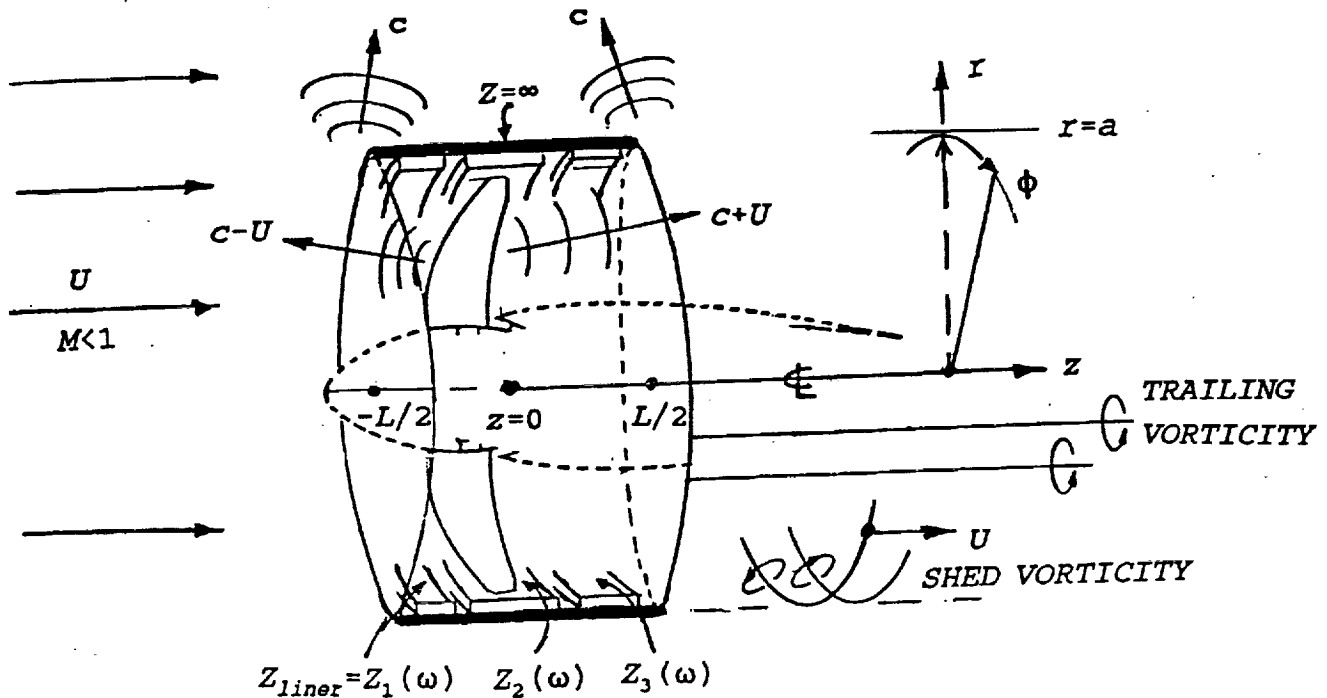issues of interest to NASA. The present study addresses
some of the acoustics items on the list.

c
c
$Z=\infty$
$c-U$
$c+U$
r
$r=a$
ϕ
U
$M<1$
z
$-L/2$ $z=0$ $L/2$
TRAILING VORTICITY
U
SHED VORTICITY

$Z_{liner}=Z_1(\omega)$ $Z_2(\omega)$ $Z_3(\omega)$

Fig. 1b Current idealization of the geometry in Fig. 1a. The
dash-lined engine core is acoustically transparent. The cowl's
radius is constant and equal to "a". Its wall's thickness is
infinitesimal for the purposes of prescribing boundary conditions
on its inner and outer surfaces. The outer surface is rigid, as
indicated at the top of the sketch. The inner surface contains
an axisymmetric liner with properties that may vary with axial
coordinate z. The example liner shown contains three distinct
ring patches with as many frequency-dependent impedances, Z_1, Z_2,
and Z_3. The remaining unlined parts of the cowl's interior have
an infinite impedance.

52
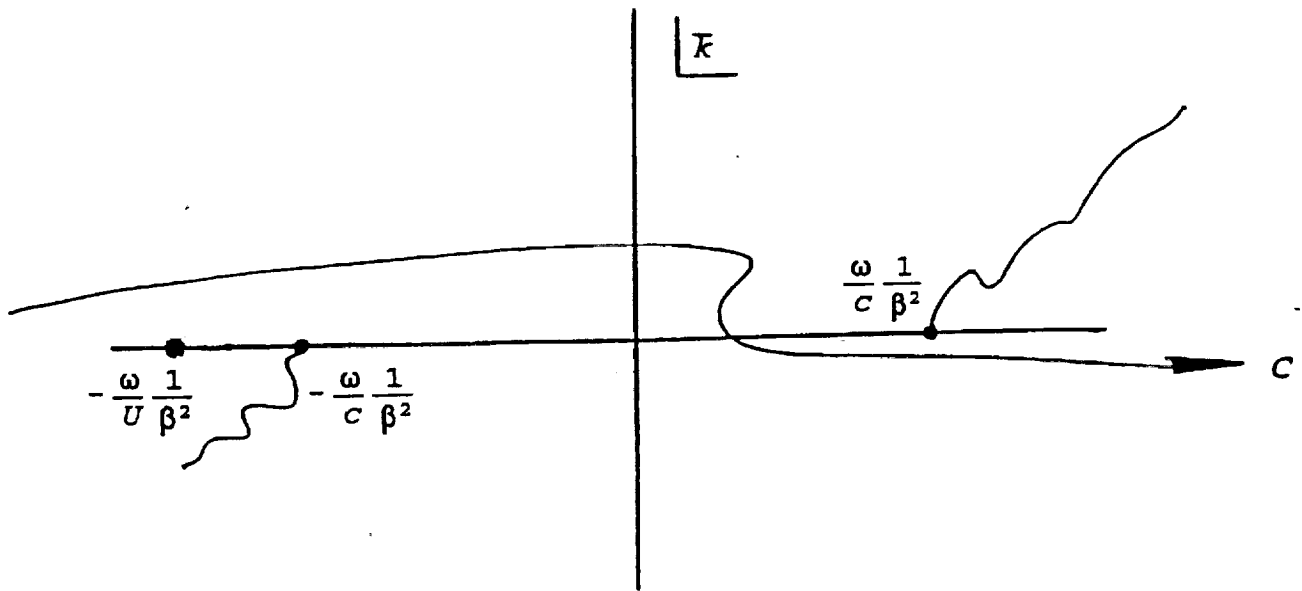
Fig. 2a   The three basic singularities of inviscid aeroacoustics. The branch points generate convected sound signals and the pole produces a shed/trailed vortex system. The implied temporal factor is exp(-iωt). This is the same picture as Fig. 2 of the author's Ref. 4c, where each wavenumber appears normalized by the relevant halfchord ("b" there, L/2 here), and where the harmonic factor is exp(+iωt). See also Fig. 2d below.
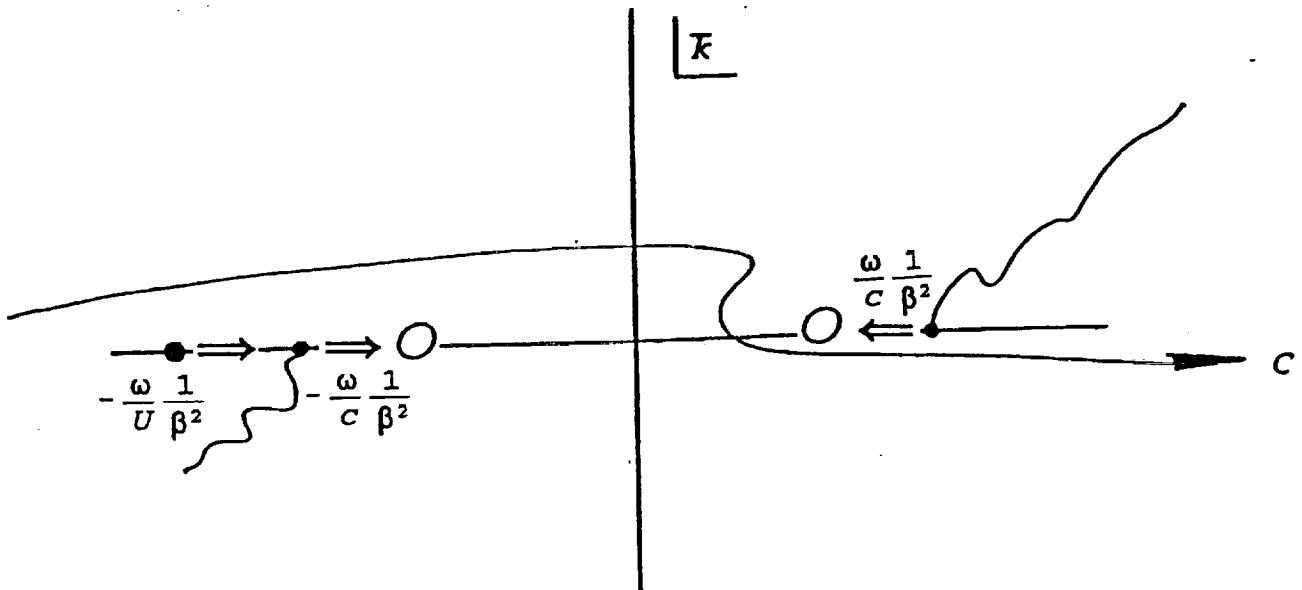

Fig. 2b   Convergence upon the $\bar{k}=0$ origin of the three singular points of Fig. 2a, for the special case of steady aerodynamics, ω=0.

53
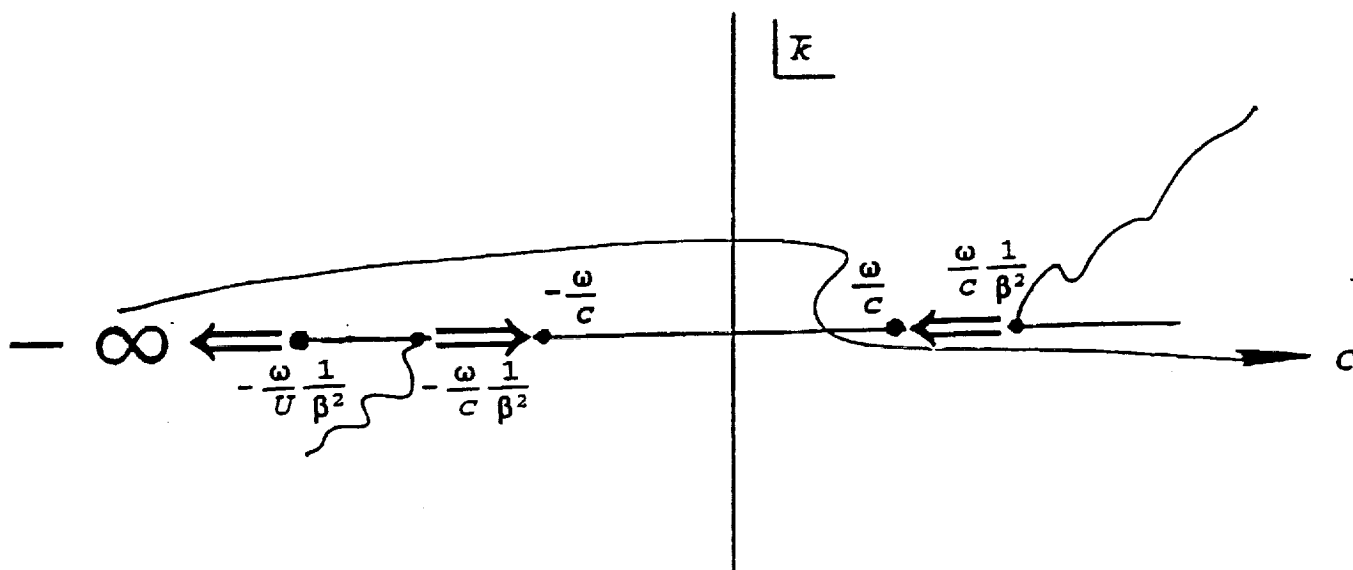
Fig. 2c   Shift of the three singular points of Fig. 2a for the special case of pure diffraction, U=0.   Factor β becomes 1 and the two branch points accordingly move toward $\pm\omega/c$.   The wake pole at $-(\omega/U)/\beta^2$ falls out to $\bar{k}=-\infty$ and out of the problem.
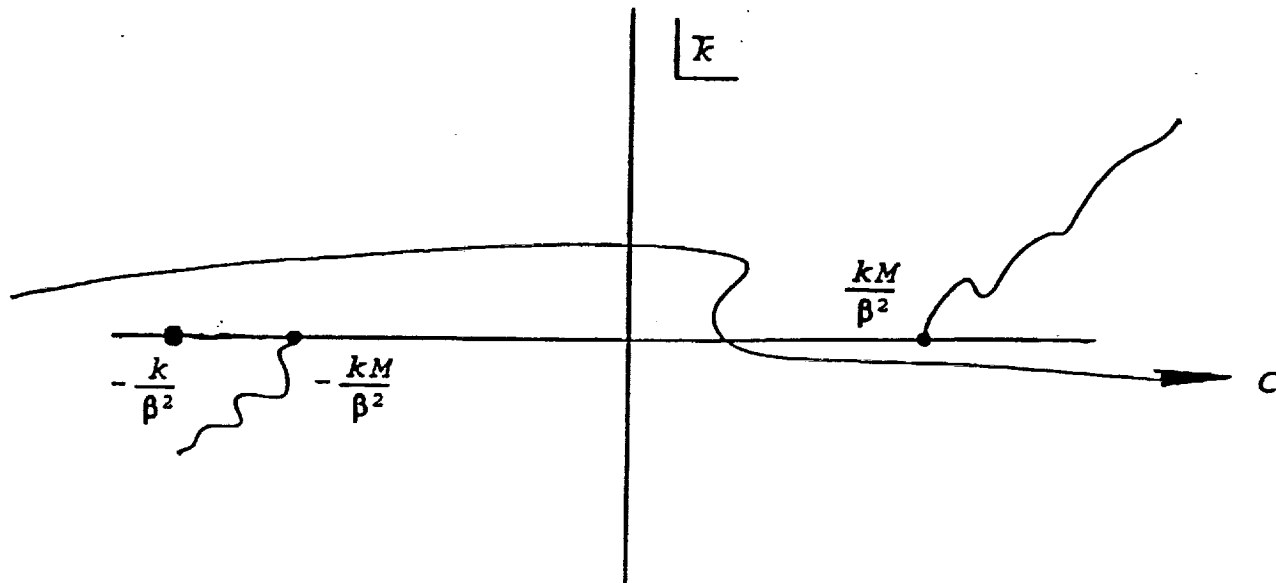
Fig. 2d   Nondimensional version of Fig. 2a.   The ring wing's halfchord L/2 has normalized the transform wavenumber $\bar{k}$.   Symbol k is the cowl's reduced frequency, $\omega L/2U$. This figure is the exp(-iωt) version of Ref. 4c's Fig. 2, where the branch point "μ" appears generalized to include oblique gusts at angle Λ.   Wavenumber μ thus collapses to the kM/β^2 wavenumber indicated above for $\Lambda=0$.

54

$$\tilde{p} \approx G\,d\bar{S}\,\Delta\!\left(\frac{\partial \tilde{p}}{\partial \tilde{r}}\right) = -\rho U G\,d\bar{S}\frac{\partial}{\partial \bar{z}}\Delta\tilde{w}$$

$$= \rho U \Delta\tilde{w}\,d\bar{S}\frac{\partial G}{\partial \bar{z}}$$

$$= -\rho U \Delta\tilde{w}\,d\bar{S}\frac{\partial G}{\partial(z-\bar{z})}$$

$$G \approx -\frac{1}{4\pi R}$$

$$\frac{\partial G}{\partial(z-\bar{z})} < 0 \quad\Big|\quad \frac{\partial G}{\partial(z-\bar{z})} > 0$$
$$\text{for } z<\bar{z} \quad\Big|\quad \text{for } z>\bar{z} \qquad\longrightarrow\; z-\bar{z}$$

$$z-\bar{z}=0$$

$$\Longrightarrow\quad \tilde{p}(z<\bar{z}) > 0 \quad \text{for } \Delta\tilde{w} = \tilde{w}^+ - \tilde{w}^- > 0$$

$$\tilde{p}(z>\bar{z}) < 0 \quad \text{for } \Delta\tilde{w} = w^+ - w^- > 0$$

$$\Longrightarrow\quad \begin{cases} \tilde{p}_v > 0 & \text{for } z<\bar{z} \\[4pt] \tilde{p}_v < 0 & \text{for } z>\bar{z} \end{cases} = -\frac{(\rho U/\beta)\,\Delta\tilde{w}_v\,d\bar{z}}{2\pi}\frac{1}{z-\bar{z}}$$

$$\text{for } \Delta\tilde{w} = \tilde{w}^+ - \tilde{w}^- = -\tilde{w}^- > 0$$

$$\tilde{w}^+ = 0$$
$$\tilde{w}^- < 0$$
$$\tilde{p}(z<\bar{z}) > 0 \qquad\qquad \tilde{p}(z>\bar{z}) < 0$$
$$U$$
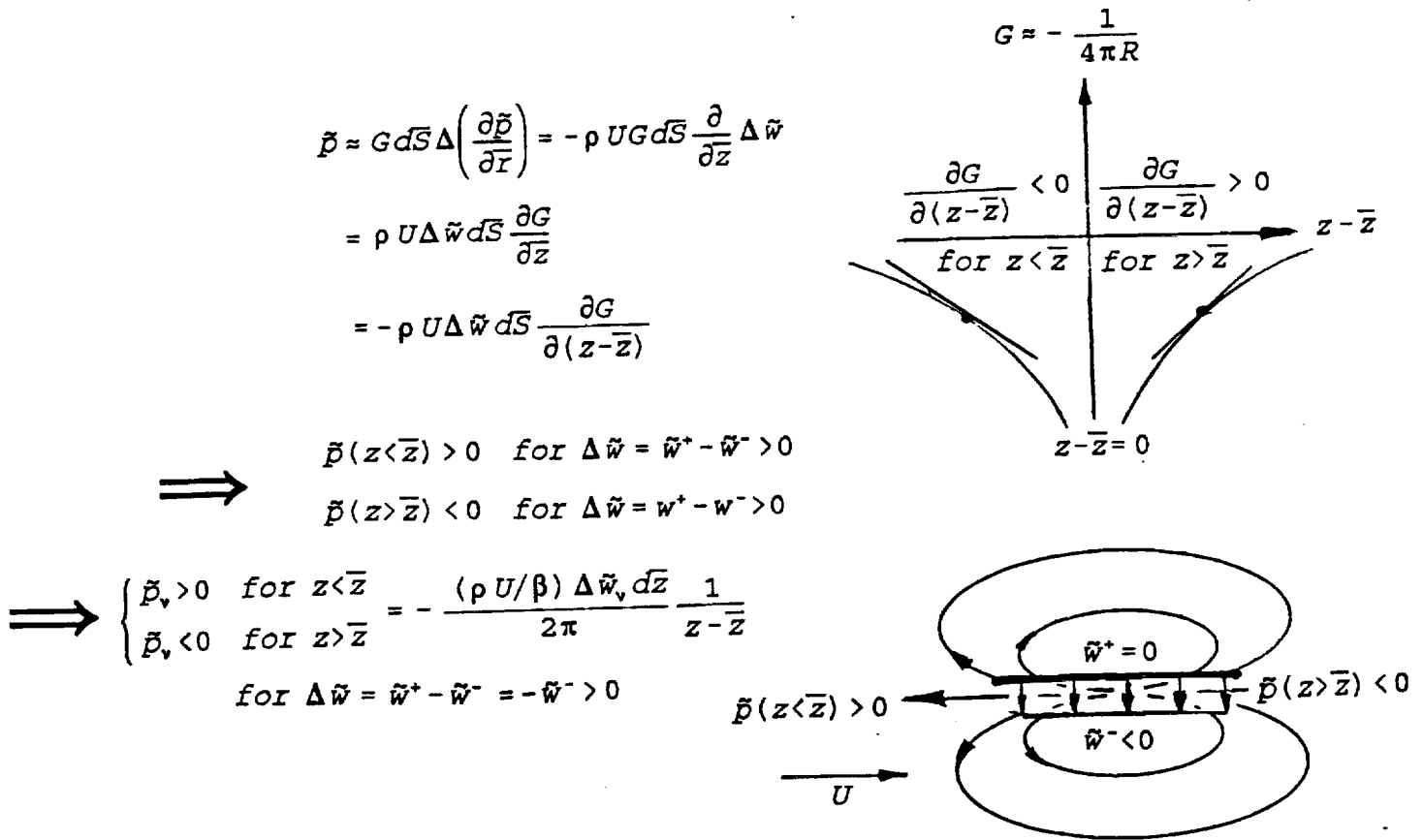
Fig. 3a Graphical confirmation of Eq. 47. The radial momentum equation changes a wall monopole locally into an axial doublet. The monopole's original strength is $\Delta\bar{w}d\bar{S}$, where $d\bar{S}$ is an elemental area patch on the cowl's midsurface. The velocity jump $\Delta\bar{w}$ is taken to be positive. R on the upper sketch is the three-dimensional distance between the source at axial position $\bar{z}$ and the receiver at nearby z. The pressure for $z<\bar{z}$ is negative, whereas $p(z>\bar{z})>0$.

$$r=a$$

$$-\Delta\tilde{u} = -(\tilde{u}^+ - \tilde{u}^-)$$
$$-\tilde{u}^+$$
$$\tilde{w}(z<\bar{z}) < 0 \qquad\qquad \tilde{w}(z>\bar{z}) > 0$$
$$\tilde{u}^-$$

$$\Delta\tilde{p}\,d\bar{S} = [\tilde{p}^+ - \tilde{p}^-]\,d\bar{S} > 0$$

$$\tilde{w}_v = \frac{\Delta\tilde{p}_v}{\rho U}\,d\bar{z}\cdot\left(\frac{\beta}{2\pi}\frac{1}{z-\bar{z}}\right) \qquad \begin{array}{l} < 0 \text{ for } z<\bar{z}, \\[4pt] > 0 \text{ for } z>\bar{z} \end{array}$$
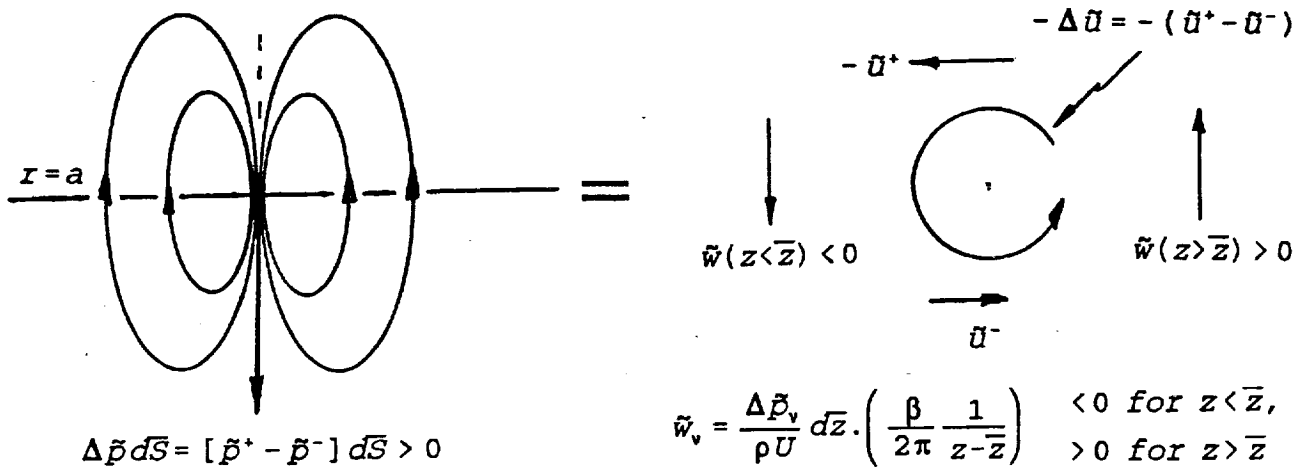
Fig. 3b Bernoulli's equation similarly turns a dipole of positive strength $\Delta\bar{p}$ (negative lift) into a bound vortex with counterclockwise circulation $-\Delta\bar{u}$. The vortex induces a negative downwash for $z<\bar{z}$ and a positive radial flow for $z>\bar{z}$. These signs are opposite those for the pressures in Fig. 3a's lower sketch, and thereby account for the "–" sign within brackets in the first term in Eq. 47.

$$\Delta\tilde{w} = \tilde{w}^+ - \tilde{w}^-$$
$$= -\tilde{w}^-$$
$$= monopole\ strength$$

$$\tilde{w}^{inc} - \tilde{w}^- = net\ velocity\ acting\ outward\ on\ r = a^+$$
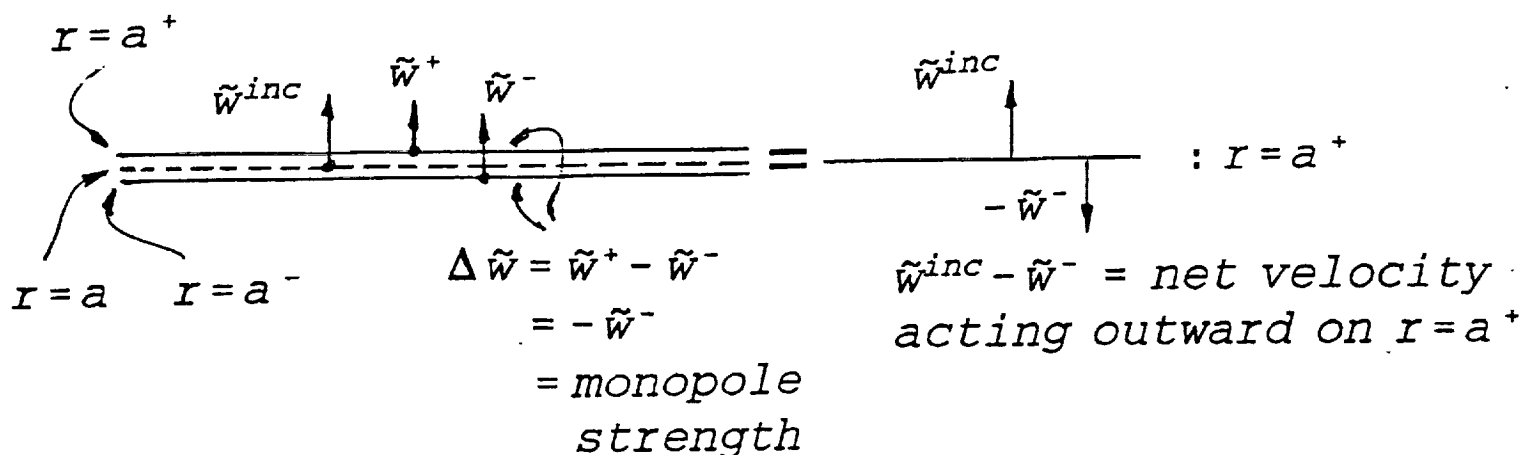
Fig. 4a   Sketch in support of the first of the two sign-check arguments discussed after Eq. 48c. The $r=a^+$ local contribution of the thickness problem is an inward velocity opposing the incident field (see also Fig. 3a's lower sketch). $\Delta\tilde{w} = -\tilde{w}^-$ because here the cowl's outer wall at $r=a^+$ is hard.
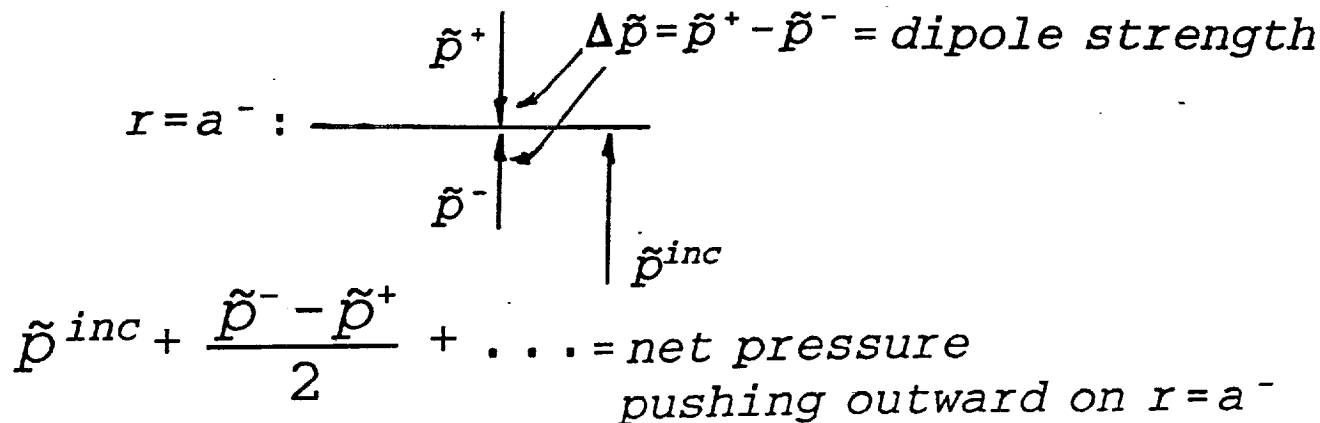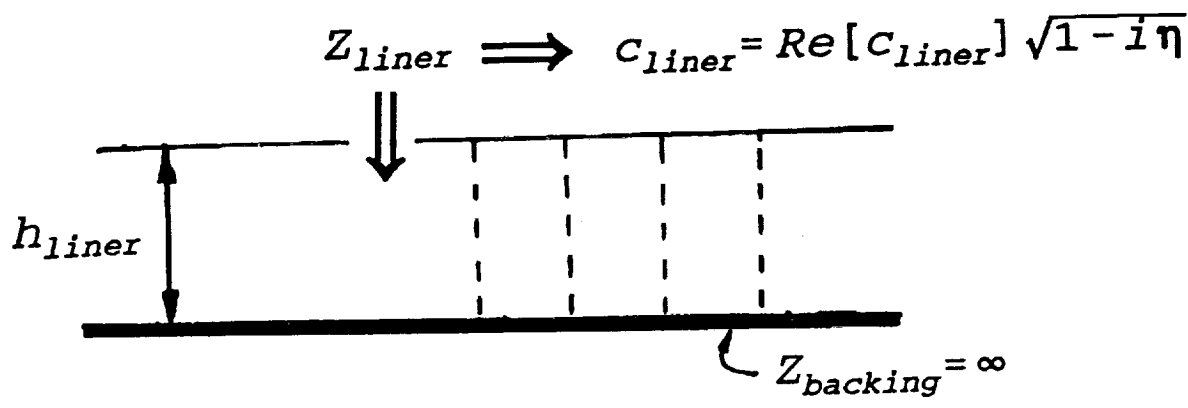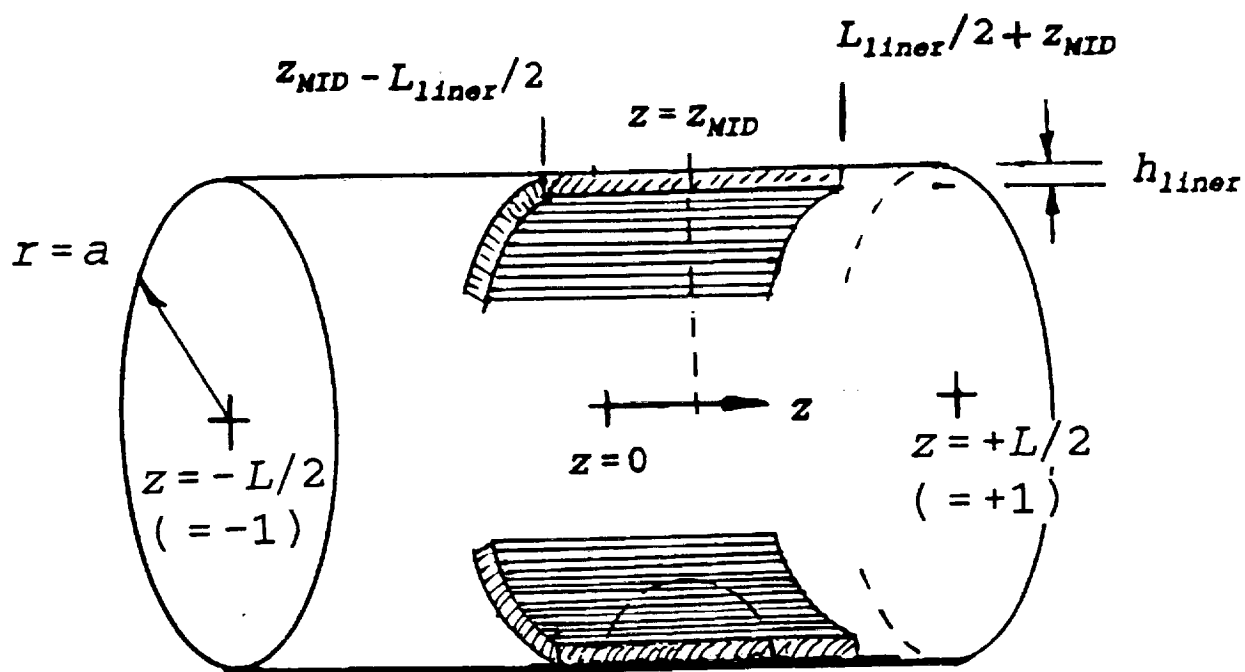

$$\Delta\tilde{p} = \tilde{p}^+ - \tilde{p}^- = dipole\ strength$$

$$\tilde{p}^{inc} + \frac{\tilde{p}^- - \tilde{p}^+}{2} + \ldots = net\ pressure\ pushing\ outward\ on\ r = a^-$$

Fig. 4b   Second of the two sign checks taken up after Eq. 48c. The inboard scattered pressure $\tilde{p}^-$ adds to that of incident field acting over $r=a^-$, as it should.

56

Figs. 5a,b (a) Geometric parameters of the liner model. The lined segment extends from $z=z_{mid}-L_{liner}/2$ to $z_{mid}+L_{liner}/2$. The picture also shows the effect of the eventual normalization of all spatial variables by the halflength $L/2$: The cowl's left end will then be at the nondimensional axial position $z=-1$, etc.

(b) Blow-up of the cropping circle in (a). The liner is a locally reacting acoustic layer with loss factor η and compressional wave speed c_{liner}. Eqs. 48b,c ignore the actual liner depth h_{liner} in prescribing the inboard boundary condition on $r=a^-$ rather than on $r=a-h_{liner}$.
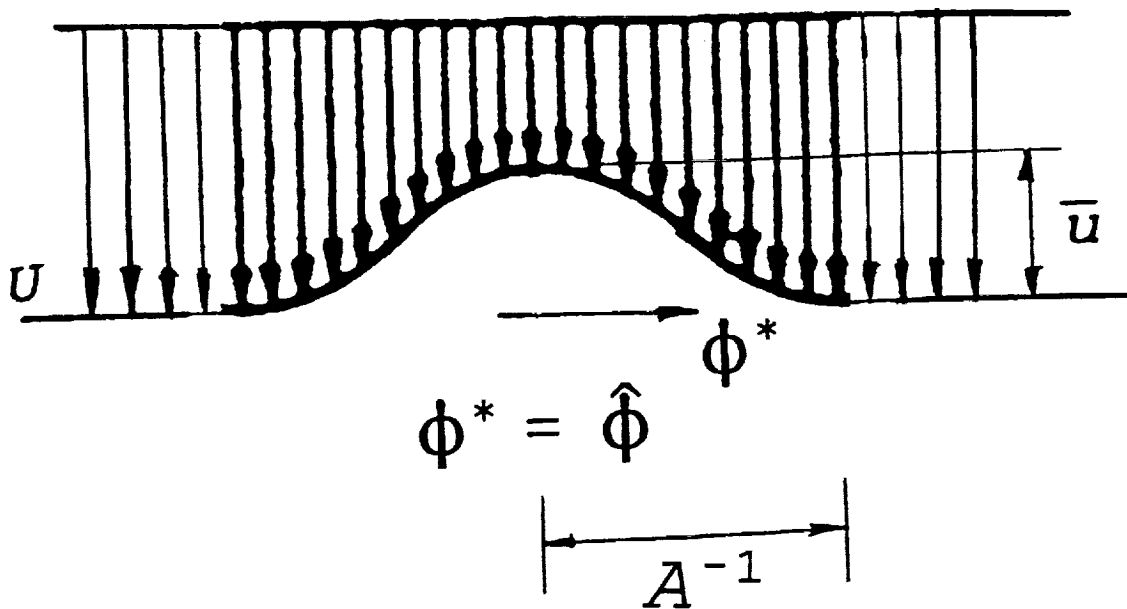
Fig. 6a Model of a stationary inflow nonuniformity being chopped by the fan. The Gaussian curve contains three parameters: (1) the absolute angular position $\hat{\phi}$ on the propeller plane for, (2) the maximum momentum deficit $\bar{u}/U$, (3) which smooths out in the ϕ^* direction at the rate A^{-1} (see Eq. 56). The nonuniformity depicted affects all r^* blade radial stations between hub (R_h) and tip (R_t).
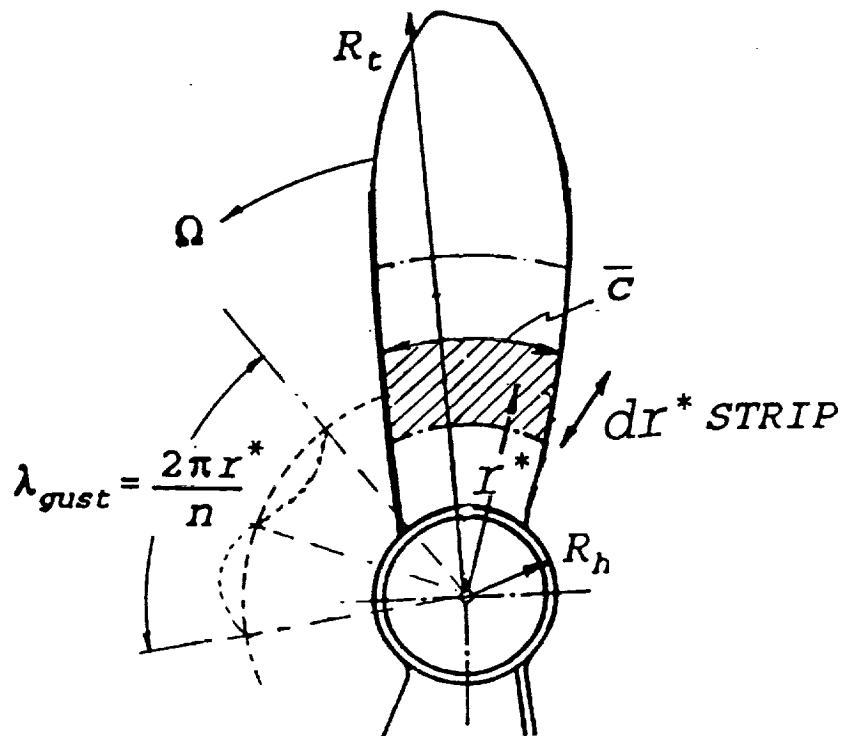
Fig. 6b Eq. 56 breaks up the inflow nonuniformity of Fig. 6a into a discrete "n" spectrum of circumferential gusts of wavelength $2\pi r^*/n$. The blades lie flat on their plane of rotation, are unswept and of constant chord $\bar{c}$. The gusts' "wavefronts" are parallel to the blades' leading edges.

$$R_o = \sqrt{(z/\beta)^2 + r^2}$$

$$\theta_o = -\tan^{-1}\left(\frac{\beta r}{z}\right)$$
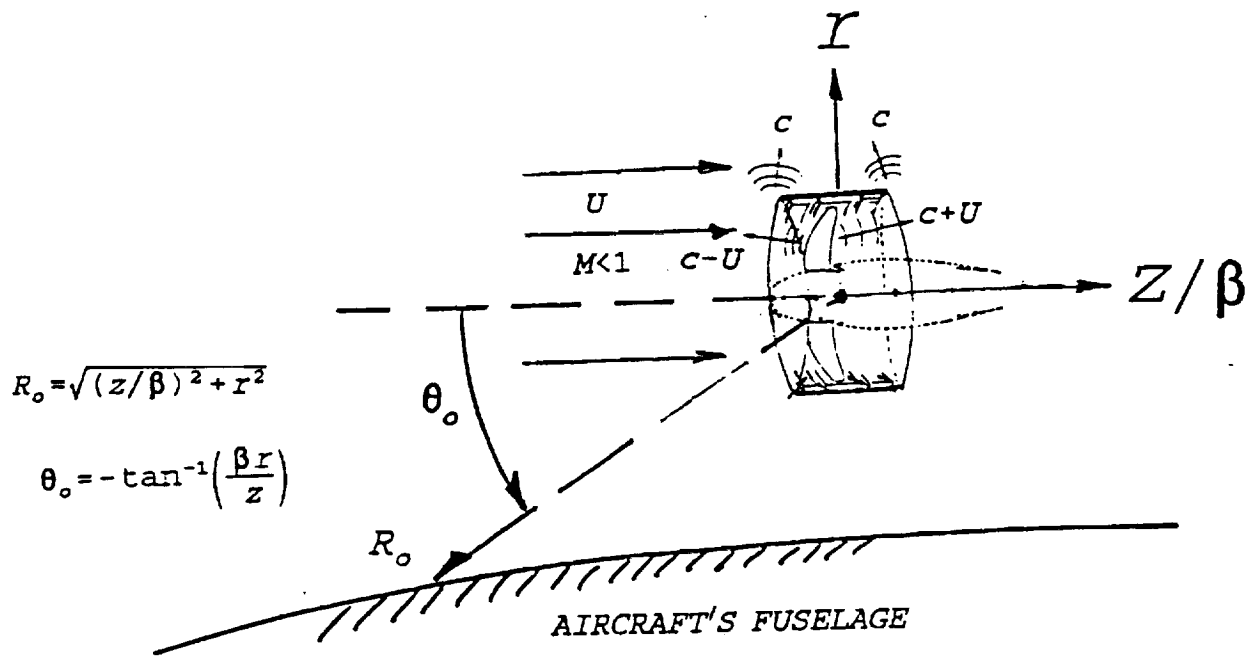
Fig. 7a Definition of range R_o and of directivity angle θ_o for the calculation of the acoustic farfield reaching the cabin's outer wall. Sound must travel through a medium moving at Mach number +M in this reference frame. Signals accordingly propagate in the downstream direction at speed c+U relative to the aircraft. Their wavelength stretches by the factor 1+M (Eq. 25). Waves travelling upstream do so at speed c−U, and their wavelength compresses by 1−M.

$$R_o = \sqrt{z^2 + r^2}$$

$$\theta_o = -\tan^{-1}\left(\frac{r}{z}\right)$$
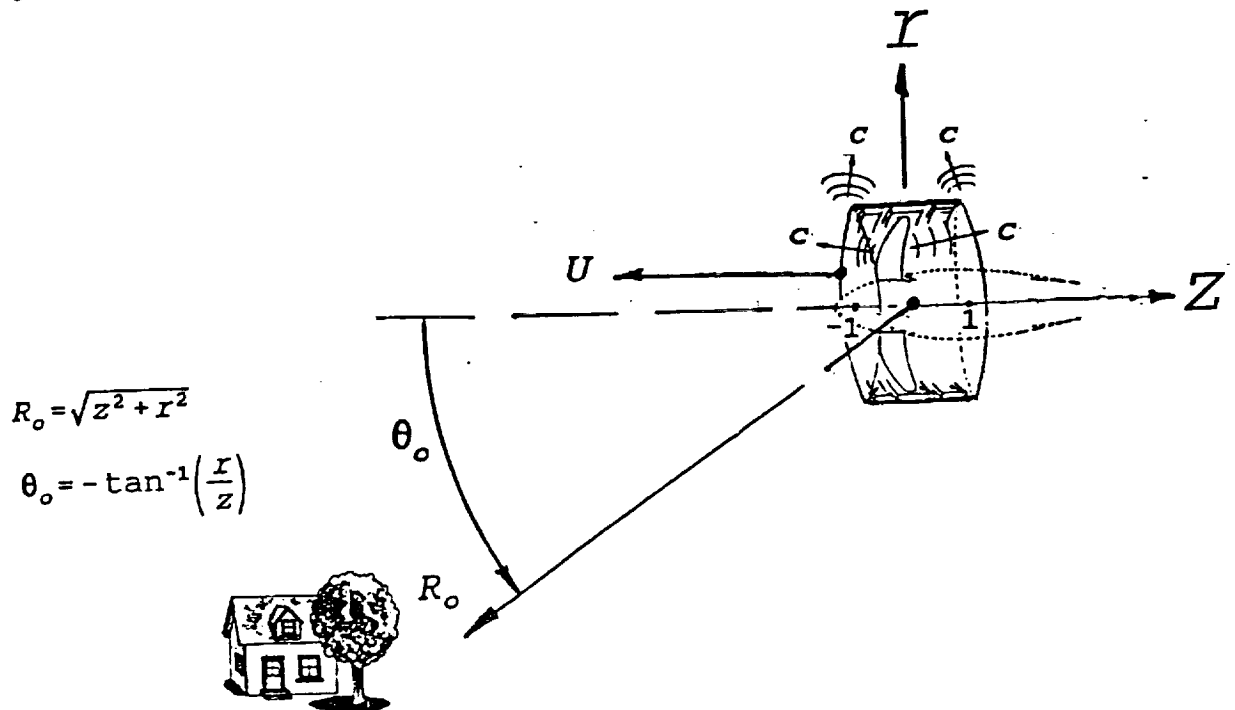
Fig. 7b Corresponding definitions for the farfield calculation for ground-based listeners. Now all real and virtual sources are in motion with speed −U, the medium is still, and all acoustic signals travel at speed c relative to all observation points. Upstream wavelengths remain shortened due to the Doppler effect (see sketch). Downstream signals stretch out for the same reason.

59
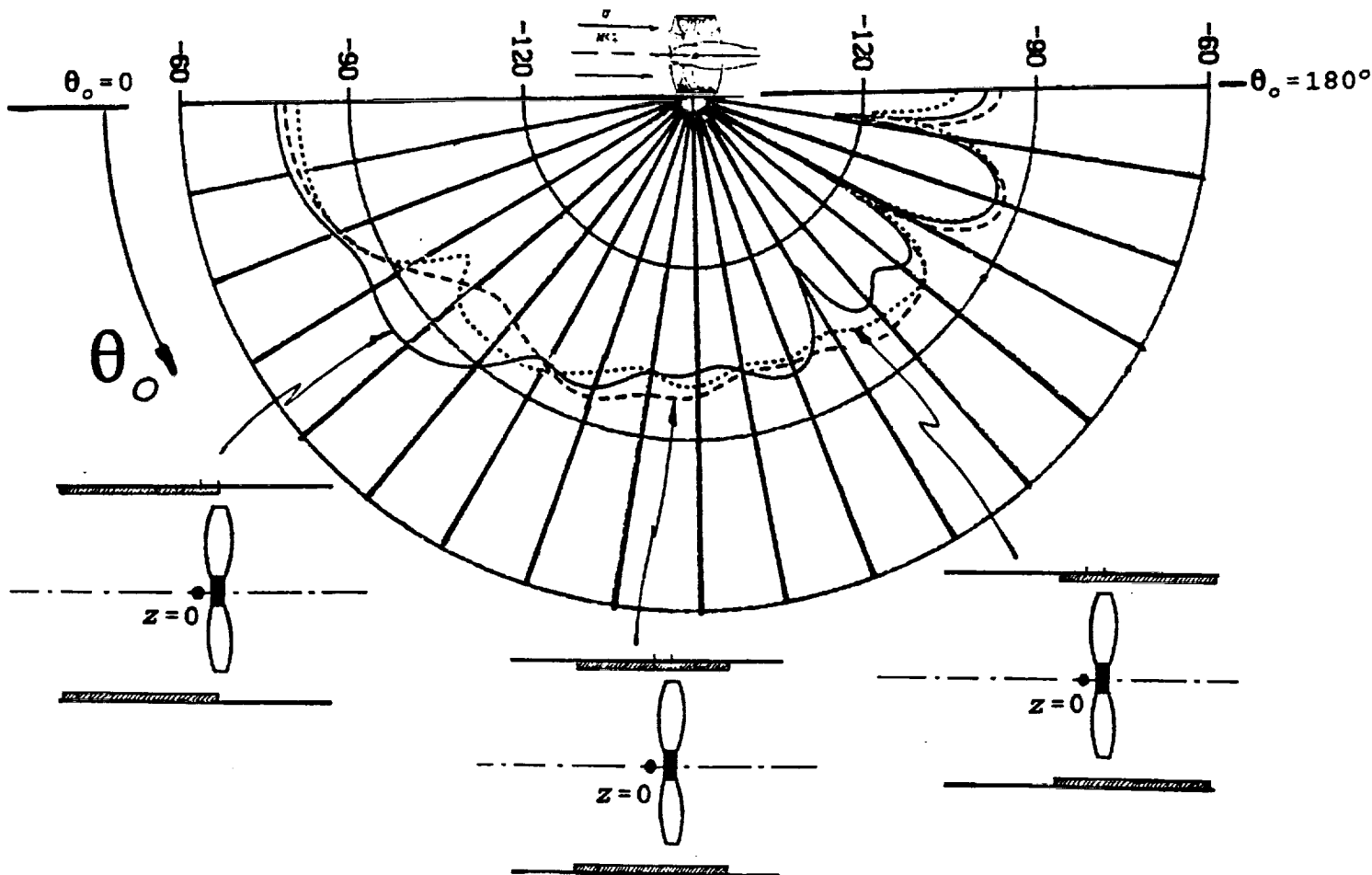
Fig. 8a Predictions of total radiated farfield for three liner
configurations. The listener is on the frame of
reference of the flying aircraft. The solid curve is
for a ring patch of liner beginning immediately after
the cowl's leading edge, etc. Each curve displays
$20\log_{10}|R_o(\bar{p}_v{}^{inc}+\bar{p}_v{}^{\ell}+\bar{p}_v{}^{th})/\rho U^2|$, with the argument of the
$\log_{10}$ provided by Eqs. 60a and 63a. R_o is the
dimensionless range to the farfield observer. Modal
index v is zero.

$\theta_o = 0$ -80 -90 -120 U NC -120 -90 -60 $\theta_o = 180°$

$IL \geqslant 0$

θ_O
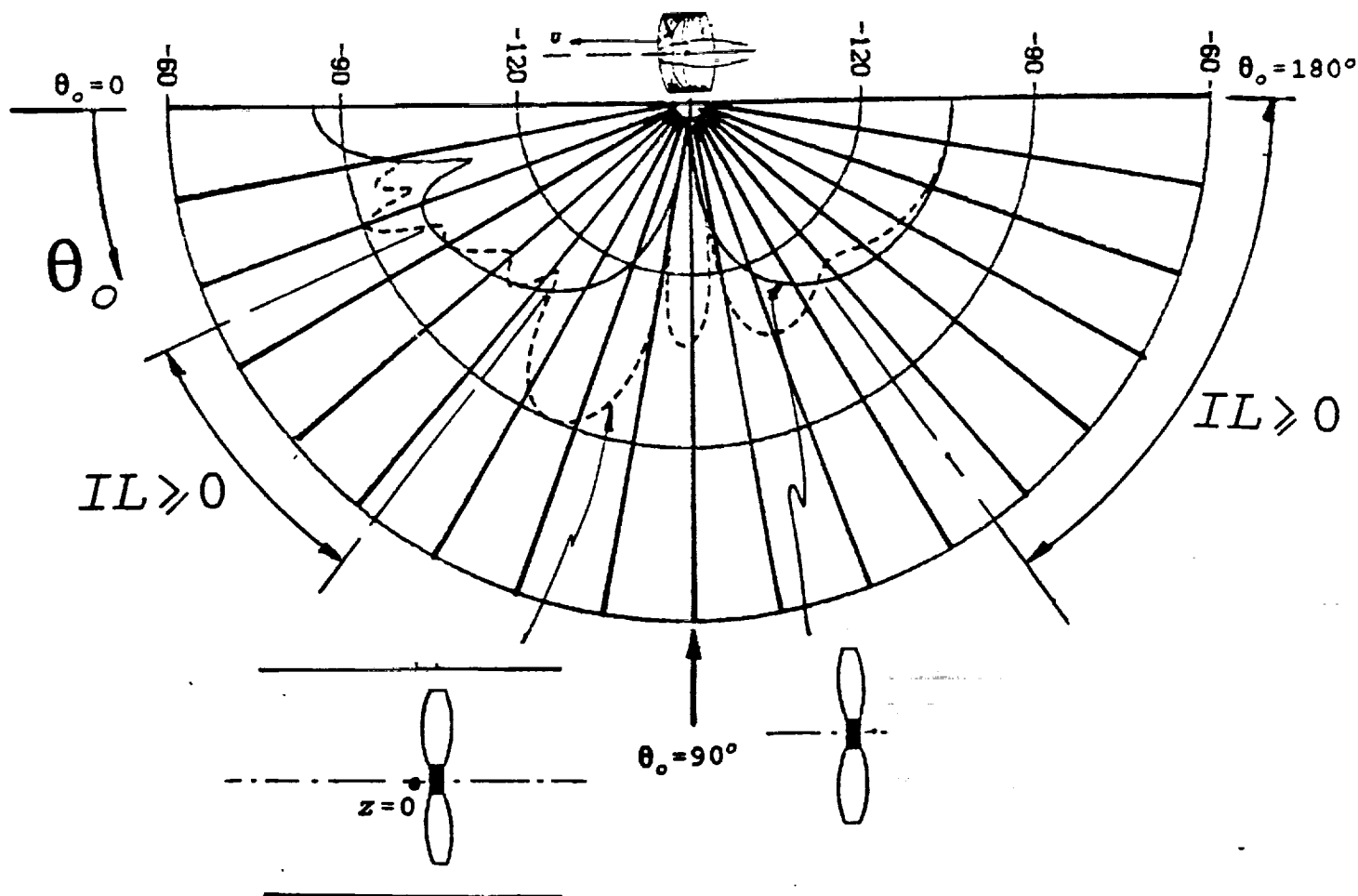
$\theta_o = 143°$

$z = 0$

$IL \geqslant 0$
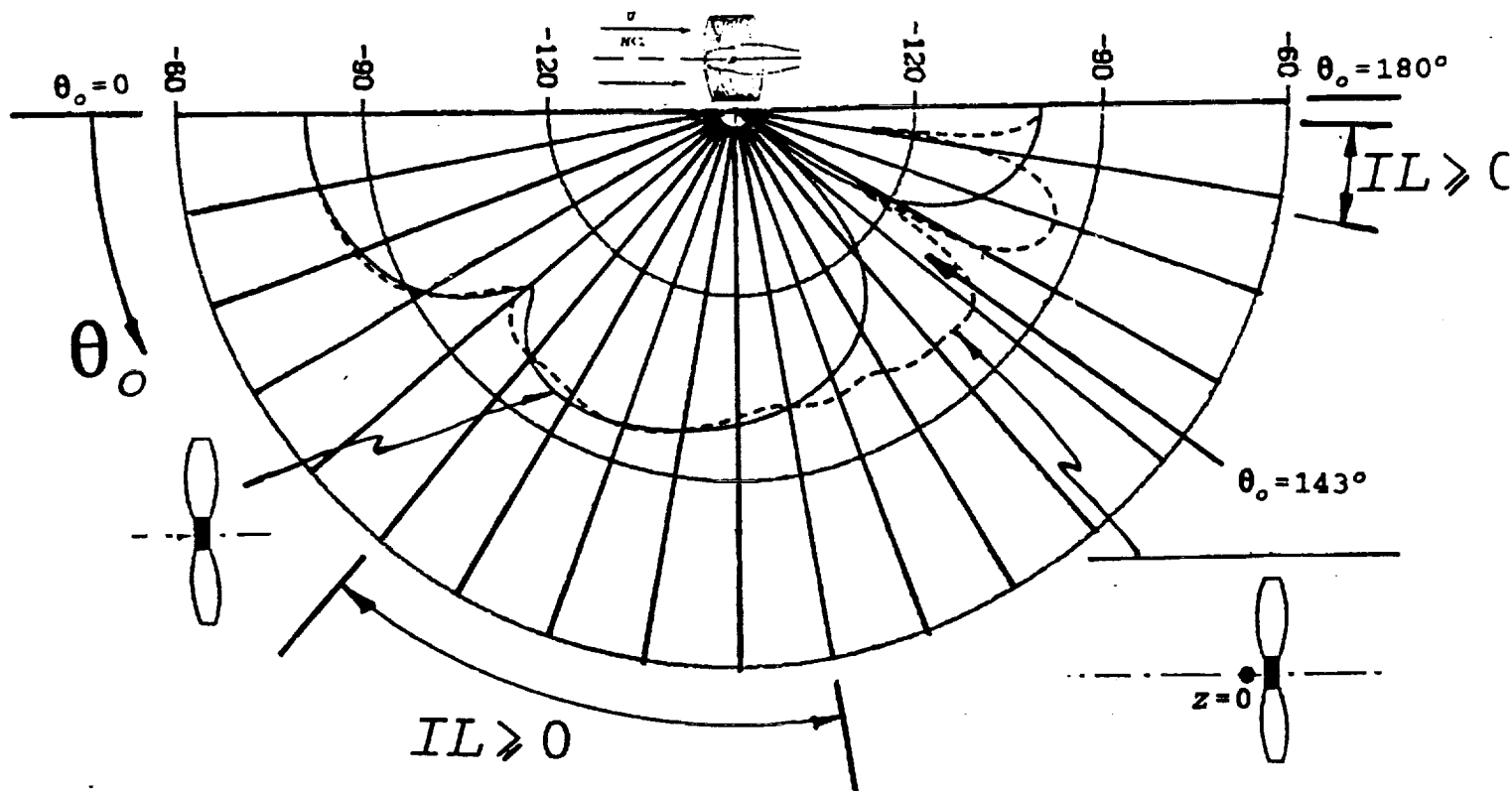
Fig. 8b Predictions of $20\log_{10}|R_o\bar{p}_v^{inc}/\rho U^2|$ and $20\log_{10}|R_o(\bar{p}_v^{inc}+\bar{p}_v^\prime+\bar{p}_v^{th})/\rho U^2|$, which respectively apply to an unducted and to a ducted propeller. The frame of reference is that of the moving aircraft. The cowl contains no liner and $\bar{p}_v^{th}$ is consequently zero. The directivity pattern for the propeller in free field (the solid curve) has a null at $\theta_o=143°$ due to the $\cos\theta_o+M$ factor on the third line of Eq. 60a. The "IL$\geq$0" label marks a pair of sectors over which the cowl has a positive, though modest noise shielding effect (a positive insertion loss). Modal index v is zero.
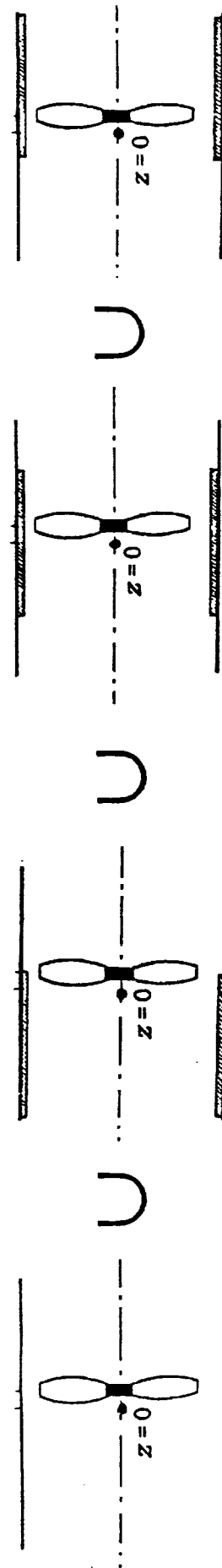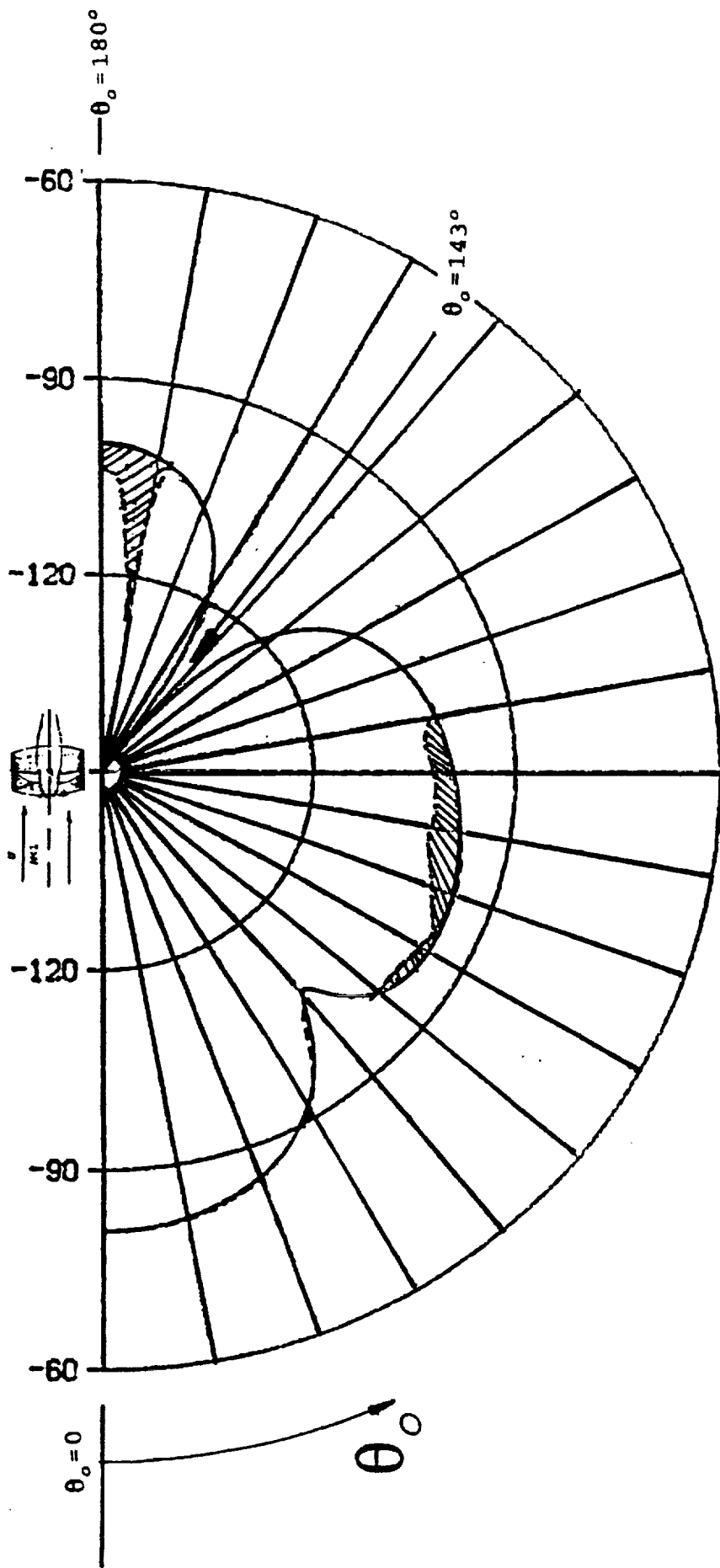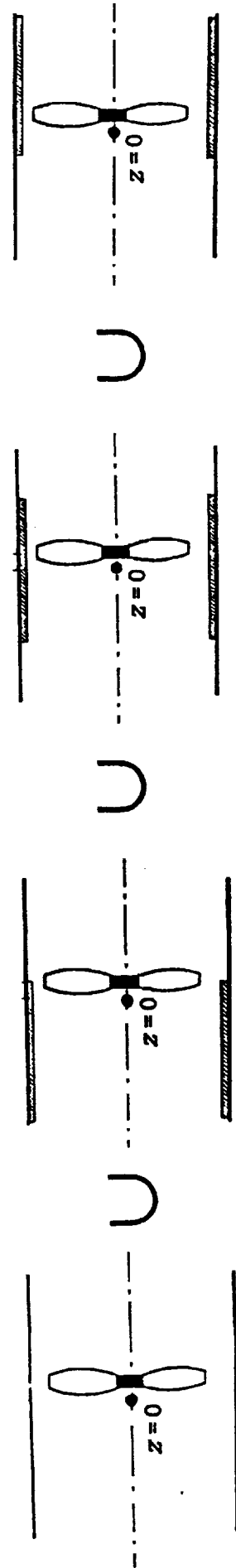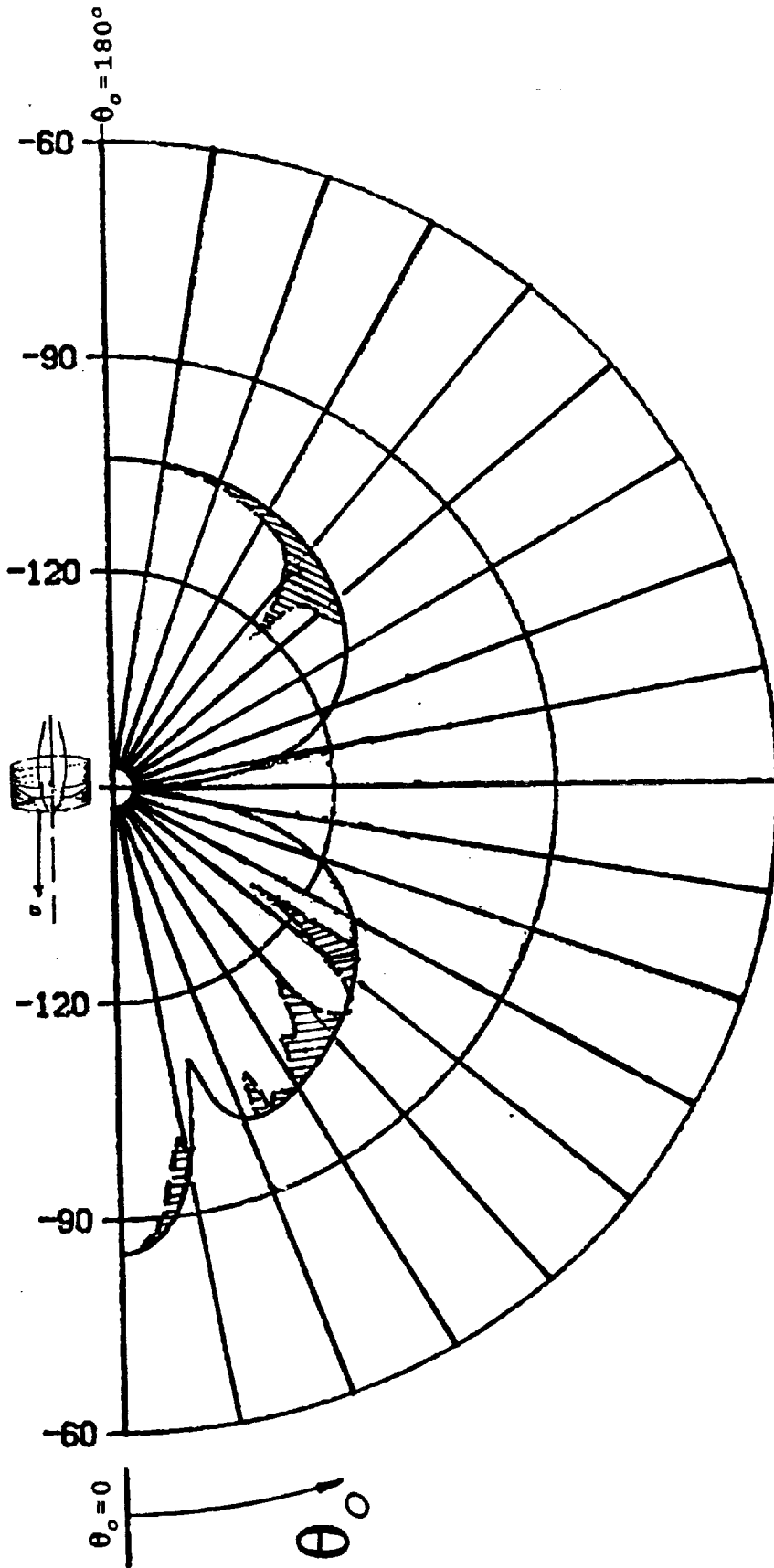
Fig. 8c Union of the IL≥0 solution sets (shaded) from the total farfields for the ducted cases in Figs. 8a,b. The solid curve repeats the unducted result in Fig. 8b. The frame of reference moves with the aircraft. Modal index v is zero.
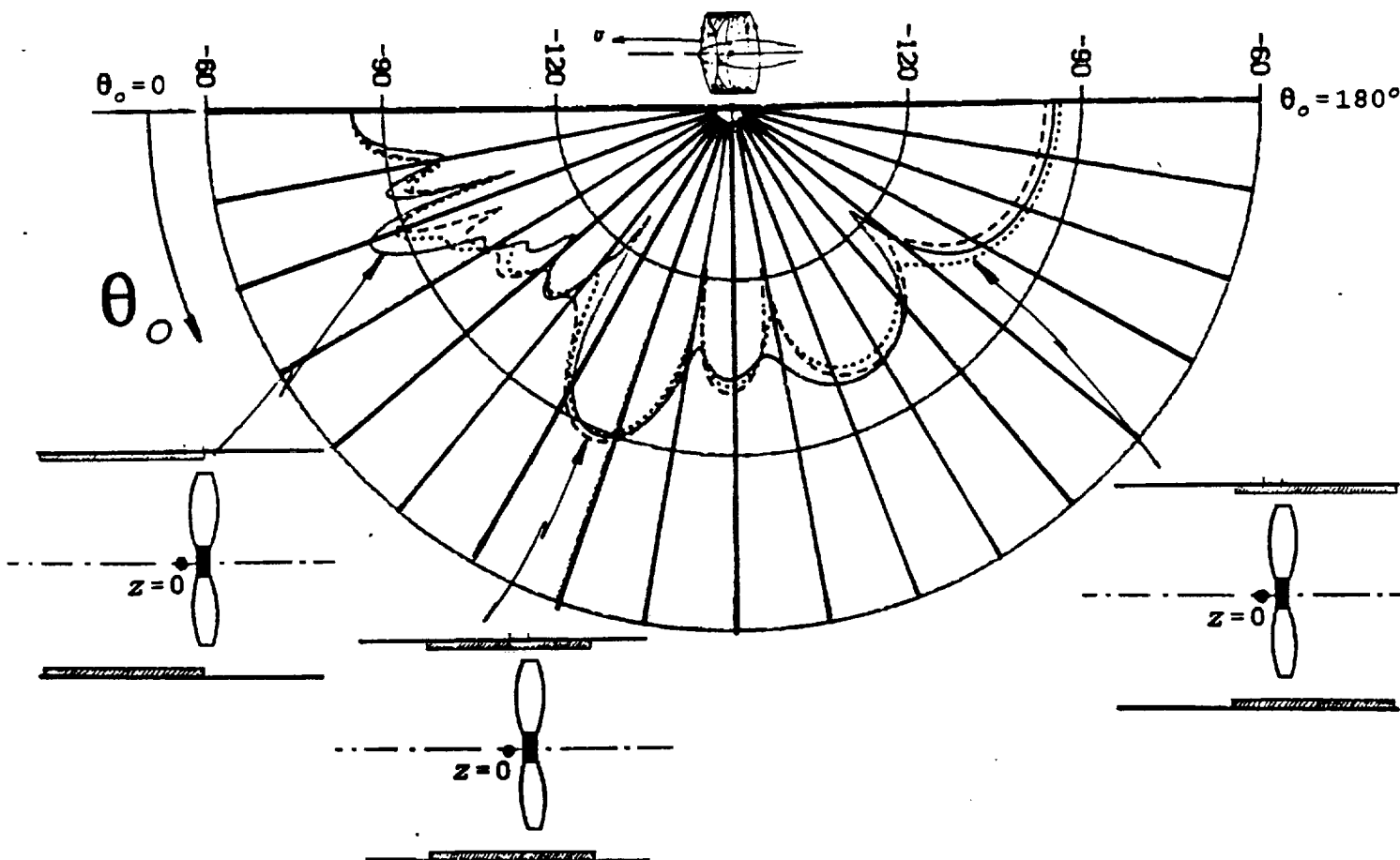
Fig. 9a   Predictions of total radiated farfield for three liner
          configurations. The listener is on the ground. The
          solid curve is for a ring patch of liner beginning
          immediately after the cowl's leading edge, etc. Each
          curve contains the result of $20\log_{10}|R_o(\bar{p}_v^{inc}+\bar{p}_v'+\bar{p}_v^{th})/\rho U^2|$,
          with the argument of the $\log_{10}$ provided by Eqs. 60b and
          63b. R_o is the dimensionless range to the farfield
          observer. Modal index v is zero.

Fig. 9b Predictions of $20\log_{10}|R_o\bar{p}_v{}^{inc}/\rho U^2|$ and
$20\log_{10}|R_o(\bar{p}_v{}^{inc}+\bar{p}_v{}^{\ell}+\bar{p}_v{}^{th})/\rho U^2|$, which respectively apply to
an unducted and to a ducted propeller. The incident-
field curve displays a null at $\theta_o=90°$ as required by the
$\cos\theta_o$ factor on the third line of Eq. 60b. The listener
is on the ground. The cowl contains no liner and $\bar{p}_v{}^{th}$ is
consequently zero. The "IL≥0" label marks a pair of
sectors over which the cowl has a positive noise-
shielding effect (a positive insertion loss). Modal
index v is zero.

64

Fig. 9c Union of the IL≥0 solution sets (shaded) from the total farfields for the ducted cases in Figs. 9a,b. The solid curve repeats the unducted result in Fig. 9b. The frame of reference is anchored on the ground. Modal index ν is zero.
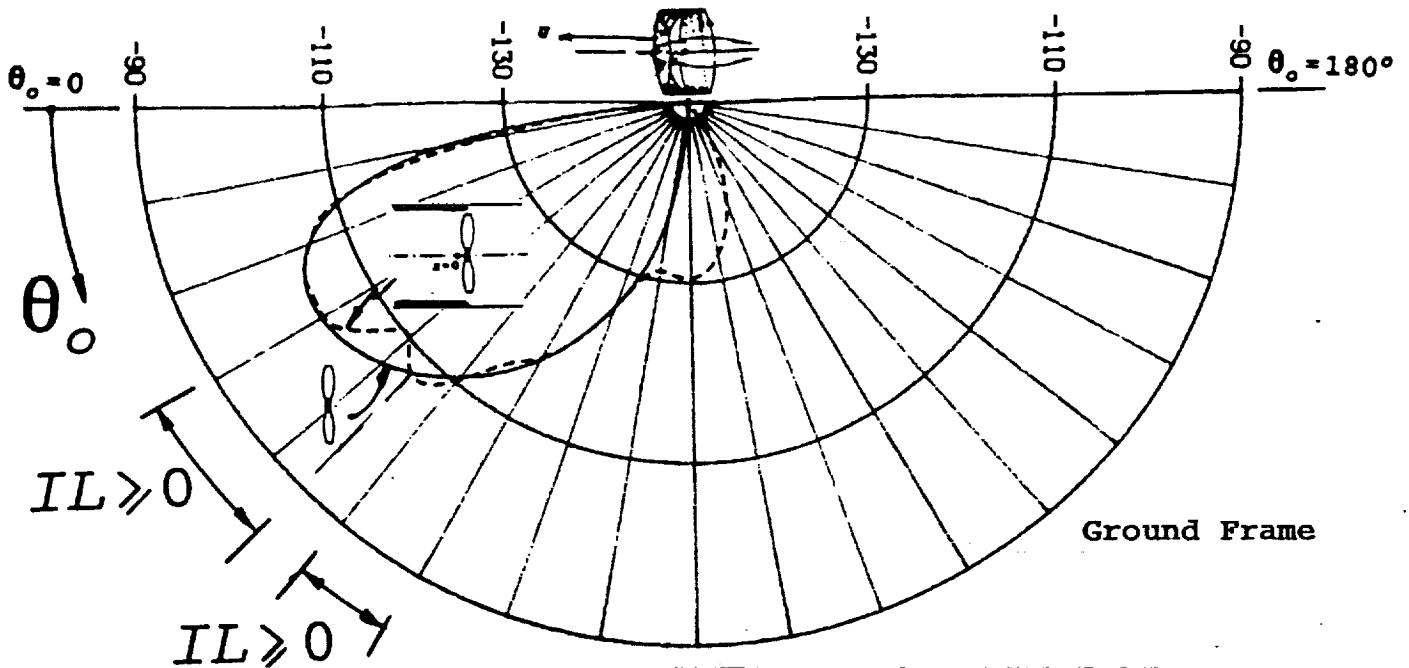
Fig. 10a Comparison of radiated patterns for ducted and unducted
cases for $|v|$=5. The tuned liner for the ducted case
abuts the cowl's leading edge (see insert). Its loss
factor η is unity. "IL≥0" labels mark those field
positions for which the cowl has a beneficial effect.
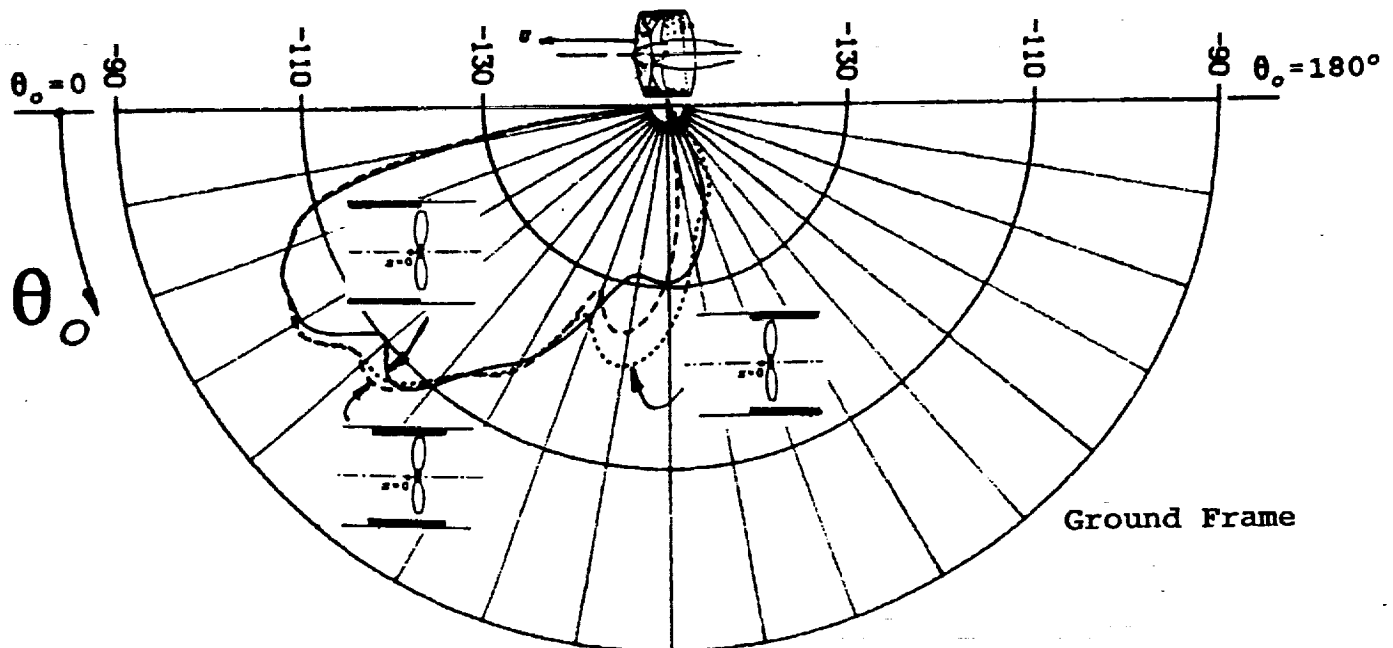
Fig. 10b Comparison of total radiated patterns for the three
liner-patch layouts of previous figures, for $|v|$=5.
Each patch is resistance-controlled (resonating and
highly damped) and the three curves do not differ
significantly except in their lower levels.

66

REPORT DOCUMENTATION PAGE

1. AGENCY USE ONLY (Leave blank)	2. REPORT DATE	3. REPORT TYPE AND DATES COVERED
	April 1993	Final Contractor Report

4. TITLE AND SUBTITLE

Aeroacoustic Diffraction and Dissipation by a Short Propeller Cowl in Subsonic Flight

5. FUNDING NUMBERS

WU–535–03–10
C–NAS3–26598

6. AUTHOR(S)

Rudolph Martinez

7. PERFORMING ORGANIZATION NAME(S) AND ADDRESS(ES)

Cambridge Acoustical Associates, Inc.
80 Sherman Street
Cambridge, Massachusetts 02140

8. PERFORMING ORGANIZATION REPORT NUMBER

E–7717

9. SPONSORING/MONITORING AGENCY NAMES(S) AND ADDRESS(ES)

National Aeronautics and Space Administration
Lewis Research Center
Cleveland, Ohio 44135–3191

10. SPONSORING/MONITORING AGENCY REPORT NUMBER

NASA CR–190801

11. SUPPLEMENTARY NOTES

Project Manager, James H. Dittmar, Propulsion Systems Division, (216) 433–3921.

12a. DISTRIBUTION/AVAILABILITY STATEMENT

Unclassified - Unlimited
Subject Category 71

12b. DISTRIBUTION CODE

13. ABSTRACT (Maximum 200 words)

This report develops and applies an aeroacoustic diffraction theory for a duct, or cowl, placed around modelled sources of propeller noise. The regime of flight speed is high subsonic. The modelled cowl's inner wall contains a liner with axially variable properties. Its exterior is rigid. The analysis replaces both sides with an unsteady lifting surface coupled to a dynamic thickness problem. The resulting pair of aeroacoustic governing equations for a lined "ring wing" is valid both for a passive and for an active liner. Their numerical solution yields the effective dipole and monopole distributions of the shrouding system and thereby determines the cowl-diffracted component of the total radiated field. The sample calculations presented here include a preliminary parametric search for that liner layout which maximizes the cowl's shielding effectiveness. The main conclusion of the study is that a short cowl passively lined should provide moderate reductions in propeller noise.

14. SUBJECT TERMS

Propeller noise; Ducted propeller

15. NUMBER OF PAGES
67

16. PRICE CODE
A04

17. SECURITY CLASSIFICATION OF REPORT	18. SECURITY CLASSIFICATION OF THIS PAGE	19. SECURITY CLASSIFICATION OF ABSTRACT	20. LIMITATION OF ABSTRACT
Unclassified	Unclassified	Unclassified	